1-1-2014

Communication Protocol Design Considerations For Highway Vehicle Platoons And Enhanced Networked Robustness By Stochastic Dithers

Lijian Xu

Wayne State University,

COORDINATED COMMUNICATION PROTOCOL DESIGN FOR HIGHWAY VEHICLE PLATOONS AND ENHANCED NETWORK ROBUSTNESS BY STOCHASTIC DITHERS

by

LIJIAN XU

DISSERTATION

Submitted to the Graduate School

of Wayne State University,

Detroit, Michigan

in partial fulfillment of the requirements

for the degree of

DOCTOR OF PHILOSOPHY

2014

MAJOR: COMPUTER ENGINEERING

Approved by:

_____

Adviser Date

_____

_____

_____

_____

ACKNOWLEDGEMENTS

This dissertation could not have been completed without the contributions of many individuals. In particular, I wish to express my deepest gratitude and sincerest appreciation to my advisor Professor Le Yi Wang for proposing me an exciting topic for my dissertation, for his exceptional guidance, constant inspiration, consistent support, and endless care during my graduate study at Wayne State University. His direction and support were crucial for the completion of the work.

I would also like to thank Professor Gang George Yin and Professor Weixing Zheng for introducing me to the area of stochastic problems. I greatly admire their mathematical perspectives, and I am thankful for the opportunity to have learned from them. Their comments, suggestions and support have resulted in much improvement of this work.

I am taking this opportunity to thank Professor Harpreet Singh and Professor Caisheng Wang for serving on my committee.

I am grateful to all my professors, including the Professor Xiaoyan Han, Professor Feng Lin, Professor Yang Zhao, Professor Robert Erlandson, Professor Chengzhong Xu and Professor Abhilash Pandya who have contributed to my solid formation in engineering, who have nurtured my curiosity and given me the opportunities to learn from them.

My thanks also go to Dr. Ge Chen, Dr. Jin Guo and Dr. Biqiang Mu for their help and encouragement in one way or another.

I am indebted to my beloved parents for their love, support, and inspiration since

I was born. This dedicated to my dearest Mother Suyun Xie and Father Shishan Xu.

Special thanks go to my wife and my kids for their love, support, encouragement, and their confidence in me.

Last, but not least, I would like to express my appreciation to the entire Department of Electrical and Computer Engineering for their hospitality and services. I have enjoyed the warm and friendly atmosphere in the department, and appreciate the support I have received during my study at Wayne State University.

TABLE OF CONTENTS

LIST OF TABLES

LIST OF FIGURES

1 INTRODUCTION

1.1 Objectives and Motivations

Highway platooning of vehicles has been identified as a promising framework in developing intelligent transportation systems [1, 2]. By autonomous or semi-autonomous vehicle control and inter-vehicle coordination, an appropriately managed platoon can potentially offer enhanced safety, improved highway utility, increased fuel economy, and reduced emission. In a platoon formation and maintenance, high-level distributed supervisors adjust vehicle spatial distributions based on inter-vehicle information such that roadway utilization is maximized while the risk of collision is minimized or avoided and robustness of control is enhanced. Controllers at vehicle levels, sensors, and communication systems interact intimately in vehicle platoon formation, control and robustness. This thesis investigates several such key issues and introduces a new method to enhance feedback robustness against communication multiplicative uncertainties, especially transmission gains. The method employs a fundamental property in stochastic differential equations to add a scaled dither under which tolerable gain uncertainties can be much enlarged to include sign changes and system delay. Unlike additive noise, uncertain gains and random delay directly impact feedback stability and must be dealt with by feedback mechanism. Beyond the traditional maximum feedback robustness against gain uncertainty, the new method can potentially enhance large multiplicative uncertainties such as gains, phase shift, delays, etc. This research is focused on first-order systems. Algorithms, stability, convergence, and

robustness are presented. Challenges in extending this idea to higher-order systems are discussed.

1.2 Literature Review

Platoon control has drawn substantial attention lately [3, 4]. During the 90s, there were substantial contributions on platoon control, including PATH projects [5, 6], FleeNet, among others. Intelligent platoon control algorithms were introduced with demonstration and experimental validation [7, 8]. The most common objectives in platoon control are safety, string stability, and team coordination [9, 10]. Early studies of platoon control were not communication focused, due to less-advanced communication systems at that time. In our recent work [11, 12], a weighted and constrained consensus control method was introduced to achieve platoon formation and robustness. At present, on-board front radars are used in vehicle distance measurements. [12] employs convergence rates as a performance measure to evaluate benefits of different communication topologies in improving platoon formation, robustness, and safety.

Recent advance in communication technologies and networked systems in mobile agents, parallel computing, intelligent vehicle systems, tele-medicine, smart grids, has generated much intensified interests and research efforts on integrated feedback systems with communication channels. Control designs that aim at dealing with unique issues from communication channels have emerged. The basic control configuration in such control systems involves a plant with local sensors and actuators and a re-

mote controller, which are interconnected by communication channels. For example, minimum channel capacities of noisy communication channels for a feedback system to stabilize an unstable plant have been sought [13]. Control-oriented communication design, including data compressions, quantization, coding schemes, has opened new avenue of integrated control and communication design [14]. [15] presents solutions to output variance minimization of systems involving Gaussian channels in the feedback loop. The optimal stochastic methodologies are used in [16] in an LQG (Linear-Quadratic-Gaussian) problem with delay statistics. Complexity issues in networked system identification are studied also [17].

Communication channels introduce some unique challenges to feedback systems. Traditionally, uncertainties from communication channels are dominantly modeled as additive noise. Since additive noises will not directly affect feedback stability, such pursuit is mostly concentrated on performance such as output variance. Recently, feedback stability and robustness have been pursued for channel latency (time delays), packet losses, quantization errors, often accommodate random uncertainties. At present, feedback robustness against channel uncertainties are still studied by applying the traditional control techniques, and hence limited by the optimal robustness bounds on gain uncertainty, etc. Communication channels insert new dynamic subsystems into control loops. Impact of communication systems on feedback loops can be treated as added uncertainty such as additive and multiplicative noise, delays and errors [15, 18, 19].

1.3 Problems Statement

In terms of coordination of control and communication systems in a platoon, some intrinsic questions arise: (1) How much improvement of safety can be achieved by including communication channels? (2) What information should be communicated? What are the values of such information? (3) How will communication uncertainties such as latency, packet loss, and error affect safety? (4) How do we choose the proper information content and its data rate in multi-information vehicle ad hoc network (VANET) environment in order to achieve a platoon control goal? (5) How do we enhance the platoon stability robustness?

This thesis aims to answer these questions with quantitative characterization. To facilitate this exploration, we consider various information structures: (1) Front radars only, (2) combined radars and wireless communications. In addition, we investigate the information contents: (1) distances only, (2) distance and speed, (3) additional early warning of the driver's braking action. Typical communication standards such as IEEE 802.11p and related communication latency are used as benchmark cases in this study, These findings are applied to the Information Harmonization Module (IHM) design. IHM is a network/control interface. This module includes two control methods. The first method is weighted multi-information structure control. By applying weighted coefficients γ on each received information, control objects of collision free and efficiency of highway usage can be achieved. This control method can be implemented by feedback system designs where γ is embedded in control gains. The

second method is communication data rate control. By applying varied data rate, the same control object with weighted multi-information structure control can be achieved. The method entails a dramatically improvement of bandwidth usage. This is essentially important for vehicle platoons due to the limitations of communication resources on highway environment. We can implement this novel idea by switching data rate based on the vehicle's feedback states and dynamic control goals instead of varying built-in vehicle parameters.

1.4 Originality and Contributions

The main contributions of this thesis are in the following aspects. (1) Thesis establishes quantitatively the impact of communication delay and package deliver rate on vehicle safety in a platoon framework. (2) Relationships among channel throughput, safety, and highway utility are derived. Such relationships can be used to guide integrated design of control and communications. (3) Platoon communication design involves information selection, network topologies, and resource allocation. We establish results for information contents (such as vehicle distance, speed, braking action), network information topologies, and bandwidth allocations. (4) It establishes new platoon control methods in the wireless multi-information framework, this benefits from the recent advances of Wireless Access in Vehicular Environments (WAVE). (5) Analysis of dynamic vehicle system control by adjusting communication system are derived, this is new by comparisons with previous vehicle control models. (6) We establish the results for platoon control oriented communication Media Access Control

(MAC) design. The results include request/response data acquisition mechanism, Orthogonal frequency-division multiplexing (OFDM) data rate selection model and time division multiple access (TDMA) design guide. (7) This research first introduce the method of adding scaled dither to feedback networked system. Enhancement of network robustness is discussed in scalar and high order cases.

1.5 Thesis Overview

The rest of the thesis is organized into the following sections. Section 2 introduces the basic platoon control problem and safety issues, this section also defines control strategies and sets up evaluation scenarios for comparative studies of different information structures and contents, The section also starts with safety analysis. Section 3 describes typical wireless communication uncertainties including analog signals with additive or multiplicative noise, digital communication with delay and package erasure models. Then in section 4, under some simplified scenarios, basic relations are derived, including speed-distance relationship for safe stopping distance and collision avoidance, distance progression in a platoon, and delay-distance functions for communication latency. This section details typical communication scenarios. Communication latency characterization and related experimental data are presented, the section also investigates impact of information structure by comparing radar-based distance sensing and communications. Front radars are the current commercial automotive technology. By expanding information structures to include wireless communication networks, improvement on safety is quantitatively studied. The roles of information

contents are explored, in which improvements on safety by including more information on vehicle speeds and drivers' actions are studied. we investigate impact of communication latency on vehicle safety. Typical scenarios of communication latency are considered. Section 5 details typical communication scenarios with erasure channel. Communication channel erasure characterization and related packet delivery rates (PDR) are presented. This section investigates the impact of information structure and channel erasures. Typical scenarios of communication channel erasures are considered. Section 6 outlines the main functions of the Weighted Multi-information Structure Control and the Data Rate Control. Simulations and case studies are also presented. Section 7 presents the key methodologies of scaled dithers. The theoretical foundation of the scaled dither methodology is first established by using the limit SDE method. The concept of the loop gain margin is first introduced that characterizes feedback robustness bounds. By using the features of the scaled dither, we show that the feedback robustness ranges can be extended to a larger set involving sign changes. Explicit robustness bounds are established. Issues with extending this idea to higher-order systems are discussed. Then we introduce consensus control. Consensus control may be viewed as a networked first-order system, which can potentially benefit from state-dependent dithers. The theoretical foundation of the state-dependent dither methodology is established by using the limit SDE method. Algorithms and their convergence properties are presented. It establishes gain robustness of the dithered consensus control. It is shown that by appropriate design of the dithers, a very large gain uncertainty set on network connections can be tolerated. Some design consider-

ations are discussed. Planning of implementation and verification described. Finally, Section 8 summarizes the main findings of this thesis.

2 PRELIMINARIES

2.1 Vehicle Dynamics and Platoon Information Structure

This thesis is concerned with inter-vehicle distance control in a highway platoon. For clarity of investigation, we use simplified, generic, but representative vehicle dynamic models from [22]

$$m\dot{v} + f(v) = F, \tag{2.1}$$

where m (Kg) is the consolidated vehicle mass (including vehicle, passengers, etc.), v is the vehicle speed (m/s), $f(v)$ is a positive nonlinear function of v representing resistance force from aerodynamic drag and tire/road rolling frictions, and F (Newton or Kg-m/s^2) is the net driving force (if $F > 0$) or braking force (if $F < 0$) on the vehicle's gravitational center. Typically, $f(v)$ takes a generic form $f(v) = av + bv^2$, where the coefficient $a > 0$ is the tire/road rolling resistance, and $b > 0$ is the aerodynamic drag coefficient. These parameters depend on many factors such as the vehicle weight, exterior profile, tire types and aging, road conditions, wind strength and directions. Consequently, they are determined experimentally and approximately. This thesis focuses on longitude vehicle movements within a straight-line lane. Thus, the vehicle movement is simplified into a one-dimensional system.

Vehicles receive platoon movement information by using sensors and communication systems. We assume that radars are either installed at front or rear of the vehicle. The raw data from the radars are distance information between two vehicles. Although it is theoretically possible to derive speed information by signal processing

(derivatives of the distances), this thesis works with the direct information and leaves signal processing as part of control design. As a result, radar information is limited to distances. In contrast, a communication channel from vehicle i to vehicle j can transmit any information that vehicle i possesses. We consider the following information contents for transmission: (1) vehicle i's distance that is measured by its front sensor, (2) vehicle i's speed, which is available by its own speedometer, (3) vehicle i's braking action. Information structures are depicted in Fig. 1. A vehicle may receive information from its front distance sensor (on its distance to the front vehicle), or its rear sensor (on its distance to the vehicle behind it), or wireless communication channels between two vehicles. The wireless communication channels may carry different information contents such as distance, speed, driver's action, etc.

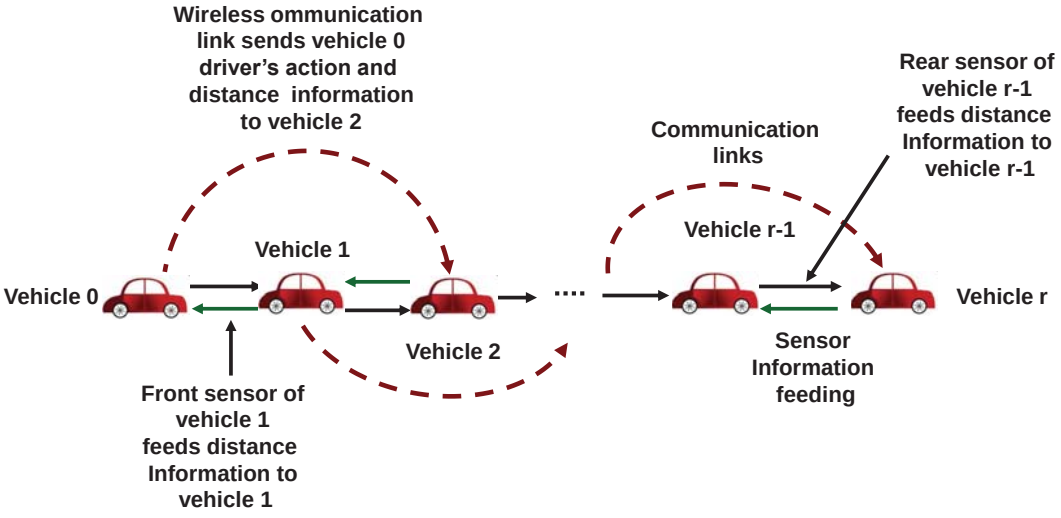

Figure 1: Information structures.

For concreteness, we use a basic three-car platoon to present our key results.

Although this is a highly simplified platoon, the main issues are revealed clearly in this system. Three information structures are studied, shown in Fig. 2. "Information Structure (a)" employs only front sensors, implying that vehicle 1 follows vehicle 0 by measuring its front distance d_1, and then vehicle 2 follows vehicle 1 by measuring its front distance d_2. For safety consideration, this structure provides a baseline safety metric for comparison with other information structures. "Information Structure (b)" provides both front and rear distances. Then "Information Structure (c)" expands with wireless communication networks.

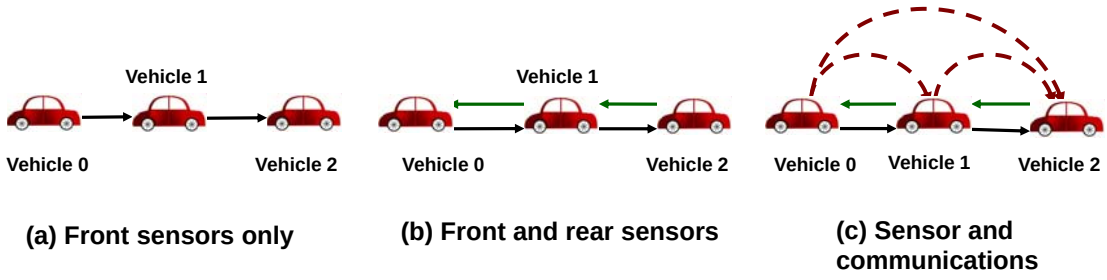

Figure 2: Three main information structures: (a) Only front distance information is available for vehicle control. (b) Both front and rear distances are available. (c) Additional information is transmitted between vehicles.

Although we employ a three-car platoon for simplicity, it forms a generic base for studying platoon safety issues for more general platoons. This is graphically explained in Fig. 3. Here the vehicles in between the leading vehicle and the vehicle of interest are grouped as one pack of perfectly running sub-platoon, and we treat this sub-platoon as one vehicle and this leads to the generic structure of Fig. 2. This

also implies that the communication distance between the two vehicles may be high.

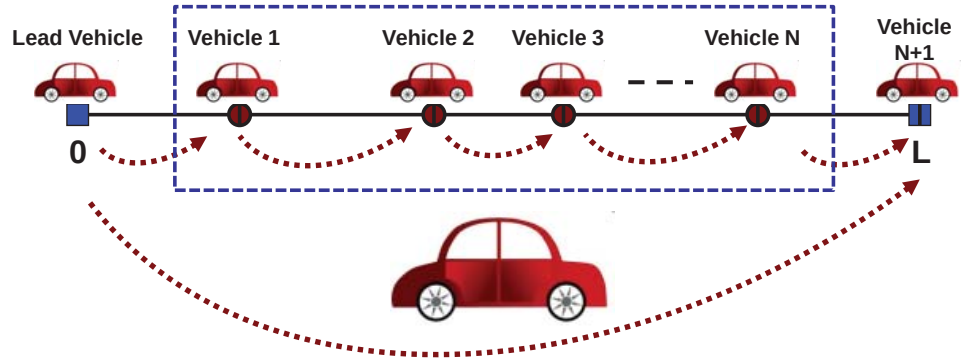

Figure 3: Grouping vehicles.

The platoon in Fig. 2 has the following local dynamics,

$$\begin{cases} \dot{v}_0 &= \frac{1}{m_0}(F_0 - (a_0 + b_0 v_0^2)) \\ \dot{v}_1 &= \frac{1}{m_1}(F_1 - (a_1 + b_1 v_1^2)) \\ \dot{v}_2 &= \frac{1}{m_2}(F_2 - (a_2 + b_2 v_2^2)) \\ \dot{d}_1 &= v_0 - v_1 \\ \dot{d}_2 &= v_1 - v_2, \end{cases} \tag{2.2}$$

where F_0 is the leading vehicle's driving action. F_1 and F_2 are local control variables. Since the vehicle lengths are fixed and can be subtracted from distance calculations, in this formulation a vehicle is considered as a point mass without length.

2.2 Control and Evaluation Scenarios

2.2.1 Feedback Control

For safety consideration, the inter-vehicle distances d_1 and d_2 have a minimum distance $d_{min} > 0$. To ensure that vehicles 1 and 2 have sufficient distances to stop when the leading vehicle 0 brakes, a cruising distance d_{ref} is imposed. Apparently, the larger d_{ref}, the safer the platoon, under any fixed control strategies. However, a larger d_{ref} implies more occupation of the highway space, and less efficiency in highway usage. As a result, it is desirable to use as small d_{ref} as possible without compromising the safety constraint.

There are numerous vehicle control laws which have been proposed or commercially implemented [20, 21]. Since the focus of this thesis is on impact of information structures and contents rather than control laws, we impose certain simple and fixed control laws. For safety consideration, we concentrate on the case when the distance is below the nominal value $d < d_{ref}$. The control law involves a normal braking region (small slope) and an enhanced braking region of a sharp nonlinear function towards the maximum braking force, as shown in Fig. 4. We denote this function as $F = g_1(d)$.

Similarly, if vehicle i's speed information is transmitted to another vehicle j (behind i), the receiving vehicle can use this information to control its braking force. This happens when $v_j > v_i$. The larger the difference, the stronger the braking force. This control strategy may be represented by a function $F = g_2(v_j - v_i)$, shown in Fig.

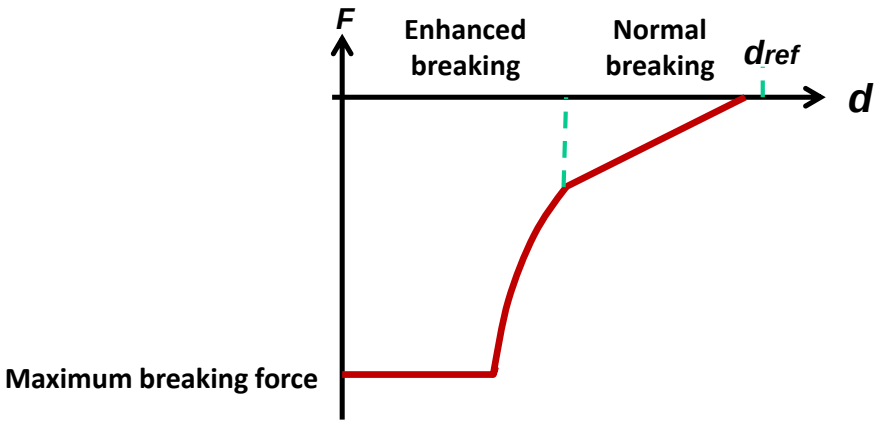

Figure 4: Braking functions based on distance information.

5.

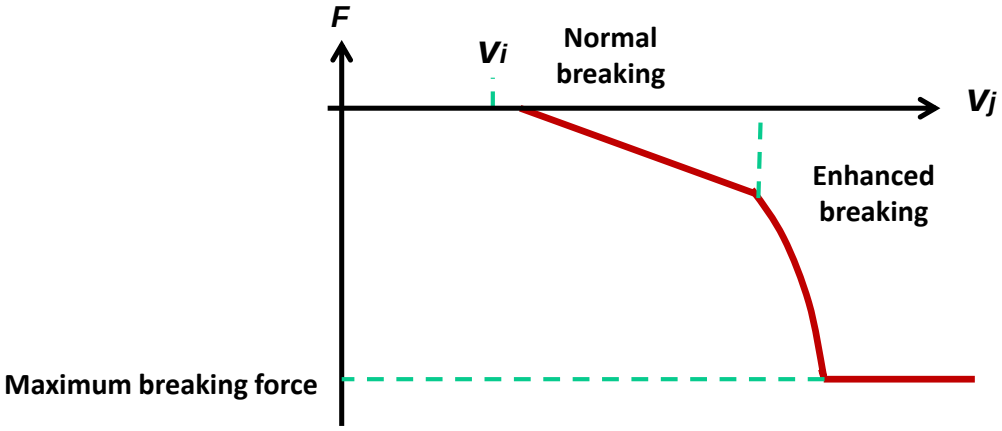

Figure 5: Braking functions based on speed information.

2.2.2 Evaluation Scenarios

To investigate impact of information structures and contents on platoon safety, we need a reasonable platform to comparative studies. Since vehicle safety involves so

many factors, we must define a highly simplified platform in which only key elements are represented. For this reason, we define the following basic scenarios.

We use some typical vehicle data from [22]. Under the MKS (metre, kilogram, second) system of units, the vehicle mass m has the range $1400 - 1800$ Kg, the aerodynamic drag coefficient b has the range $0.35 - 0.6$ Kg/m. During braking, a (as the rolling resistance) is changed to tire/road slipping, which is translated into the braking force F (negative value in Newton). As a result, a is omitted.

Three identical cars form a platoon as in Fig. 2. The vehicle masses are $m_0 = m_1 = m_2 = m = 1500$ Kg. The aerodynamic drag coefficients $b_0 = b_1 = b_2 = 0.43$. The nominal inter-vehicle distance $d_{ref} = 40$ m. The cruising platoon speed is 25 m/s (about 56 mph). The road condition is dry and the maximum braking force is 10000 N. This implies that when the maximum braking is applied (100% slip), the vehicle will come to a stop in 3.75 second. The braking resistance can be controlled by applying controllable forces on the brake pads.

The feedback control function $F = g_1(d)$ is depicted in Fig. 6. The actual function is

$$\max\{k_1(d - dref) + k_2(d - dref)^3, -F_{max}\} \tag{2.3}$$

where $d_{ref} = 40$ (m), $k_1 = 50$, $k_2 = 4$, $F_{max} = 10000$ (N). The function applies smaller braking force when the distance is only slightly below the reference value, but increases the braking force more dramatically in a nonlinear function when the distance reduces further until it reaches the maximum braking force. We comment that if one views the braking function purely from safety aspects, it is desirable to

impose the maximum braking as soon as the distance drops. This, however, will compromise drivability and smoothness of platoon operation. In fact, the braking function of Fig. 6 is already on the aggressive side.

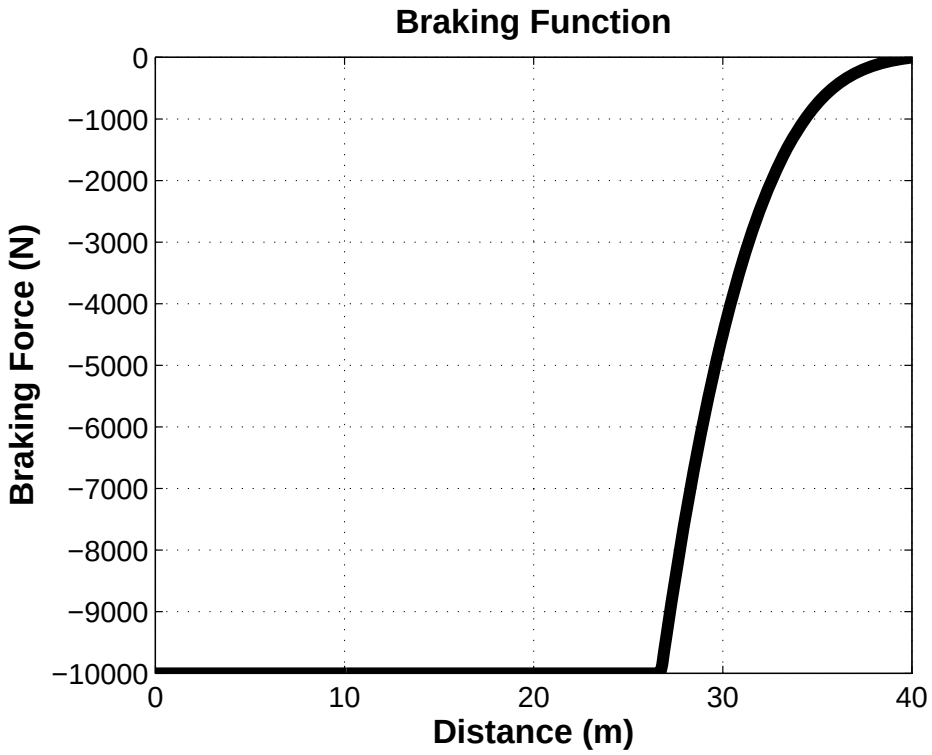

Figure 6: Braking function for Example 9.

To see this, consider the slow braking condition: Suppose that the leading vehicle applies a braking force 1000 N, which brings it to a stop from 25 m/s in 37.5 second. The distance trajectories of d_1 and d_2 are shown in Fig. 7. In this case, the minimum distances are 30.9 m for d_1 and 24.2 m for d_2. This is acceptable for safety. On the other hand, the transient period shows oscillation, indicating that the braking action has been aggressive already under normal driving conditions.

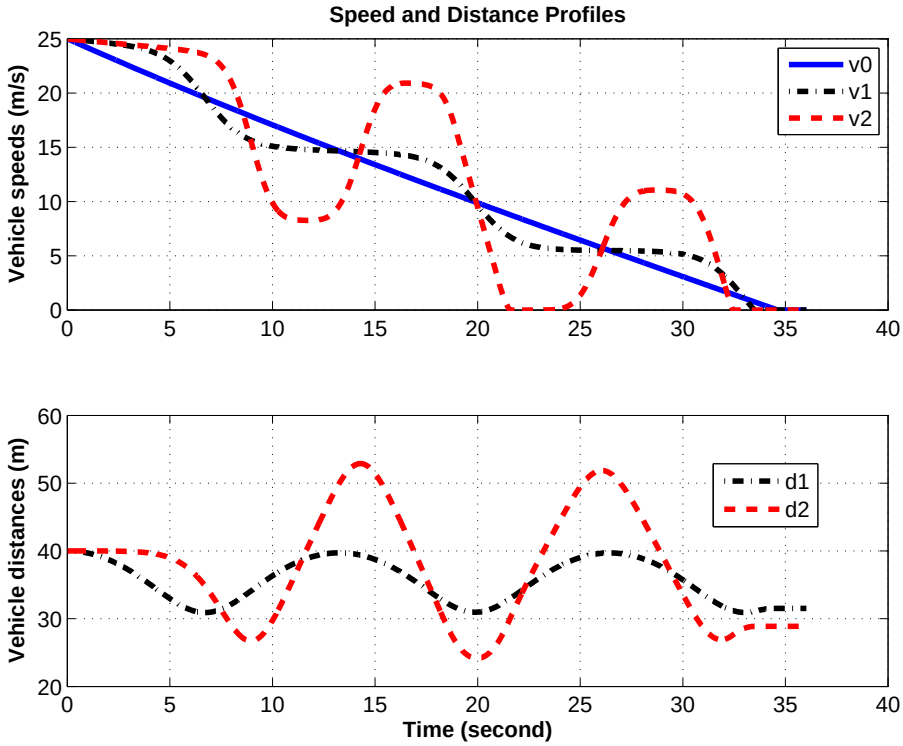

Figure 7: Distance trajectories under slow braking.

For evaluations, we will use the fast braking scenario defined as follows.

Fast Braking: The leading vehicle uses a braking force 5000 N. If the cruising speed of the platoon is 25 m/s, then this braking force brings the leading vehicle to a stop from 25 m/s in 7.5 second.

In some derivations, we also use the extreme case in which the maximum braking force 10000 (N) is applied. This is for the worst-case analysis. But the Fast Braking case is representative for understanding safety issues. In this thesis, the minimum vehicle distance $d_{min} = 15$ (m) is used to distinguish "acceptable" and "unsafe" conditions. When a distance is reduced to 0, a collision occurs.

2.3 Safety Analysis

We conduct safety analysis under the scenario specified in Section 2.2.2. Some simplifications will be made so that explicit expressions can be derived to clarify the main underlying safety issues.

We observe that under this braking force, the influence of the tire/road resistance and aerodynamic drag force bv^2 is relatively small. a is proportional to the tire deformation and inversely proportinal to the radius of the loaded tire. The rolling resistance of a normal car 1500 kg on convrete with rolling coefficient 0.01 can be estimated:

$$F_r = 0.01(1500kg)(g) = 0.03(1500kg)(9.81m/s^2) = 147(N), \tag{2.4}$$

When $b = 0.43$ and $v = 25$ m/s, the aerodynamic drag force is 268.75 (N). This is only 8.3% of the braking force. In the subsequent development, we omit the aerodynamic drag force in our derivations, but include it in all simulation studies.

Assuming that the platoon cruising speed is $v_0(0) = v_1(0) = v_2(0) = 25$ (m/s) and the leading vehicle brakes at $t = 0$ with $F_0 = -\alpha$, where α is a constant (for the Fast Braking, $\alpha = 5000$ (N); and the worst-case $\alpha = F_{max} = 10000$ (N)). The braking

function (2.3) is used. It follows that the dynamics of the three-car platoon are

$$\begin{cases} \dot{v}_0 &= -\frac{\alpha}{m} \\ \dot{v}_1 &= -\frac{g_1(d_1)}{m} \\ \dot{v}_2 &= -\frac{g_1(d_2)}{m} \\ \dot{d}_1 &= v_0 - v_1 \\ \dot{d}_2 &= v_1 - v_2, \end{cases} \tag{2.5}$$

with the initial conditions $v_0(0) = v_1(0) = v_2(0) = 25$ (m/s) and $d_1(0) = d_2(0) = d_{ref} = 40$ (m).

2.3.1 Safety Regions

In a platoon, usually vehicle 2 acts later than vehicle 1 due to information cascading structures (vehicle 1 sees the slowdown of the leading vehicle before vehicle 2). Suppose that after vehicle 1 applied the maximum braking force at an earlier time, vehicle 2 starts to apply the maximum braking force at t_0.

Theorem 1 *Assume that* $v_1(t_0) < v_2(t_0)$. *Denote* $\eta = v_2^2(t_0) - v_1^2(t_0)$, *and* $\delta = d_2(t_0)$. *The final distance is*

$$d_2^{final} = \delta - \frac{\eta m}{2F_{max}}.$$

Proof: For $t \geq t_0$, the two vehicles have the dynamics $\dot{v}_1 = -\frac{F_{max}}{m}$, $\dot{v}_2 = -\frac{F_{max}}{m}$, which implies $v_1(t) = v_1(t_0) - \frac{F_{max}}{m}(t - t_0)$, $v_2(t) = v_2(t_0) - \frac{F_{max}}{m}(t - t_0)$.

Vehicle 1 stops after travelling the total stoping time $v_1(0)m/F_{max}$ and the total length $\Delta_1 = v_1^2(t_0)m/(2F_{max})$. Similarly, the total length travelled by vehicle 2 to a complete stop is $\Delta_2 = v_2^2(t_0)m/(2F_{max})$. Thus, the final distance is

$$d_2^{final} = \delta - \frac{(v_2^2(t_0) - v_2^1(t_0))m}{2F_{max}} = \delta - \frac{\eta m}{2F_{max}}.$$

□

For any given final distance $d_2^{final} = C$, the function

$$\eta = \frac{2F_{max}}{m}(\delta - C)$$

defines the iso-final-distance line on the $\delta - \eta$ space, shown in Fig. 8, in which the acceptable region and collision avoidance region are also marked.

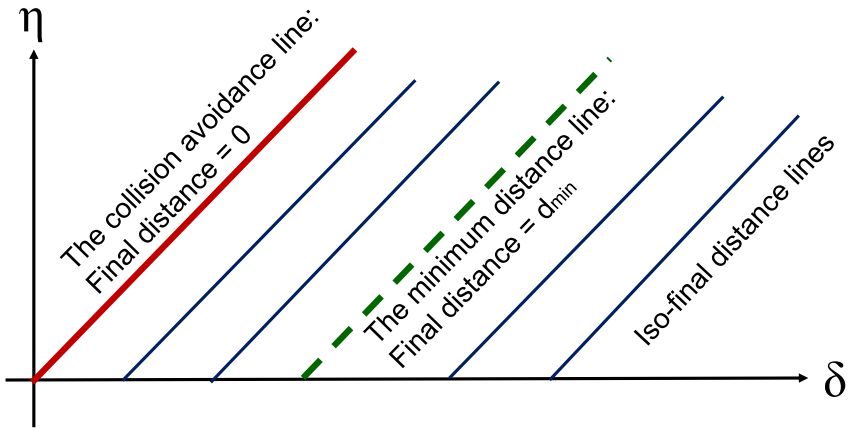

Figure 8: $\delta - \eta_v$ lines under a given final distance. Acceptable safety regions and collision avoidance regions can be derived from such curves.

2.3.2 Platoon Distance Progression

A platoon consists of many vehicles. Under typical information structures, there is a phenomenon of inter-vehicle distance progression that must be considered in platoon management.

Assumption 1 (1) At $t = 0$, the platoon of n following vehicles is at the cruising condition with equal distance d_{ref} and speed $v(0)$. (2) The information on the braking action $F_0 = -F_{max}$ of the leading vehicle at $t = 0$ is passed to the following vehicles in a progressive manner: For $t > 0$, $F_1(t) \leq F_2(t) \leq \cdots \leq F_n(t)$, and the equalities are valid only when both braking forces reach -10000 (N). (3) Suppose that vehicle j starts to apply the maximum braking force at t_j. We assume that $t_1 < t_2 < \cdots < t_n$.

Theorem 2 *Under Assumption 1, the total travel length L_j of vehicle j before a complete stop satisfies*

$$L_0 = \frac{v(0)m}{2F_{max}} < L_1 < L_2 < \cdots L_n.$$

The minimum final distance is

$$\min_{j=1,\ldots n} d_j^{final} = d_{ref} - \max_{j=1,\ldots,n} (L_j - L_{j-1}).$$

Proof: The expression $L_0 = \frac{v(0)m}{2F_{max}}$ is proved in Theorem 1.

Let the braking force for vehicle j be $-f_j(t)$ with $f_j > 0$. The speed profile is

$$v_j(t) = v(0) - \int_0^t \frac{f_j(\tau)}{m} d\tau.$$

The total travel time T_j satisfies

$$\int_0^{T_j} \frac{f_j(\tau)}{m} d\tau = v(0).$$

The total length travelled by vehicle j until a complete stop is

$$L_j = \int_0^{T_j} v_j(t)dt = v(0)T_j - \int_0^{T_j} \int_0^t f_j(\tau)d\tau dt.$$

Under Assumption 1, we have the inequalities

$$v_1(t) < v_2(t) < \cdots < v_n(t), t > 0 \tag{2.6}$$

which implies that

$$T_1 < T_2 < \cdots T_n. \tag{2.7}$$

These imply

$$L_1 < L_2 < \cdots L_n.$$

Now, the final distance d_j^{final} is

$$d_j^{final} = d_{ref} - (L_j - L_{j-1})$$

which implies that

$$\min_{j=1,\ldots,n} d_j^{final} = d_{ref} - \max_{j=1,\ldots,n} (L_j - L_{j-1}).$$

This completes the proof. □

3 COMMUNIATION UNCERTAINTIES

3.1 Analog Communication Uncertainties

Traditionally, analog signal is modeled as additive and multiplicative noise when it is transmitted. it is broadcasted and propagates through multiple pathways, depending on terrain conditions, buildings, weather conditions, echoes, interferences, and correlations with other signals showing at Figure 9.

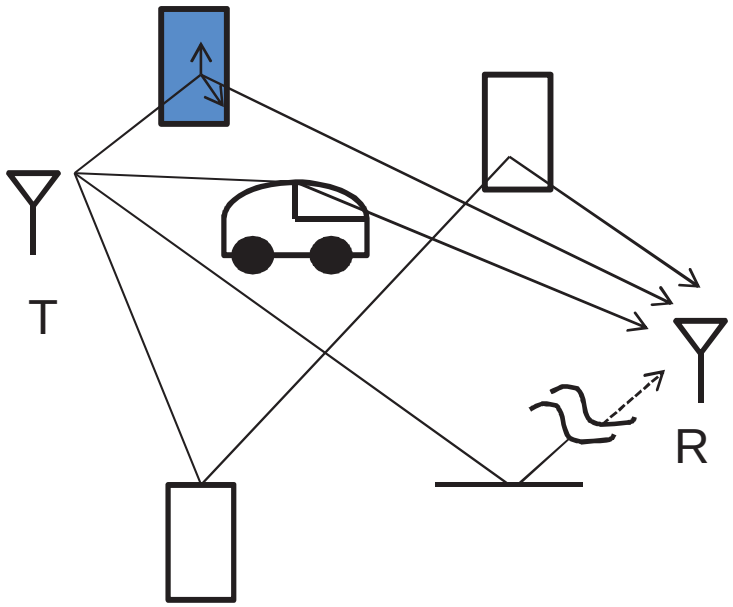

Figure 9: Multiple Wireless Signals

They are then collected at the receiver, combined, and decoded. Such a scenario is better represented by variations on transmission gains whose values can vary over a large range and may change signs as well. Feedback robustness against such gain uncertainties require consideration of large uncertainty sets on gains. Unfortunately,

due to fundamental limitations of feedback systems, large gain uncertainties, especially sign changes, cannot be overcome by the feedback mechanism alone. This thesis introduces a new method to enhance feedback robustness in this unique aspect for vehicle platoons.

3.2 Digital Wireless Communication Latency

Typical digital communications consist of several essential function blocks, such as sampling, data compression, quantization, source coding, channel coding, modulation at the sending side, and demodulation, decoding, and signal reconstruction at the receiving side, that are summarized in Figure 10. Although a remotely controlled system involves always signal forward communication links and control signal feedback links, even multiple paths and routs in each direction, to avoid unnecessary notational complexity in system analysis, it is a common strategy that we group system blocks in a path into a lumped subsystem. As a result, we will lump the links as one in the feedback loop and view the communication link as a sensing link from the system output y to its estimate $\grave{y}$. Consequently, the control signal $u = \tilde{u}$.

To study more realistically how communication systems and control interact, we use a generic communication scheme shown in Fig. 11. In this scheme, a data packet is generated and enters the queue for transmission. The queuing time depends on network traffic and data priorities. The packet contains both data bits and error checking bits. We assume that the error checking mechanism is sufficient to detect any faulty packet. If the packet transmission is successful, the receiver returns an

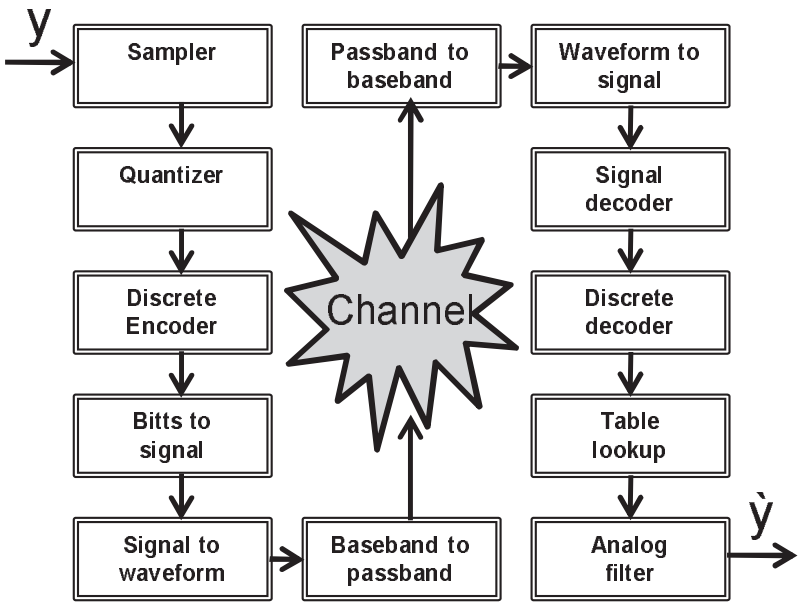

Figure 10: Typical Digital Communication Channel

acknowledgment message to the sender, which completes the transmission. If the packet is received with error, it will be discarded and a request is sent back to the sender to re-transmit the same packet. The permitted total time for transmission of a packet is pre-determined by the control updating times. If a packet was not successfully transmitted when the control updating time is up, the packet will be considered as lost.

Inter-vehicle communications (IVC) can be realized by using infrared, radio, or microwaves waves. For instance, in IEEE 802.11p, a bandwidth 75 MHz is allotted in the 5.9 GHz band for dedicated short range communication (DSRC) [23, 24]. Alternatively, ultra-wideband (UWB) technologies have been used for IVC. IEEE 802.11x, where $x \in \{a, b, g, p \ldots\}$ have been studied for inter-vehicle use. At present,

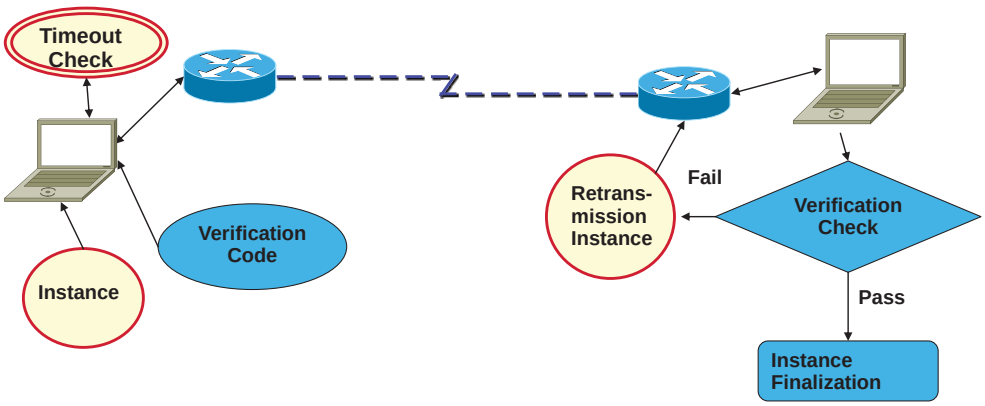

Figure 11: Data transmission schemes.

many applications use DSRC with IEEE 802.11p (a modified version of IEEE 802.11 (WIFI) standard) at the PHY and MAC layers. IEEE 802.11g and IEEE 802.11p are used for experimental studies in this thesis.

In the middle of protocol stack, DSRC employs IEEE 1609.4 for channel switching, 1609.3 for network service, and 1609.2 for security service. In the network service, users have a choice between the wireless access for vehicle environments short message protocol (WSMP) or the internet protocol version 6 (IPv6) and user datagram protocol (UDP)/transmission control protocol (TCP). Single-hop messages typically use the bandwidth-efficient WSMP, while multi-hop packets use the IPv6+UPD/TCP for its routing capability.

Inter-vehicle communications use wireless networks that are subject to severe uncertainties. For example, the signal-to-interference-plus-noise ratio (SINR) [25] attenuates with distance (it decreases inverse proportionally to the cubic of the distance between the two vehicles). It is also affected by obstructions such as buildings,

bridges, other vehicles, etc. Other factors include queue delays, network data traffic conditions, routes, signal fading, signal interference from other vehicles, Doppler shifts, and traffic and weather conditions. These uncertainties depend significantly on channel coding schemes and communication networks. These factors collectively determine packet delivery delays, packet loss rates, etc. This thesis will focus on delay effects. To be concrete in treating communication systems, we will employ IEEE 802.11 standards as our benchmark systems and the related latency data [23].

Bandwidth-delay product is often used to characterize the ability of a network pathway in carrying data flows [26, 27]. When the TCP protocol is used in data communications, packet-carrying capacity of a path between two vehicles will be limited by this product's upper bound. For more detailed discussions on capacity/delay tradeoffs, the reader is referred to [23] and the references therein. Note that latency is further caused by delays in each hub's queues, routes (multi-hub), packet delivery round-trip time, channel reliability, re-transmission, scheduling policies in interference avoidance strategies. Although typical transmission delays can be as low as several millisecond, vehicular traffic scenarios introduce combined latency of several hundreds of milliseconds even several seconds. In this thesis, we will show that delays of such scales will have significant impact on vehicle safety.

3.3 Digital Wireless Communications with Erasure Channel

The block-erasure channel represents a channel model where transmitted packets are either received or lost. The loss of a packet may be caused by erasure of one or

multiple bits within the packet during transmission. Typically, block-erasure channels are simple models for fading channels. Due to power limitation, transmission noises, signal interferences, some codewords in a packet may be completely lost [28, 29, 30]. Probability of packet erasures can be reduced by introducing error detection and correction bits, which increase data lengths and reduce information flow rates.

We consider block-erasure channels with certain channel codings that include error detection. Generic discussions are sufficient at this point, and the actual channel coding schemes will be specified in case studies. In this protocol, channel error detecting codes such as parity-check matrices are encapsulated and are used by the receiver to either detect transmission errors or in some cases correct the missing or erroneous bits. The detection/correction mechanism is shown in Fig. 12.

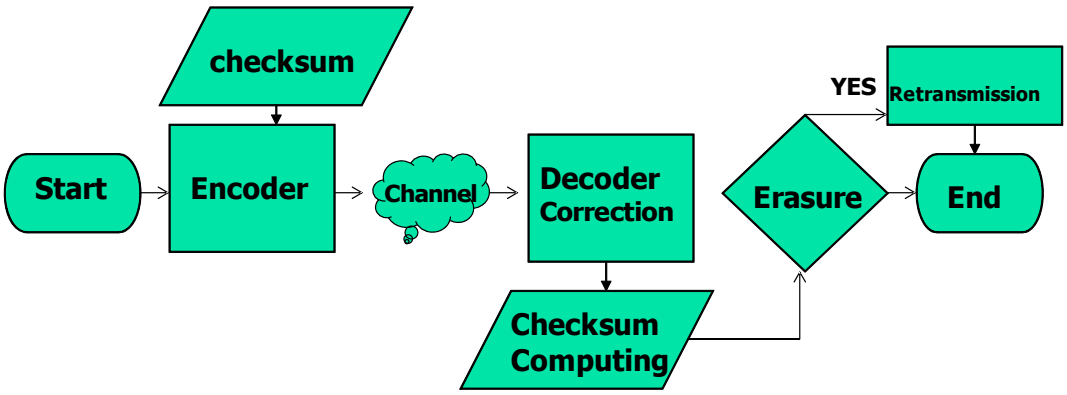

Figure 12: An erasure channel with check-sum error detection and re-transmission

During one round-trip of this scheme starting at time t_k, the source generates a data block, which is channel coded with codeword c_{t_k} and transmitted. Due to channel uncertainties, the decoder receives the codeword $\widehat{c}_{t_k}$ with possible erasure of

one or more bits. After decoding and error correcting, the receiver either acknowledges receipt of the data, or indicates a packet erasure. Suppose that the round-trip time for this scheme is τ. If $t_k\tau < t_{k+1}$, a re-transmission is implemented and the above transmission process renews.

At t_{k+1}, the data is either received correctly or declared to be lost. In the later case, the channel is equivalently disconnected during $[t_k, t_{k+1})$ since no data are received. Since this event is random, the channel is modelled as a random link, with probability p_k to be linked and $1 - p_k$ to be disconnected. Applying this scenario to all channels, we have a randomly switching network topology such that the probability for each topology is generated from individual link connection probabilities.

In the next subsections, we derive probabilistic models for erasure channels. Our pursuit involves two objectives: (1) Understand what is the minimum signal-to-noise ratio (SNR) for a required safety level. To this end, we must derive erasure probability's lower bounds. Information-theoretical analysis will be employed. (2) Employ a practical system and its corresponding erasure probability characterization to characterize concretely the required information for platoon control. We use the low density parity-check (LDPC) coding as a benchmark coding scheme to carry out this study. The LDPC codes have appealing properties in their theoretical foundation and implementation efficiency. Their main advantages in computational efficiency and code length utility have resulted in successful commercial products.

3.3.1 Probabilistic Error Models of Erasure Channels

We consider an erasure channel whose packet contains B bits for information transfer.[1] The information bits are divided and used either for data or for error checks. In this section, it is not necessary to specify such divisions. For simplicity, all coding schemes in this thesis are over the binary field $\mathbb{F}_2 = \{0, 1\}$, although the results of this thesis can be easily extended to other fields. For the same reason, we consider standard erasure channels instead of block-erasure channels, although it is straightforward, but a little tedious in expressions, to derive probabilistic error models for block-erasure channels.

To transmit a code S of size $K = \log_2 |S|$ with the codeword of length L, we have the coding rate $r = K/L$ per channel usage. Let the codeword be denoted by $c = [c_1, \ldots c_L]$ where $c_j \in \{0, 1\}$ is the jth bit of the codeword c. The erasure pattern is indicated by the vector $\eta = [\eta_1, \ldots, \eta_L]$ such that $\eta_j = 1$ means that the jth bit is erased, and $\eta_j = 0$ indicates the jth bit is received correctly.

We consider a two-time-scale scenario for link communication and control. Control actions are updated every T seconds, and the communication round-trip time is τ. For simplicity, assume $T = k\tau$ for some integer $k \geq 1$. If a transmission results in an ambiguity at the receiver's side such that the transmitted code cannot be uniquely determined, it will label it as "failure" for this transmission and a re-transmission request is returned to the sender. Consequently, the maximum number of transmissions

[1] As a common practice for information and error analysis, packet heading and other auxiliary segments are not considered in our analysis.

of the same code during T is k. It should be pointed out that when ambiguity arises, we do not use any method to break the tie which will cause a possible erroneous decoding, but rather demand a re-transmission. As a result, we either receive the correct code or do not have information at all.

Let the minimum Hamming distance of S be $d \geq 1$.[2] It follows that if a transmission causes less than $d-1$ erasures, the transmitted code can be uniquely determined. For a unified treatment and in consideration of the worst-case scenario, we consider erasures with d erasures or more as a failed transmission in our probabilistic models for error analysis.[3] For related but different error models and channel coding methods in erasure channels, we refer the reader to [31, 28, 29, 30] for further details.

Suppose that bit transmissions are independent and identically distributed (i.i.d.) and the bit erasure probability is ε. In one transmission, the error probability can be

[2]The Hamming distance between two codes is the number of positions at which the corresponding symbols are different.

[3]Depending on the actual code, some specific erasure patterns with d or more bit erasures may not result in ambiguity. However, such cases defy unified treatment. For practical implementations, these details can be considered to improve transmission efficiency.

calculated from the standard Bernoulli trials and binomial distributions [32],

$$
\begin{aligned}
P_e^1 &= \mathbf{P}\{\eta : \eta \text{ contains 1's at } d \text{ locations or more}\} \\
&= \sum_{j=d}^{L} \mathbf{P}\{\eta : \eta \text{ contains 1's at exactly } j \text{ locations}\} \\
&= \sum_{j=d}^{L} \begin{pmatrix} L \\ \\ j \end{pmatrix} \varepsilon^j (1-\varepsilon)^{L-j} \\
&= \sum_{j=d}^{L} \frac{L!}{j!(L-j)!} \varepsilon^j (1-\varepsilon)^{L-j}.
\end{aligned}
$$

Under independent transmissions of channel usage, we have the link erasure probability after k usages of the channel as

$$
P_e^k = (P_e^1)^k = \left(\sum_{j=d}^{L} \frac{L!}{j!(L-j)!} \varepsilon^j (1-\varepsilon)^{L-j} \right)^k . \tag{3.4}
$$

It is noted that in the worst-case sense, the probability model in (3.4) is exact. For practical codes, (3.4) provides an upper bound on the erasure errors during one time interval of control action update.

Example 3 Suppose that the code length is $L = 20$ and the minimum Hamming distance is d. Fig. 13 depicts packet erasure probabilities as functions of bit erasure probabilities ε under various minimum Hamming distances d. Furthermore, when communication round-trip time τ is smaller than control updating time T, multiple retransmission becomes possible and can be used to reduce packet erasure probabilities.

This is shown in Fig. 14 under a code of length $L = 20$ and minimum Hamming distance $d = 4$.

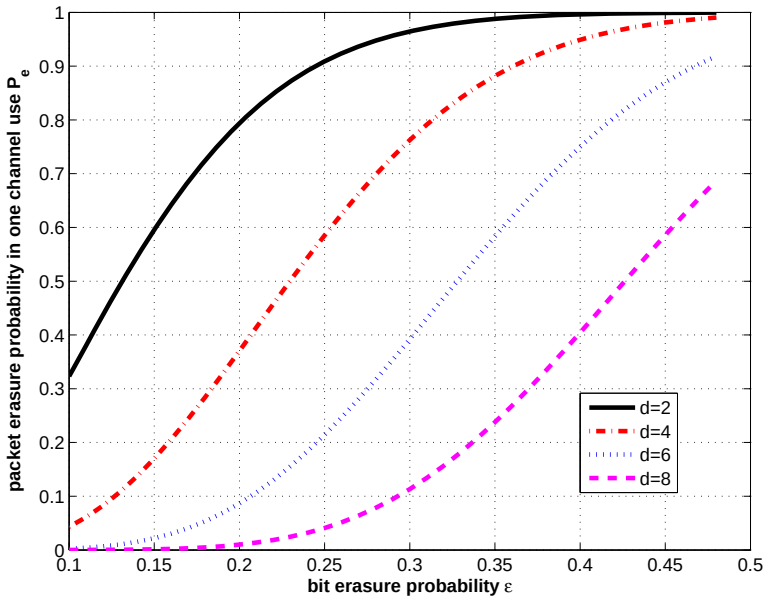

Figure 13: Packet erasure probabilities under one transmission: $L = 20$

3.3.2 Communication Resources and Erasure Probabilities

The bit erasure probability ε depends on communication resources such as power and bandwidths, and also transmission media. In a mobile system such as highway vehicles, vehicle-to-vehicle (V2V) communication links are affected by inter-vehicle distances, weather conditions, obstacles, interference, signal fading, etc. Consequently, a detailed and accurate description of bit erasure probability for a practical system is ad hoc and extremely difficult. On the other hand, the principles and generic function forms of bit erasure probability can be established and used as a guideline in design considerations. This subsection discusses such principles and function forms.

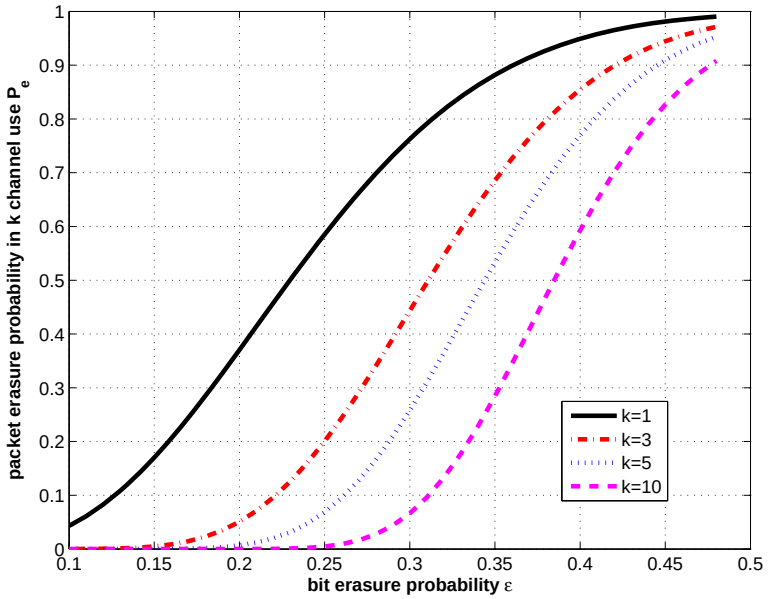

Figure 14: Packet erasure probabilities under k transmissions: $L = 20$, $d = 4$

We use the Binary Additive White-Gaussian-Noise Channel (BAWGNC) for this exploration. The source symbol x takes values in $\{-1, 1\}$. With the BPSK (Binary Phase-Shift Keying), signal energy E_N, additive channel noise of independent zero-mean Gaussian distribution with variance σ^2, and hard-decision decoding, it is well known [33, Chapter 4] that the error probability (including both events "1 is sent but 0 is received" and "0 is sent but 1 is received") is

$$\varepsilon = Q(\sqrt{E_n/\sigma^2}), \tag{3.5}$$

where the Q function is

$$Q(x) = \int_x^\infty \frac{1}{\sqrt{2\pi}} e^{-\frac{y^2}{2}} dy.$$

In our framework, this error is interpreted as the erasure probability with the understanding that erasure detection is achieved by channel coding and error detection

decoding.

Here ε is a function of the signal-to-noise ratio (SNR) E_N/σ^2. Also, following the standard practice of representing noise variance by its power $N_0 = 2\sigma^2$ (single-sided power-spectral density), we have

$$\varepsilon = Q(\sqrt{2E_n/N_0}). \tag{3.6}$$

Combining (3.4) and (3.6), we may link the packet erasure probability directly to the SNR

$$P_e^k(E_n/N_0) = \left(\sum_{j=d}^{L} \frac{L!}{j!(L-j)!}(Q(\sqrt{2E_n/N_0}))^j(1-Q(\sqrt{2E_n/N_0}))^{L-j}\right)^k. \tag{3.7}$$

Usually, the SNR is expressed in dB, namely $10\log_{10}(E_N/N_0)$. Fig. 15 illustrates how the SNR of the channel affects the packet erasure probability.

4 IMPACT OF COMMUNICATION DELAY

In this subsection, a relationship between the communication delay time and its detrimental effect on inter-vehicle distance is derived. To single out the delay effect, we impose the following assumption.

(1) Direct Transmission of Braking Action

Suppose that the leading vehicle transmits its braking action directly to the vehicle behind it. This is the fastest way to inform the following vehicle to take action. If no time delay is involved, then the following vehicle will brake immediately and the inter-vehicle distance will be kept contact until both vehicles come to the complete stop. However, communication delays will postpone the following vehicle's action.

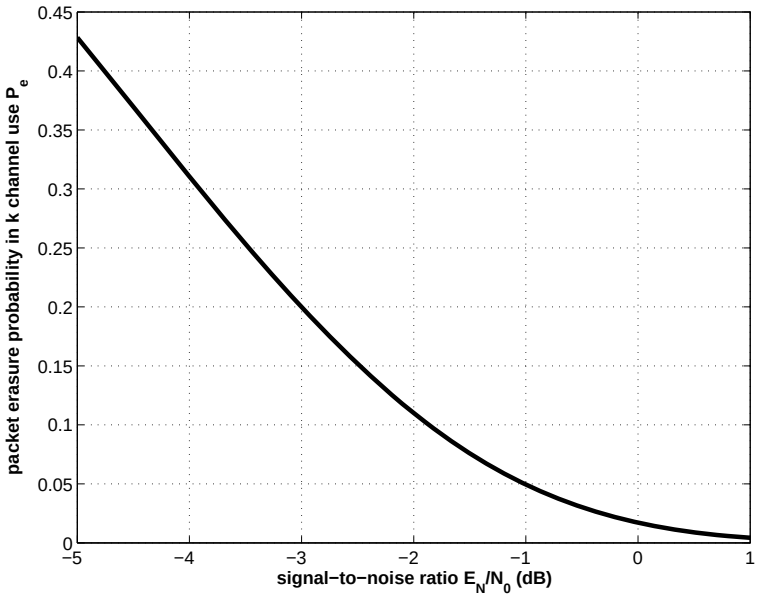

Figure 15: Packet erasure probabilities as a function of the signal-to-noise ratio

The main question is: How much delay can be tolerated?

Assumption 2 (1) The leading vehicle and following vehicle travel at the cruising condition with distance d_{ref} and speed $v(0)$. (2) The information on the braking action $F_0 = -F_{max}$ of the leading vehicle at $t = 0$ is immediately transmitted to vehicle 1 with a communication delay τ. (3) No other information is available to vehicle 1.

Theorem 4 *Under Assumption 2, the final distance* d_1^{final} *is*

$$d_1^{final} = d_{ref} - v(0)\tau + \frac{F_{max}}{2m}\tau^2.$$

Proof: Since the braking force for the leading vehicle is $-F_{max}$, its speed profile is

$$v_0(t) = v(0) - \frac{F_{max}}{m}t.$$

At time τ, its speed is

$$v_0(\tau) = v(0) - \frac{F_{max}}{m}\tau.$$

Vehicle 1 receives the braking information at τ and immediately applies the maximum braking force $-F_{max}$ with the initial speed $v(0)$. As a result, $\eta = v^2(0) - v_0^2(\tau)$.

By Theorem 1, the final distance is

$$d_1^{final} = d_{ref} - \frac{\eta m}{2F_{max}} = d_{ref} - v(0)\tau + \frac{F_{max}}{2m}\tau^2.$$

Corollary 5 *For a given required minimum distance* d_{min}*, the maximum tolerable communication delay is*

$$\tau_{max} = \frac{v(0) - \sqrt{v^2(0) - 2\frac{F_{max}}{m}(d_{ref} - d_{min})}}{2}.$$

Proof: By Theorem 4, to satisfy $d_1^{final} \geq d_{min}$, the maximum tolerable τ is solved from $d_{min} = d_{ref} - v(0)\tau + \frac{F_{max}}{2m}\tau^2$ or

$$\frac{F_{max}}{2m}\tau^2 - v(0)\tau + (d_{ref} - d_{min}) = 0$$

whose smaller solution is

$$\tau_{max} = \frac{v(0) - \sqrt{v^2(0) - 2\frac{F_{max}}{m}(d_{ref} - d_{min})}}{2}.$$

□

In particular, for collision avoidance, $d_{min} = 0$ and we have

$$\tau_{max} = \frac{v(0) - \sqrt{v^2(0) - 2\frac{F_{max}}{m}d_{ref}}}{2}.$$

For the evaluation scenario in Section 2.2.2, $v(0) = 25$, $F_{max} = 10000$, $m = 1500$, $d_{ref} = 40$, and $d_{min} = 15$. The corresponding maximum tolerable delay is $\tau_{max} = 3.9609$ second. For collision avoidance, $d_{min} = 0$ and $\tau_{max} = 7.7129$ second.

However, if the vehicle weight is increased to $m = 1800$ (Kg) and the platoon cruising distance is reduced to $d_{ref} = 30$, the tolerable delay is reduced to $\tau_{max} = 1.7956$ second.

Typical vehicle braking control must balance safety and driveability. Consequently, inter-vehicle distances may reduce more significantly than the scenario of this subsection. As a result, the maximum tolerable delay may be significantly less. These will be evaluated in the subsequent case studies.

(2) Broadcasting Schemes and Consequence

The leading vehicle's braking action can be broadcasted to the platoon. The average communication latency depends on the distance between the sending (leading vehicle) node and the receiving node. Using the basic square relationship, if the first following vehicle experiences a delay $\tau_1 = \tau$, then the second vehicle will have a delay around $\tau_2 = 4\tau$, the third vehicle with $\tau_3 = 9\tau$, and so on.

For example, if $d_{ref} = 40$ (m) and $\tau_1 = 100$ (ms), then $\tau_2 = 400$ (ms) (at 80 (m)), ..., $\tau_7 = 4.9$ (s) (at 280 (m)), which implies that d_7 will fall below 15 m, violating the minimum distance requirement.

This analysis indicates that communication schemes need to be carefully designed when a platoon has many vehicles.

4.1 A Single-Hop Experimental Study

We assume the three-vehicle scenario in Fig. 2. Communication channels between v_0 and v_2 use the WSMP protocol. This protocol can carry messages on both the Control Channel (CCH) and the Service Channel (SCH). The WSMP allows direct control of the lower-layer parameters such as transmission power, data rates, channel numbers, and receiver MAC addresses. The WSMP over the CCH can skip the steps of forming a WAVE Basic Service Set (BSS) that delivers IP and WAVE short message (WSM) data on the SCH. Those methods can potentially reduce communication latency.

The round trip time (RTT) under this protocol includes measurement time for the variables (vehicle distance, speed, etc.), source data creation time (creating packets, adding verification codes, scheduling, etc), communicating the packet to v_2, receiver

verification, travel time for sending back acknowledgment from v_2. Fig. 16 sketches some of the time delays from these steps.

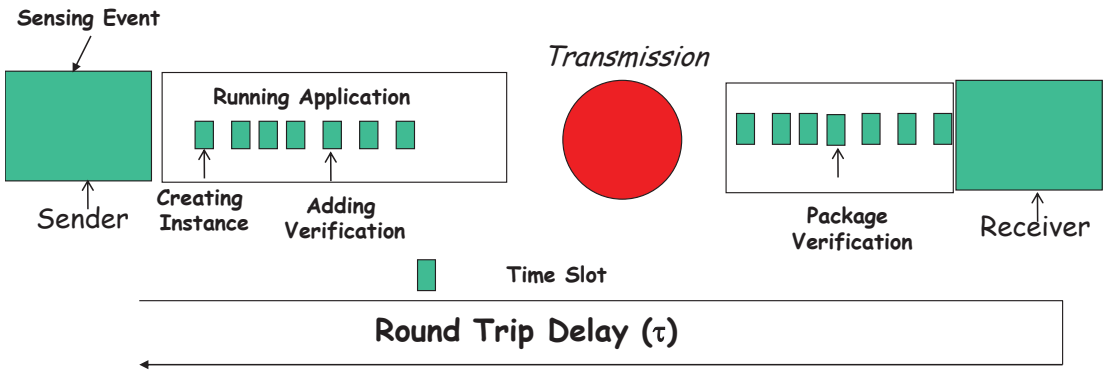

Figure 16: A Round Trip Delay.

In an ideal case that v_0 can capture the CCH during each CCH time slot, v_0 can send its beacon and update its status to v_2 at the rate of 10 Hz. If a package is successfully transmitted and verified during the first round, the Package Delivery Rate(PDR) is 1, the RTT $\tau^0 \leq 100$ ms since IEEE 1609.4 specifies the reoccurrence of the CCH at the rate of every 100 ms.

The physical limitations on wireless channels (bandwidth and power constraints, multi-path fading, noise and interference) present a fundamental technical challenge to reliable high-speed communication. One or several retransmissions are often necessary to meet a PDR requirement. In this case, delay is $\tau = n\tau^0$ where n is the number of average rounds for a successful transmission. In the following examples, we show how modulation rates and channel interferences affect the number of retransmission and delay τ. Due to the network system heterogeneity and highway environments,

we are using the truth-ground data, rather than ns-3 simulations.

Example 6 [34] reports experimental data of IEEE 802.11p DSRC from a team of vehicles driving on certain Michigan highways. Package Delivery Rates (PDR) are measured under different driving conditions, traffics, and surroundings. A typical curve from [34] is re-generated in Fig. 17. When the modulation rate is 6 Mbps, the Package Delivery Rate (PDR) is about 75% at a distance of 85 m. The first round-trip takes about 100 ms. Each subsequent round-trip must catch the next CCH and it takes on average more than three retransmissions to achieve a PDR over 98.5%. Consequently, the average delay is $\tau \approx 0.3$ second. When the modulation rate is increased to 18 Mbps, the PDR is reduced to 36% at 85 m. In order to meet the same PDR 98.5%, the delay is more than 1 second.

Example 7 In this experimental study, we use the IEEE 802.11g standard to analyze the affects of multi-path interference. The communicating nodes reside on laptop computers and are moved from a short distance of 20 m to 95 m. In the first experimental setting, the transmission pathway does not have obvious obstacles, except low grass on the open field. Communication latency is recorded by the synchronized clocks on these computers. Fig. 18 provides the experiment data on recorded latency for different inter-node distances. A simplified curve can be obtained by data fitting, which is also shown in the same figure. It is noted that latency between 100 ms to 600 ms is typical in this case study.

Example 8 Extending on the experiment in Example 7, we now evaluate impact of

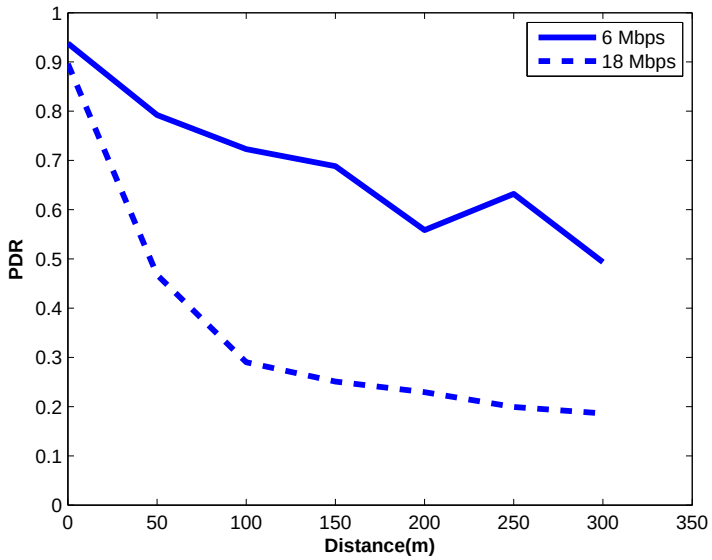

Figure 17: PDR vs. separation distance under different data rates in the Rural Road (RR) environment (with 95% Confidence Interval). Here, the data rates are 6 Mbps and 18 Mbps. The transmission power is 20 dBm.

obstacles on transmission pathways. Under the same experimental protocols as in Example 7, we select a field with many trees, but not overly dense. Consequently, depending on distances, the transmission pathways are obstructed by several trees. Fig. 19 demonstrates the experimental data on communication latency under different transmission distances. It is seen clearly that with obstacles, communication latency increases significantly to a range of 3.4 second.

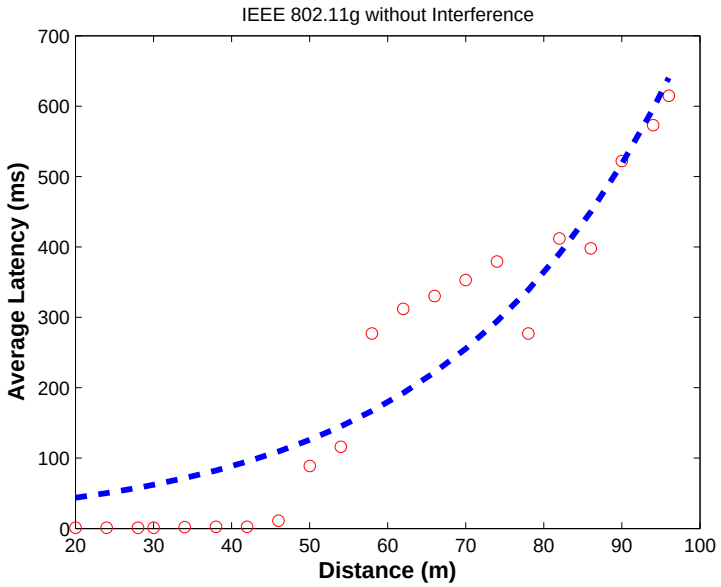

Figure 18: Dependence of latency on distance without obstacles on the transmission pathway.

4.2 Multi-Hop Communication Data

Inter-vehicle communications may involve multi-hops which create further delays. Typically, the IPv6+UDP/TCP protocols can be used in such systems. Unlike the WSMP protocols which use 11 bytes overhead, the IPv6 protocol requires a minimum overhead of 52 bytes. Although this is more complicated in coding and less efficient in using the data resource, this protocol provides more flexible routing schemes. There are many experimental studies of IEEE 802.11p under multi-hop and highway environment. Since we are only concerned with latency data, we quote here the studies in [23] that contain extensive experimental results. A typical curve from [23] is regenerated in Fig. 20. It is noted that although IEEE 802.11p uses higher power and

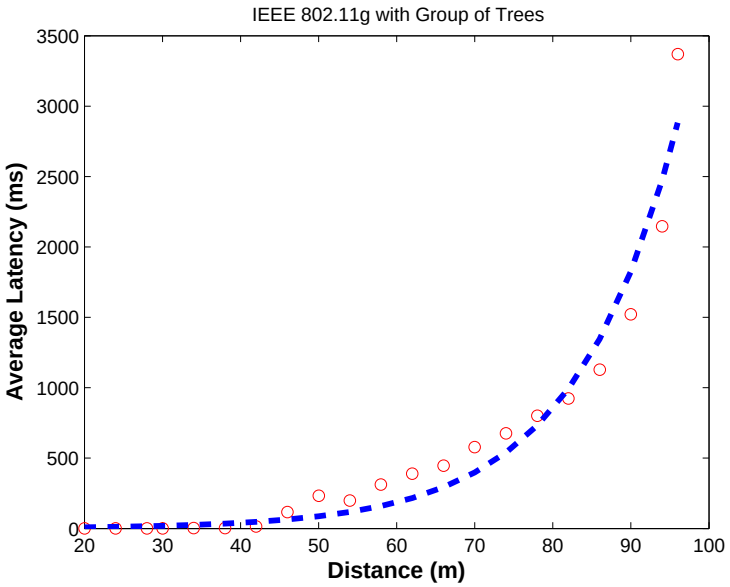

Figure 19: Dependence of latency on distance with trees on the transmission pathway.

faster speed, a latency of hundreds of milliseconds is typical in highway conditions.

4.3 Platoon Information Structure

4.3.1 Safety under Front Sensor Information

We start with the basic information structure of using front distance sensors only. For the three-car platoon in Fig. 2 and the control law $F = g_1(d)$ in Fig. 4, the

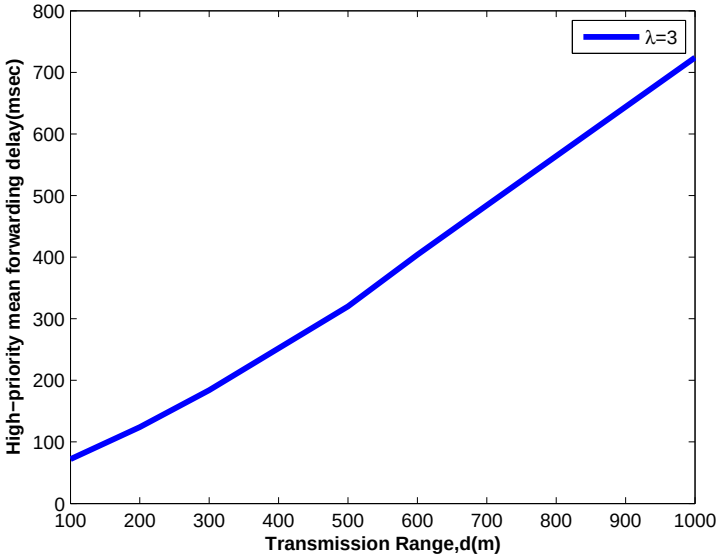

Figure 20: Average delay of high-priority message dissemination for 5 hops of communication as functions of the transmission range.

closed-loop system becomes

$$\begin{cases} \dot{v}_0 &= \frac{1}{m_0}(F_0 - (a_0 v_0 + b_0 v_0^2)) \\ \dot{v}_1 &= \frac{1}{m_1}(g_1(d_1) - (a_1 v_1 + b_1 v_1^2)) \\ \dot{v}_2 &= \frac{1}{m_2}(g_1(d_2) - (a_2 v_2 + b_2 v_2^2)) \\ \dot{d}_1 &= v_0 - v_1 \\ \dot{d}_2 &= v_1 - v_2 \end{cases} \tag{4.4}$$

Example 9 We consider the scenario defined in Section 2.2.2. Suppose that the platoon uses only front sensors to measure inter-vehicle distances, namely the information structure (a) in Fig. 2 is in effect. The feedback control function $F = g_1(d)$ is depicted in Fig. 6. We will use the following fast braking condition for comparison.

Under the **Fast Braking** scenario from Section 2.2.2, suppose that the leading vehicle uses a braking force 5000 N, which brings it to a stop from 25 m/s in 7.5 second. The distance trajectories of d_1 and d_2 are shown in Fig. 21. In this case, the minimum distances are 20.6 m for d_1 that is acceptable, but 0 m for d_2. This means that vehicle 2 will collide with vehicle 1 during the transient time.

To explain this scenario, we note in the top plot of Fig. 21 that since vehicle 2 relies on d_2 to exercise its braking control function, there is a dynamic delay in initiating its braking. d_2 is reduced to about 20 m when vehicle 2 starts to act. For a large platoon, this dynamic delay from vehicle to vehicle is a serious safety concern.

4.3.2 Adding Distance Information by Communications

We next expand on the information structures beyond front sensors by adding distance information by communications.

Example 10 Continuing from Example 9, we consider the same three-car platoon under the same initial conditions: The nominal inter-vehicle distances are 40 m; the cruising vehicle speeds are 25 m/s; the maximum braking force is 10000 N.

Under the **Fast Braking** scenario as in Example 9, suppose now that vehicle 1 sends d_1 information to vehicle 2 by communication. As a result, vehicle 2 can use

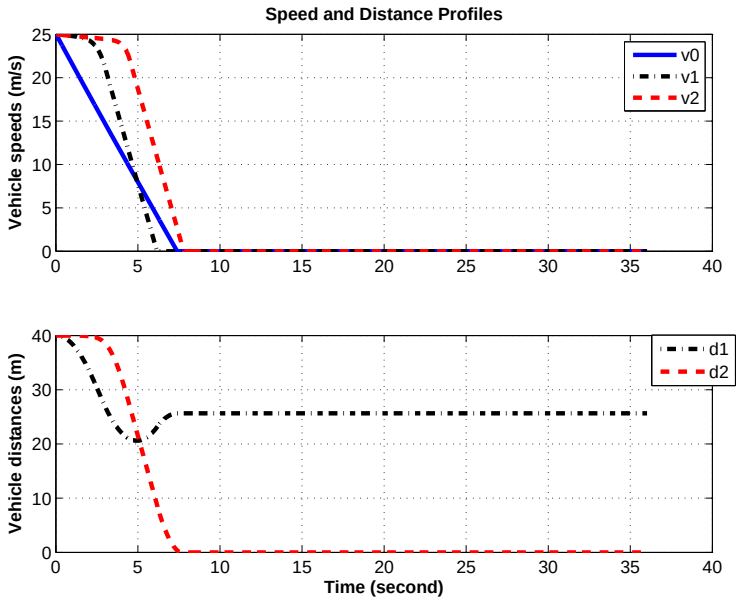

Figure 21: Distance trajectories under fast braking.

both d_1 and d_2 in its control function; see Fig. 22.

Suppose that vehicle 2 modifies its braking control function from the previous $F_2 = g_1(d_2)$ to the weighted sum $F_2 = 0.5g_1(d_2) + 0.5g_1(d_1)$ that uses both distances. The resulting speed and distance trajectories are displayed in Fig. 23. Now, the minimum distances are 20.6 m for d_1 and 15.9 m for d_2, both are within the safety region.

To compare Fig. 21 and Fig. 23, we note that with information feeding of d_1 into vehicle 2, vehicle 2 can slow down when d_1 is reducing before d_2 changes. Consequently, it is able to act earlier, resulting in a reduced distance swing for d_2 during the transient.

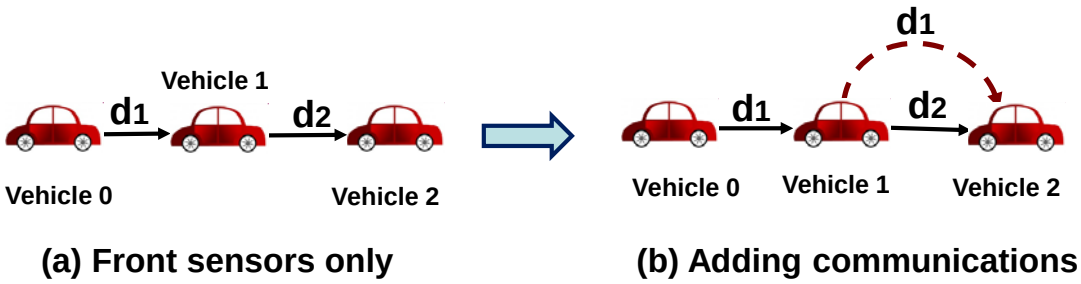

Figure 22: Enhanced information structure by sending d_1 to vehicle 2 by communication links in Example 10

4.4 Platoon Information Contents

4.4.1 Adding Speed Information by Communications

We now add the speed information of the leading vehicle to both vehicles 1 and 2 by communication.

Example 11 For the same three-car platoon under the same initial conditions as Example 10, we add the leading vehicle's speed v_0 into the information structure. This information is transmitted (or broadcasted) to both vehicles 1 and 2. Under the **Fast Braking** scenario as in Example10, suppose that vehicles 1 and 2 receive the additional speed information v_0, resulting in a new information structure shown in Fig. 24.

From the control functions of Example 10, additional control actions $g_2(v_0, v_1)$ and $g_2(v_0, v_2)$ are inserted. The resulting speed and distance trajectories are displayed in Fig. 25. Now, the minimum distances are 28.3 m for d_1 and 27.1 m for d_2, a much improved safety performance.

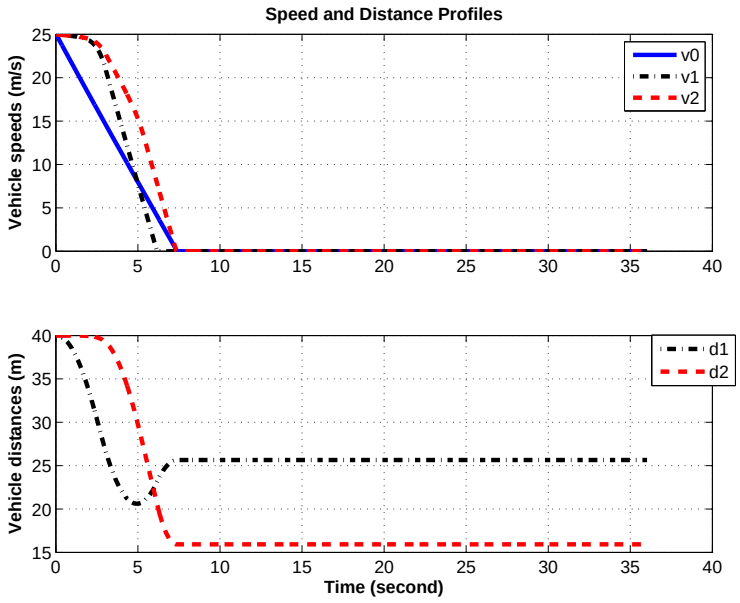

Figure 23: Distance trajectories when the distance information d_1 is made available to vehicle 2. It shows improvement over Fig. 21.

4.4.2 Adding Braking Event Information by Communications

Intuitively, if the leading vehicle's braking action can also be communicated, the following vehicles can act much earlier than their measurement data on vehicle movements. To evaluate benefits of sending the driver's action, we add the braking event information of the leading vehicle to vehicle 2 by communications.

Example 12 For the same three-car platoon under the same initial conditions as Example 11, we now further add the leading vehicle's braking event information F_0 into the information structure. To understand the impact, we purposely assume that vehicle 1 does not receive this information. In other words, this information will be transmitted only to vehicle 2 by communications. Under the **Fast Braking**

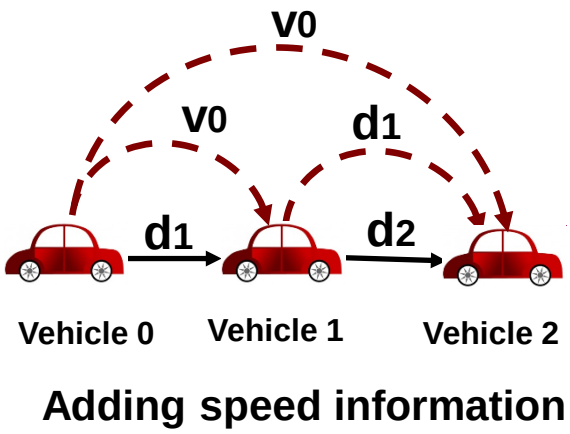

Figure 24: Enhanced information structure by sending d_1 to vehicle 2 and v_0 to both vehicles 1 and 2.

scenario as in Example 11, suppose that vehicle 2 receives the additional braking event information F_0, resulting in a new information structure shown in Fig. 26.

From the control functions of Example 11, an alternative control action F_0 is inserted when $d_2 < d_{ref} = 40$ m. The resulting speed and distance trajectories are displayed in Fig. 27. Now, the minimum distances are 28.3 m for d_1 and 30.6 m for d_2, a much improved safety over the case in Example 11. It is interesting to note that by knowing the leading vehicle's action, vehicle 2 can react faster than even vehicle 1 which does not receive the braking action data.

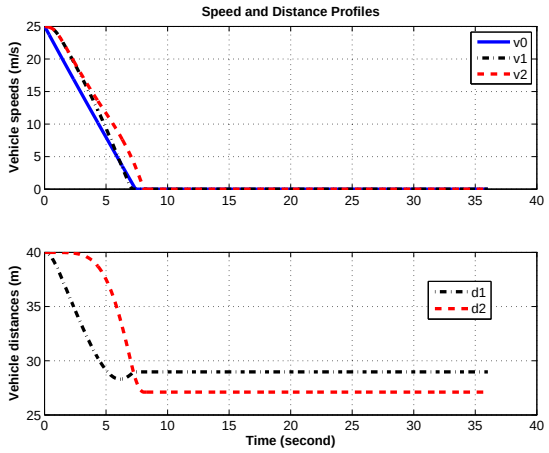

Figure 25: Distance trajectories when both distance and speed information is made available.

4.5 Impact of Radar and Communication Uncertainties

4.5.1 Impact of Radar Resolution and Missed Detection

Radar sensors provide a stream of measurement data, typically using 24, 35, 76.5, and 79 GHz radars. In general, radar sensor measurements are influenced by many factors that limit their accuracy and reliability. These include signal attenuation by the medium, beam dispersion, noises, interference, multi-object echo (clutter), jamming, etc.

We first consider the impact of radar's resolution on a platoon system. Within the same setup as Example 10, vehicle 2 receives the distance information of d_1 and d_2 in which d_2 is measured by a radar. Taking into consideration radar resolution, the measured distance is $\tilde{d}_2 = d_2 + \gamma\delta$, where γ is a resolution level and δ is a standard Gaussian noise $\mathcal{N}(0, 1)$.

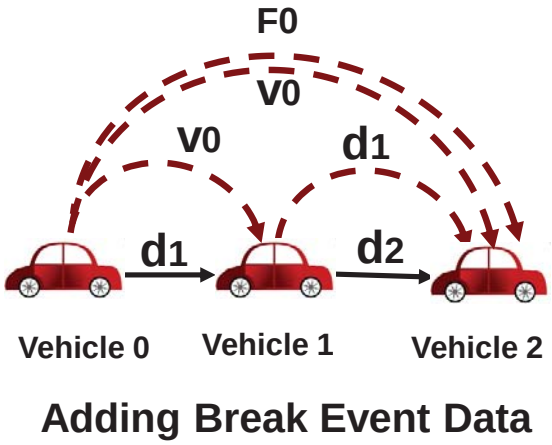

Figure 26: Enhanced information structure by sending the braking event F_0 to vehicle 2.

Fig. 28 shows a simulation result under a radar of resolution 1 m. The distribution of the minimum distances after repeated runs to account for randomness is shown in Fig. 29. Although the expectation is 8.01 m, the minimum distance has a high probability of having values close to zero. Consequently, this low resolution radar is not suitable for this application.

Next, we upgrade the radar to a higher resolution 0.1 m. A corresponding simulation is shown at Fig. 30. The minimum distances for both d_1 and d_2 are much improved. The distribution of minimum distances of d_2 is shown in Fig. 31. The random minimum distances have expectation 15.92 m and variance $\sigma^2 = 0.31$. This is an acceptable resolution for this application.

It is noted further that uncertainties of radar signals include also random false alarms or missed detection. In this scenario, the sensor does not provide information

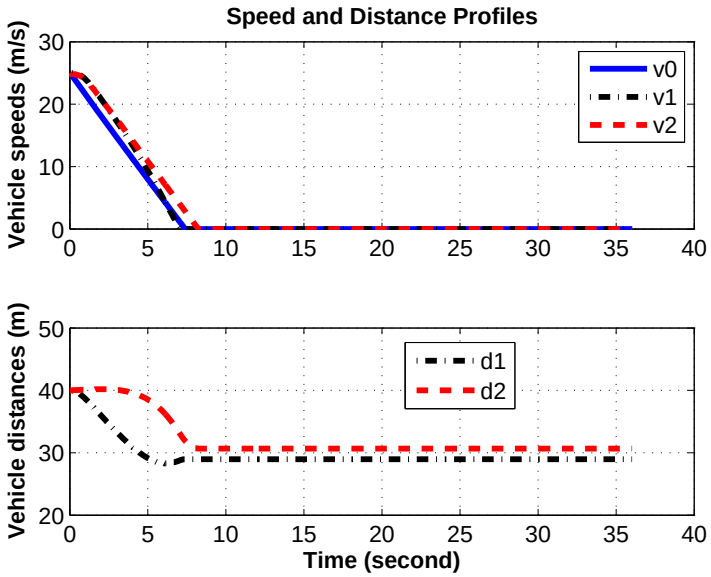

Figure 27: Distance trajectories with added braking event information.

at the sampling time, and the control/brake action must rely on its previous measurements and other available information from different resources. This situation is similar to Example 17 when communication information is unavailable, which will be detailed in the next subsection.

4.5.2 Impact of Communication Delay Analysis

Communications introduce a variety of uncertainties. Most common types are communication latency and packet loss. These can be caused by many factors as listed in the Section of Introduction. This thesis focuses on communication latency. Depending on environment and communication protocols, communication latency can be near a constant, distance dependent, or random. We cover these cases in the following subsections.

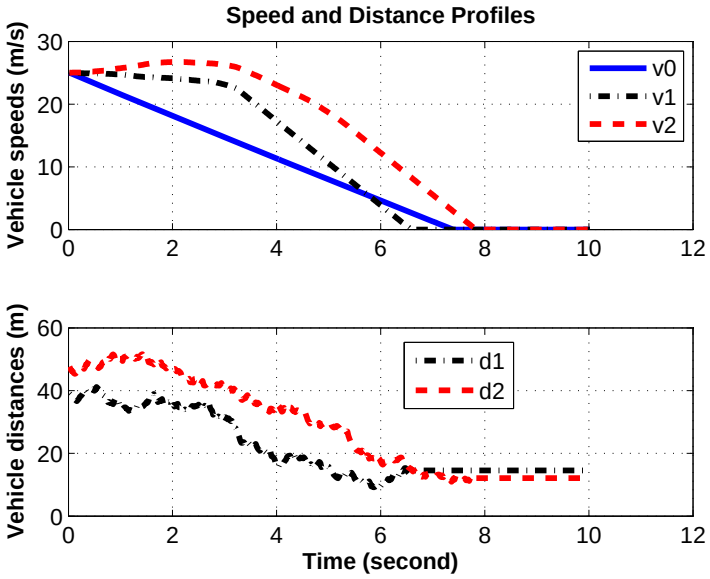

Figure 28: Distance trajectories under a radar of low resolution (1 m).

Fixed Delays:

We first consider fixed delays.

Example 13 Under the same system and operating condition as Example 10, we assume that the communication channel for the distance information has a delay of τ second. The impact of the communication delay is shown in Fig. 32. Without the delay, the minimum distance for d_2 is 15.9 m. When a delay of $\tau = 0.6$ (second) is introduced, the minimum distance for d_2 is reduced to 11 m.

Table 1 lists the relationship between the delay time and the minimum distance for d_2.

Next, we use experimental delay data in our simulation studies.

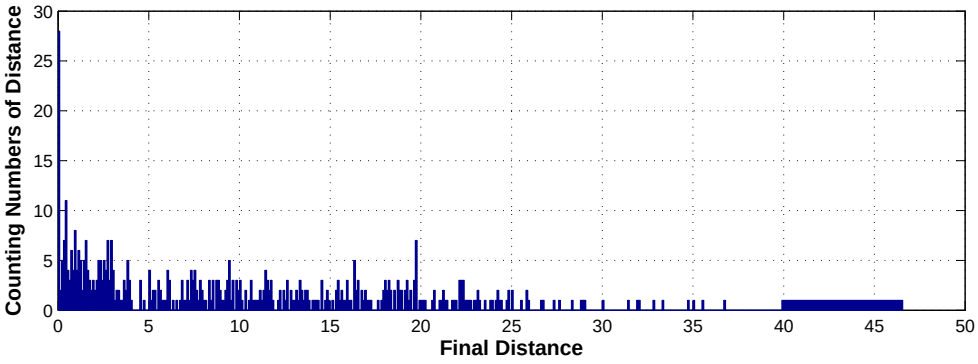

Figure 29: The distribution of minimum distances d_2 under a radar of low resolution (1 m).

Table 1: Impact of Communication Delays

delay time τ (s)	0	0.3	0.6	0.9	1.2
minimum d_2 (m)	15.9	13.6	11	8.2	5.1

Example 14 Under the same system and operating condition as Example 10, we assume that communication systems use the single-hop scenario in Section 4.1. Under a scenario of latency $\tau = 0.1$ second (CCH delay only), the minimum distance for d_2 is 15.1 m. It remains as an acceptable safe distance. Many factors affect such delays. One essential consideration is channel capacity. Shannon's channel capacity claims that if the channel is too noisy which reduces channel capacity, information cannot be effectively transmitted. This is translated into very large channel latency under a required PDR. In this sense, impact analysis of channel latency is in fact a study on

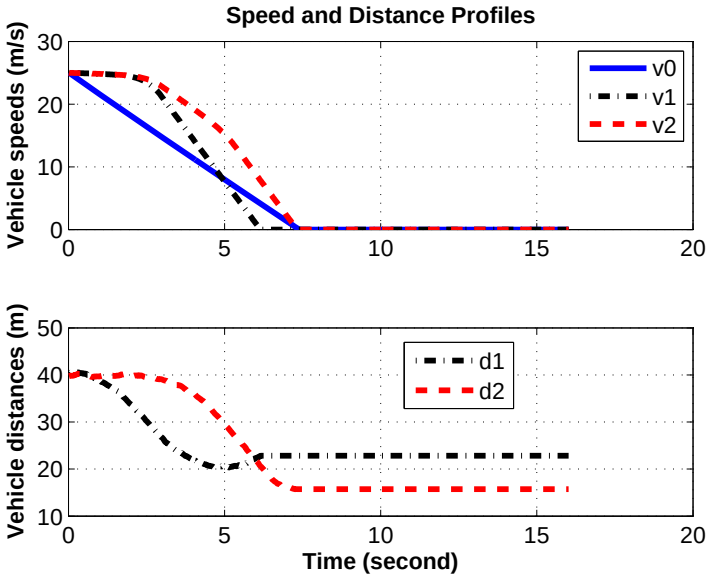

Figure 30: Distance trajectories with high Resolution Radar.

communication resources. Here we use platoon safety as a performance criterion in this study.

Distance-Dependent Delays:

In vehicle platoon environment, communication latency depends directly on inter-vehicle distances. These are reflected clearly in Figures 17, 18, and 19. It is observed that during platoon formation and braking, inter-vehicle distances change substantially. This subsection considers delays as a function of distance.

Example 15 Under the same system and operating condition as Example 14, we now use more realistic experimental data in Fig. 18 for latency which is a function of distance. Based on the relationship of distance and latency, the simulation in Fig. 33 shows that the minimum distance for d_2 is now 12.7 m. Furthermore, if signal

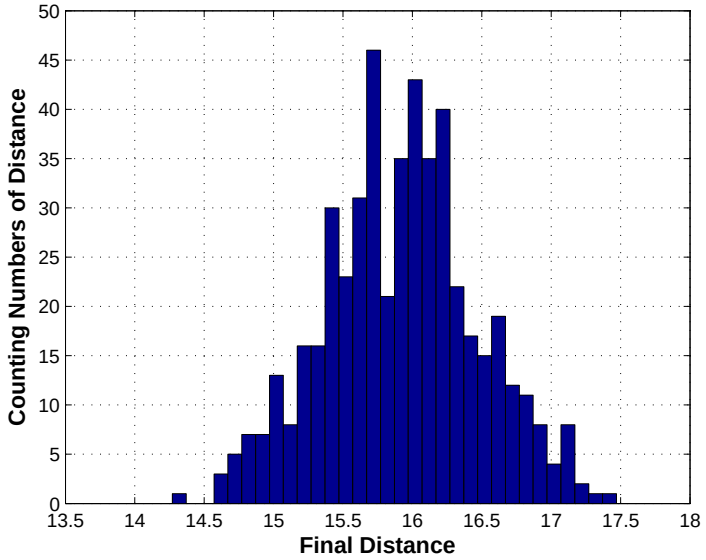

Figure 31: Distance Distribution of d_2 with high Resolution Radar .

interference, obstructions, and fading are considered, the latency is increased to these in Fig. 19. The simulation results in a minimum distance for d_2 as 5.6 m. This is shown in Fig. 34, which causes safety concerns.

Example 16 Continuing the study of Example 14, we consider the multi-hop scenario in Subsection 4.2. In that scenario, transmission from v_0 to v_2 is over 5 hops. Suppose that each hop has the same priority, and that each loses CCH once followed by one successful re-transmission. Based on the distances between the vehicles in the example, the total communication delay $\tau > 1.5$ second. The simulation shows that the minimum distance for d_2 approaches to 0, leading to a collision.

Random Delays:

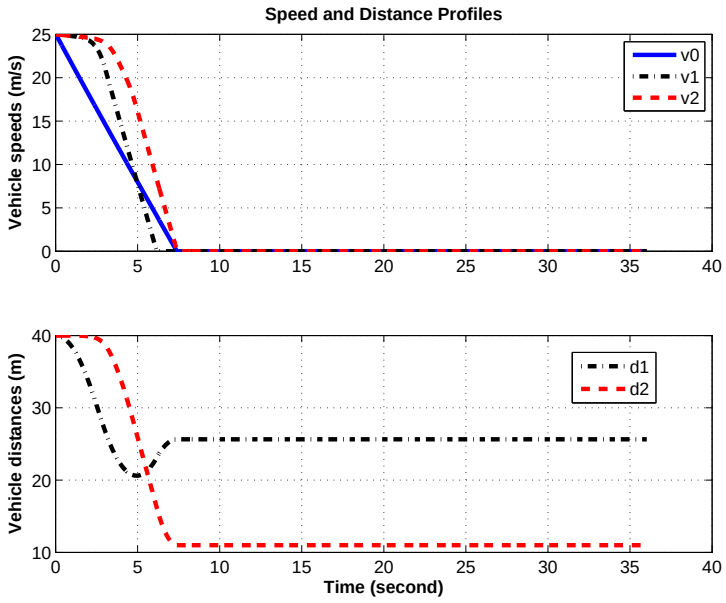

Figure 32: Distance trajectories when communication delays are considered.

Typically, communication delays are random variables with certain distributions. Depending on latency control mechanisms of transmission protocols, the latency can have different distributions. We use the common Gaussian distribution for our study in this subsection.

Example 17 Assume that communication latency is a random variable, due to the random features of wireless transmissions. In this example, we model τ as a random variable that is Gaussian distributed with $\mathbb{E}(\tau) = 1.2$ (second) and variance $\sigma^2 = 0.09$. Continuing the study of Example 16, the simulation in Fig. 35 shows that the minimum distance d_2 approaches to 5.09 m.

Simulation results of minimum distance distribution are shown at Fig. 36. The variance of d_2 is $\sigma^2 = 0.142$.

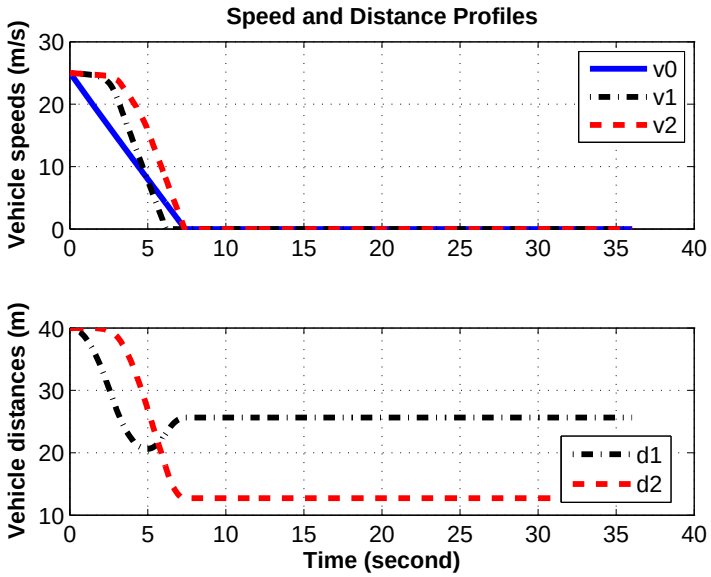

Figure 33: Distance trajectories when communication delays are dependent on vehicle distances, whose function form is given in Fig. 18 for the "no obstacle" scenario.

4.5.3 Impact of Doppler Frequency Shift and Signal Spreading

Mobility-induced Doppler spread is one of the main factors that degrade the performance of Orthogonal Frequency Division Multiplexing (OFDM) schemes. It introduces Inter-Symbol Interference (ISI) and Inter-Carrier Interference (ICI) by destroying the orthogonality between adjacent sub-carriers.

In most cases, DSRC is adequate in restoring both zero ISI and zero ICI in highly mobile, severe-fading vehicular environments, as discussed with great detail in [35]. In the physical layer of IEEE 802.11p, the bandwidth of each DSRC channel is 10 MHz, which entails less ISI and ICI than IEEE 802.11a which uses 20 MHz channel bandwidth. This brings better wireless channel propagation with respect to multi-path

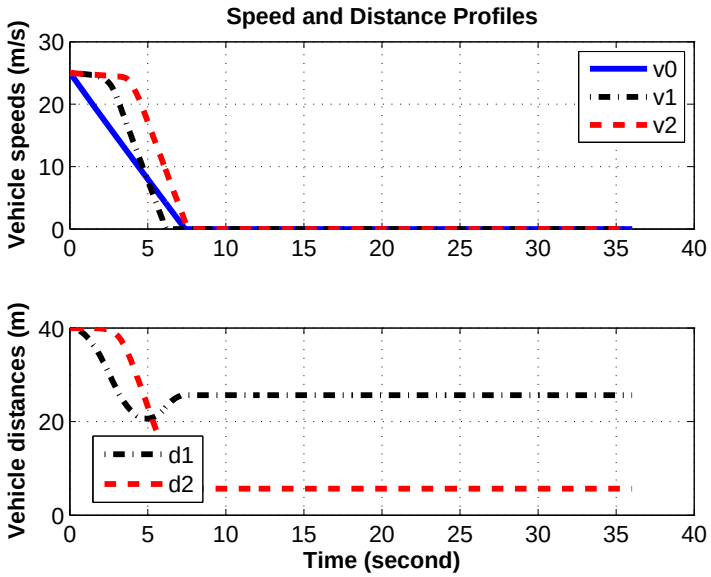

Figure 34: Distance trajectories when communication pathways are obstructed as shown at Fig. 19.

delay spreads and Doppler effects caused by high mobility and roadway environments. Also, DSRC expands Guard Band (GB) to 156 KHz and has 1.6μs guard interval for OFDM schemes. The Guard Band between sub-carriers can ensure that mobility-induced Doppler spreads do not cause two adjacent sub-carriers to overlap.

On the other hand, with high operation frequency at 5.9 GHz, IEEE 802.11p is subject to higher Doppler frequency shifts. When vehicle speeds are extremely high (such as 250 km/h on German highways), the issue of Doppler frequency shifts become more pronounced. At present, fast network topology switching and complicated road environments are still challenges with respect of ISI and ICI, and remain to be resolved by new technologies.

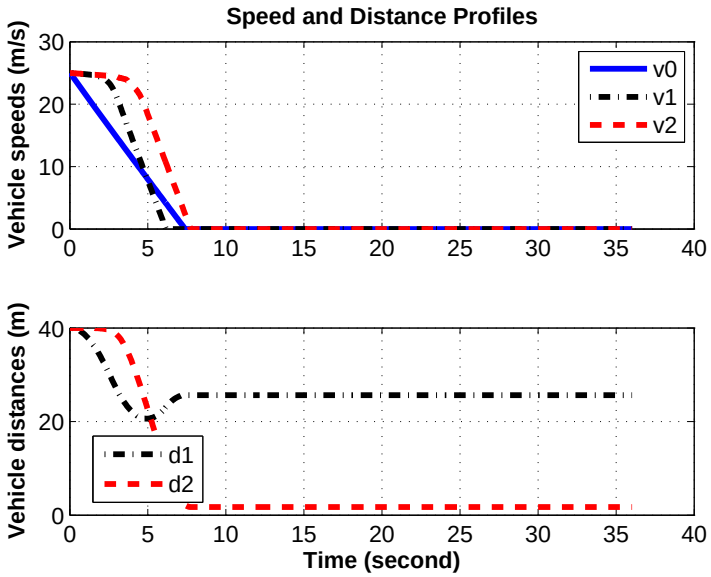

Figure 35: Distance trajectories under communication latency which is Gaussian distributed.

Fig. 37, re-produced from [34], compares the impacts of Open Field (OF) and Rural Freeway (RRF) on the PDR. The PDR remains nearly unchanged in the OF environment when relative vehicle velocities vary from 0 (m/s) to 25 (m/s). In contrast, the PDR drops dramatically in the RRF environment. For example, when the relative velocity is 12.5 (m/s), the PDR of the communication link in the RRF environment is reduced to 1/3 of that with the OF environment. This implies that in the RRF environment, much more communication resources are needed to ensure the same level of safety. As a result, it is advisable that these DSRC characteristics be incorporated into the platoon design by VANET designers.

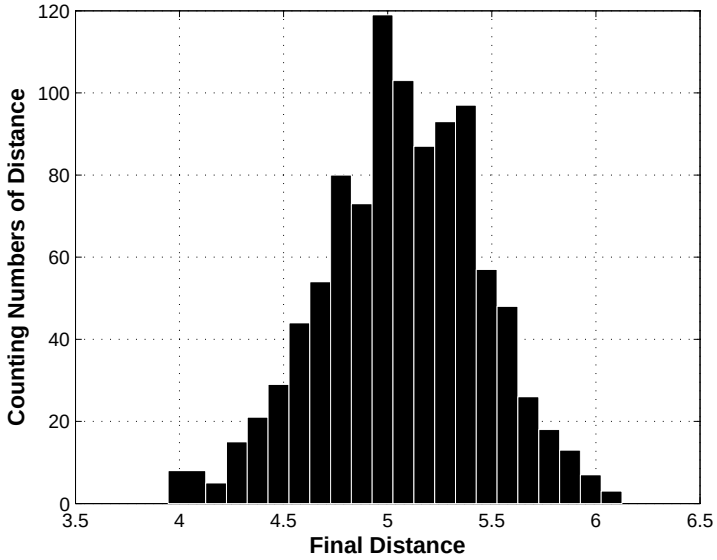

Figure 36: Distance distribution of d_2 under random communication latency .

4.6 System Integration with VANET Framework

The generic platoon model of this thesis is an important component of a VANET framework as shown in Fig. 38. In our exploration, the actual communication routes are not specified. Within a VANET, the links among vehicles can be realized by V2V communications or V2I pathways involving access points, wireless towers and other infrastructures. Our model provides a fundamental framework to study impact of communications on vehicle safety and can be specified to different communication configurations. The findings of this thesis can be used as guidelines in selecting VANET parameters. For example, transmission power, modulation rate, and coding scheme can be selected so that they meet the requirements of an acceptable minimum inter-vehicle distance. Also, a platoon can potentially enhance VANET data access

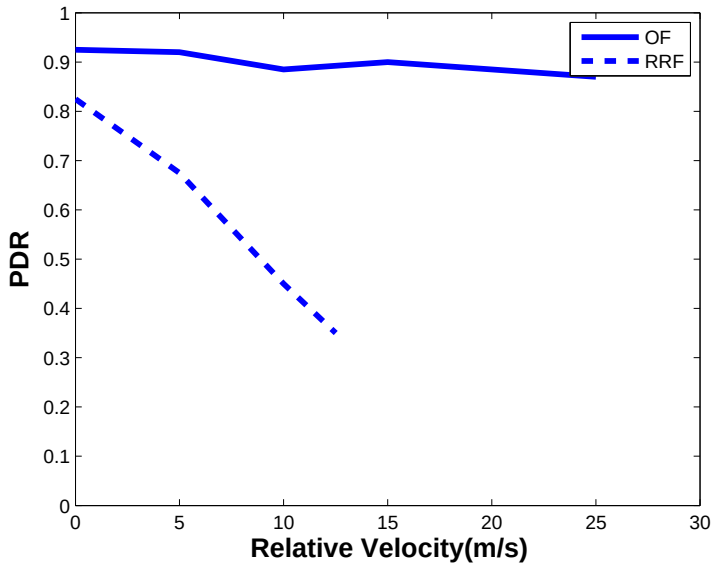

Figure 37: The impact of relative velocities on the PDR(with the 95% confidence interval). A bin of 20 packets is used to calculate PDR values as well as relative velocities.

performance. By using vehicles as transmission hubs, data can be replicated and relayed to more vehicles in the group. This structure improves VANET resources in a distributed manner and, if used properly, can improve overall performance.

While this thesis is focused on one platoon formation, a platoon experiences many dynamic variations in real implementations. These include lane change, vehicle departure and addition, platoon reformation, etc. At the network level, such changes amount to network topology variations. At the communication/physical level, some uncertainties will be introduced such as echo among vehicles and road infrastructures. A VANET can easily accommodate such topology changes by using vehicle

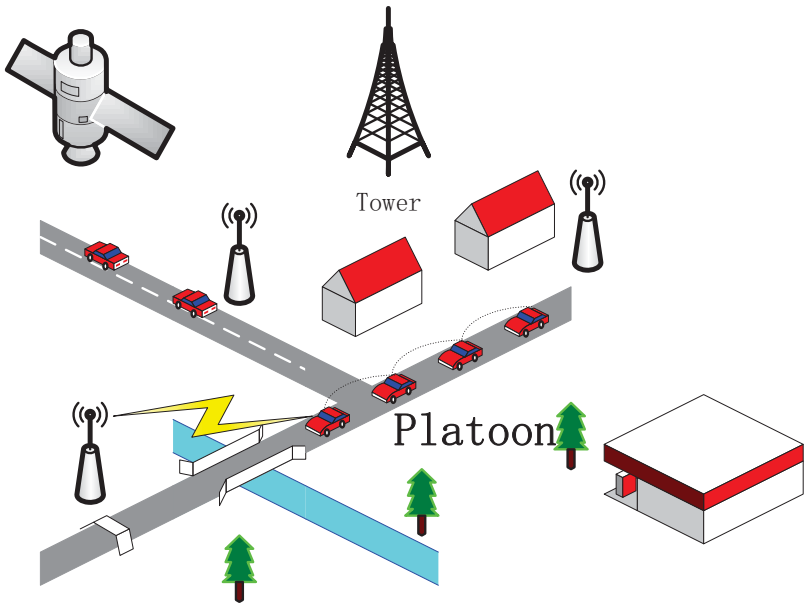

Figure 38: System integration of a platoon with a VANET framework.

IDs and their links. Furthermore, by seamless integration into a VANET, a platoon can have access to VANET resourses, including GPS, Internet, distributed live database, VANET-enabled applications, etc. Consequently, a platoon can potentially utilize additional information in its safety considerations via inter-vehicle communications and emission reduction via traffic information. These topics are, however, beyond the scope of this thesis.

5 IMPACT OF COMMUNICATION PACKET LOSS

Inter-vehicle distances are most commonly measured by radars. Radar sensors provide a stream of measurement data, typically using 24, 35, 76.5, and 79 GHz radars. In general, radar sensor measurements are influenced by many factors that limit their accuracy and reliability. These include signal attenuation by the medium, beam dispersion, noises, interference, multi-object echo (clutter), jamming, etc.; see [36] for further detail. On the other hand, when communication channels are employed, channel uncertainties become essential features in control design consideration. This thesis concentrates on communication uncertainties from erasure channels, which are described next.

5.1 Impact of Information Structures and Channel Erasure

This section lays the foundation for performance analysis in a vehicle safety framework. We concentrate on impact of erasure channels.

We then expand on the information structure by adding new information via communications. Communications introduce a variety of uncertainties, such as latency, jitter, and packet loss. We only focus on the effect of packet loss.

Example 18 We first consider distance-independent package erasure rates. Under the above evaluation scenario, now vehicle 1 sends d_1 information to vehicle 2 by communication. As a result, vehicle 2 can use both d_1 and d_2 in its control function; see Fig. 22.

Suppose that vehicle 2 modifies its braking control function from the previous $F_2 = g_1(d_2)$ to the weighted sum $F_2 = 0.5g_1(d_2) + 0.5g_1(d_1)$ that uses both distances. Assuming that the communication channels are secure (no erasures or $P_e^k = P_e = 0$), the resulting speed and distance trajectories are displayed in the left plots of Fig. 39. With information feeding of d_1 into vehicle 2, vehicle 2 can slow down when d_1 reduces before d_2 changes. Consequently, the minimum distances are increased to 20.6 m for d_1 and to 15.9 m for d_2, both are within the safety region.

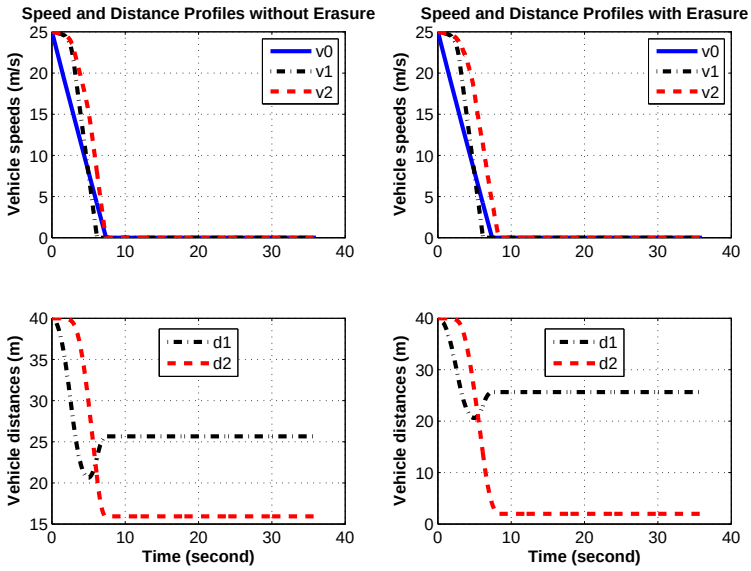

Figure 39: Distance trajectories when the distance information d_1 is made available to vehicle 2 and with Erasure rate 0 and 0.4.

Channel erasure has significant impact on vehicle safety. To show this, assume that the packet erasure probability is increased to $P_e = 0.4$. The right plots of Fig. 39 highlight a drastic reduction of the minimum distances to near zero. Fig. 40

illustrates the dependence of the minimum distances on the link erasure probability.

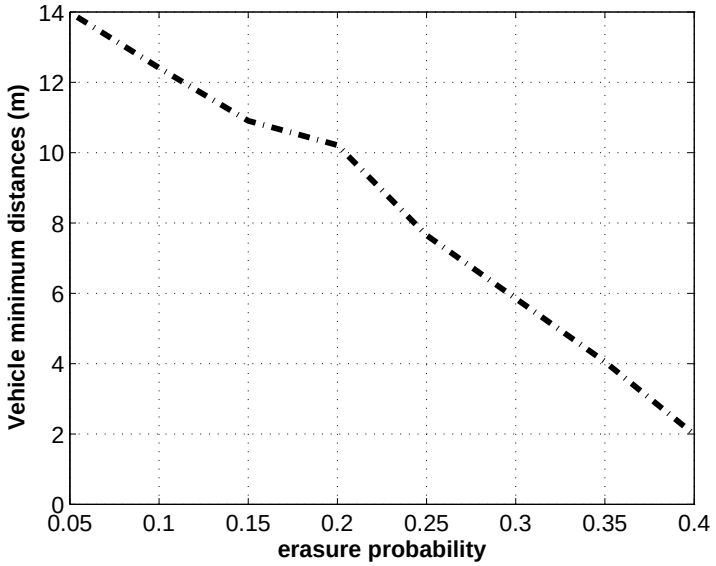

Figure 40: Minimum inter-vehicle distances and erasure probabilities on distance information

Example 19 We now add the speed information of the leading vehicle to both vehicles 1 and 2 by communication. For the same three-car platoon under the same initial conditions as Example 18, we add the leading vehicle's speed v_0 into the information structure. This information is transmitted (or broadcasted) to both vehicles 1 and 2. Under the **Fast Braking** scenario as in Example 18, suppose that vehicles 1 and 2 receive the additional speed information v_0, resulting in a new information structure.

From the control functions of Example 18, additional control actions $g_2(v_0-v_1)$ and $g_2(v_0 - v_2)$ are inserted. The resulting speed and distance trajectories are displayed in the left plots of Fig. 41. Now, the minimum distances are increased to 28.3 m for

d_1 and 27.1 m for d_2, a much improved safety performance.

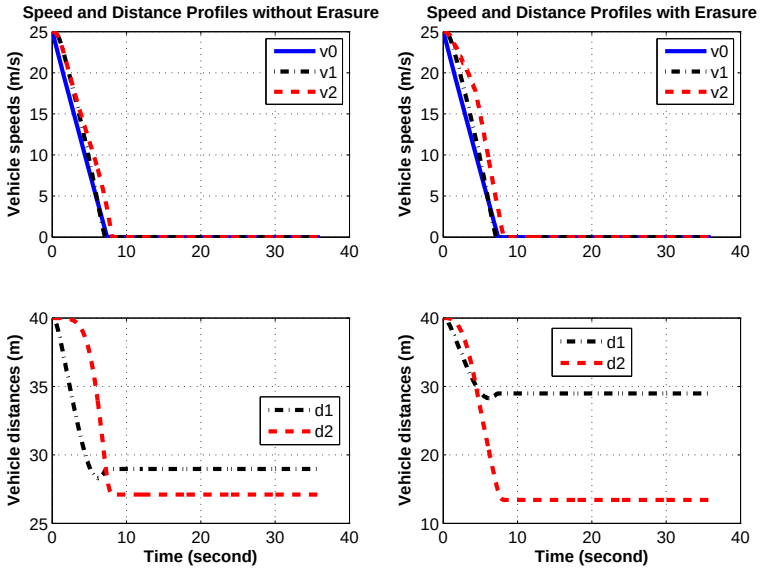

Figure 41: Distance trajectories when both distance and speed information transmitted with erasure rate 0 and 0.5.

Example 20 Similarly, we can consider impact of erasure channels for v_0 and d_1 information as in Example 18. Under the same system and operating condition as Example 19, we assume that the communication channel for the speed v_0 and d_1 information is an erasure channel. The left plots of Fig. 41 represent the secured channel without erasure. If the packet erasure probability is increased to $P_e = 0.5$, the right plots of Fig. 41 highlight a reduction of the minimum distance to 13.89 (m), which is less than an acceptable minimum distance d_{min}. Fig. 42 depicts the dependence of the minimum distances on the link erasure probability on transmission of d_1 and v_0 information.

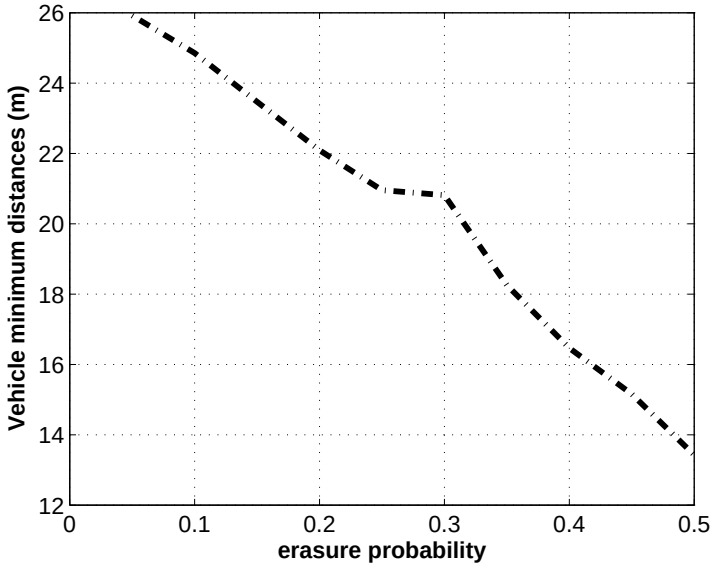

Figure 42: Minimum inter-vehicle distances and erasure probabilities on speed and distance information

Intuitively, if the leading vehicle's braking action can also be communicated, the following vehicles can act much earlier than their measurement data on vehicle movements. To evaluate benefits of sending the driver's action, we add the braking event information of the leading vehicle to vehicle 2 by communications.

Example 21 For the same three-car platoon under the same initial conditions as Example 19, we add the leading vehicle's braking event information F_0 into the information structure. From the control functions of Example 19, an alternative control action F_0 is inserted when $d_2 < d_{ref} = 40$ m. The resulting speed and distance trajectories are displayed in the left plots of Fig. 43. Now, the minimum distances are increased to 28.3m for d_1 and 30.6m for d_2, a much improved safety over the case in

Example 19.

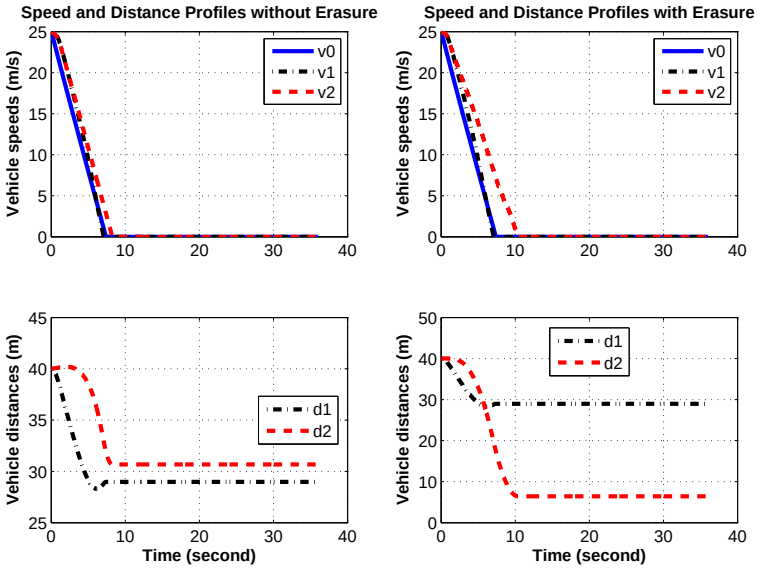

Figure 43: Distance trajectories with added braking event information.

Example 22 Under the same system and operating condition as Example 21, we assume that the communication channel for F_0, v_0, and d_1 is an erasure channel with erasure probability $P_e = 0.25$. The right plots of Fig. 43 demonstrate a drastic reduction of the minimum distance to 7.07 (m), it is less than an acceptable minimum distance d_{min}.

Fig. 44 summarizes the dependence of the minimum distance on the link erasure probability on transmission of d_1, v_0, and F_0. It shows that brake event is more sensitive to the erasure probability than the distance and speed information.

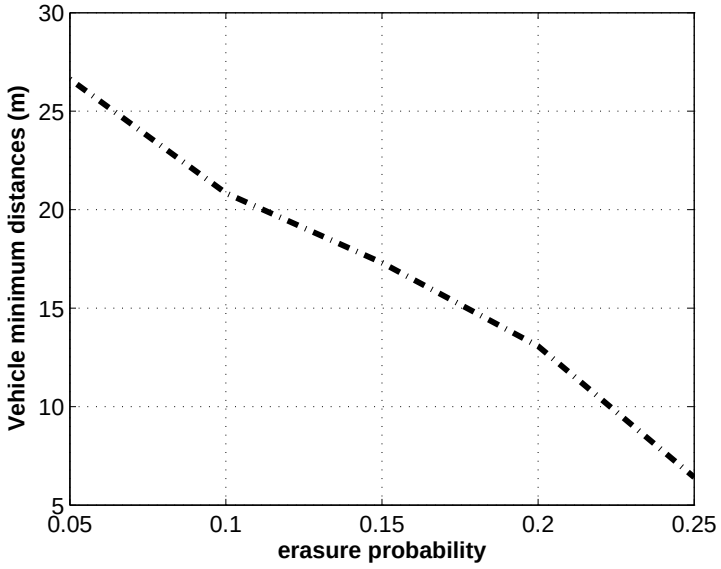

Figure 44: Minimum inter-vehicle distances and erasure probabilities

5.2 Case Studies of Erasure Channel Effects

This section presents several cases that include more details on communication systems. Due to the complexity of traffic conditions, environments, and communication facility heterogeneity, our case studies consider several basic features and main communication resources.

5.2.1 Package Erasure Rate Implications of Inter-vehicle Distance

Distance-Dependent Signal Attenuation:

There are many factors at the physical level that affect a link's package erasure rates. Here, we consider the main factor from signal fading due to variations in inter-vehicle distances.

Suppose that the leading vehicle broadcasts a complex sinusoid $e^{2\pi ift}$. The signal strength at the receiving site of distance d behind the leading vehicle is typically modeled as

$$E_s = \frac{\alpha_s(\theta, \psi, f)e^{2\pi if(t-d/c)}}{d} \tag{5.5}$$

where (θ, ψ, f) are the vertical angle, horizontal angle, and carrier frequency, respectively, and c is the speed of light. What is relevant here is the fact that the power radiated per unit area attenuates with rate $1/d^2(t)$. This in turn implies a decaying SNR as the distance increases. Consequently, P_e^k in (3.7) becomes a function of the inter-vehicle distance.

Since our platoon model accommodates various communication resources, we first use the IS95 standard from [37] in our case studies to exam the distance-dependent erasures. The IS95 is one of the major classes of cellular standards that use the modulation scheme of code division multiple access (CDMA). The modulation maps each successive 6 bit string into a 64 bit binary string. Assuming non-coherent detection and a single-tap channel filter, the erasure probability is bounded by

$$\varepsilon \leq \frac{63}{2}e^{-E_s/(2N_0)}. \tag{5.6}$$

In a narrow-band environment, this model provides a basic erasure rate expression. Other communication uncertainties, such as signal reflections, inter-symbol interferences, and Doppler shift, will further increase the error probability ε. To accommodate more realistic vehicle communication environments, in our case studies we employ the experimental package delivery rate (PDR) data from [34], shown in Fig.

45. Here, the relationship of PDR and P_e is $\rho = 1 - P_e$. For example, in a typical rural road environment, the PDR decreases from $\rho \approx 0.936$ in the range of $0 - 50$ m to $\rho \approx 0.391$ in the range of $450 - 500$ m.

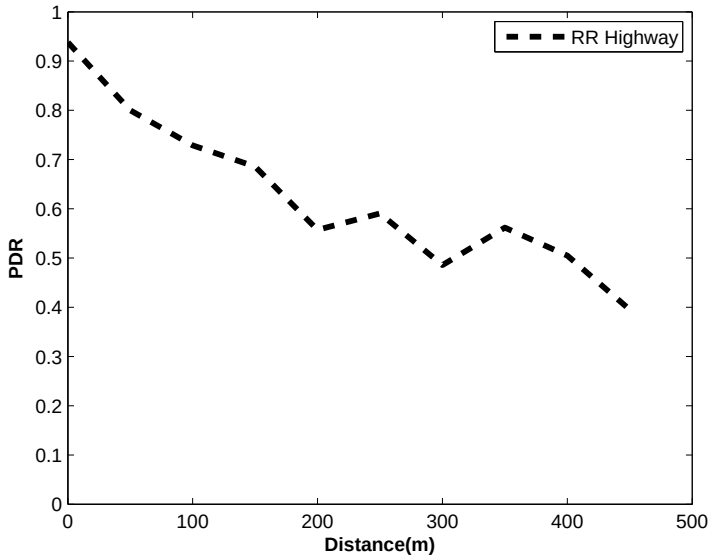

Figure 45: The impact of separation distance (with the 95% confidence interval). In this figure, a bin of 20 packets is used to calculate PDR values.

Dedicated Short Range Communications:

The PDR of a link depends also on communication protocols. Currently, the most commonly accepted vehicle communication protocol is IEEE 802.11p, which supports Dedicated Short Range Communications (DSRC). IEEE 802.11p is a modified version of IEEE 802.11**(WIFI)** standard. DSRC is a short-to-medium range communications service that supports both public and private operations in roadside-to-vehicle and vehicle-to-vehicle communications environments. It is one of the most effective means

to deliver rapidly real-time data. In the US, a spectrum of 75 MHz from 5.850 GHz to 5.925 GHz is allocated for DSRC applications. Within the spectrum, 5 MHz is reserved as the guard band, and seven 10-MHz channels are configured into one control channel (CCH) and six service channels (SCHs). The CCH is reserved for carrying high-priority short messages or management data, while other data are transmitted on the SCHs.

There are many experimental studies of IEEE 802.11p on freeway environments. Since we are only concerned with PDR, we quote here the studies in [34] which contain extensive experimental results of PDR from many possible contributing factors, such as inter-vehicle distance, signal propagation environment, relative velocity, effective velocity, received signal strength, and transmission power and modulation rate.

5.2.2 Probabilistic Characterization of PDR and Sampling Time on Vehicle Safety

Impact of the PDR on vehicle safety can be analyzed by a simplified transmission model. In this model, when a packet is lost the measured variable is not delivered. As a result, the controller must use the previous value in its control actions. Mathematically, this is similar to a sampling process with random sampling times.

Suppose that the baseline sampling interval is τ_0. At $k\tau_0$, we use a link-connection variable γ_k to indicate if the packet is delivered ($\gamma_k = 1$) or lost ($\gamma_k = 0$). As a result, assuming that γ_k is independent and identically distributed (i.i.d.), we denote the PDR by $\rho = P\{\gamma_k = 1\}$. Fig. 46 shows a sample path under $\rho = 30\%$ and $\tau_0 = 0.2$.

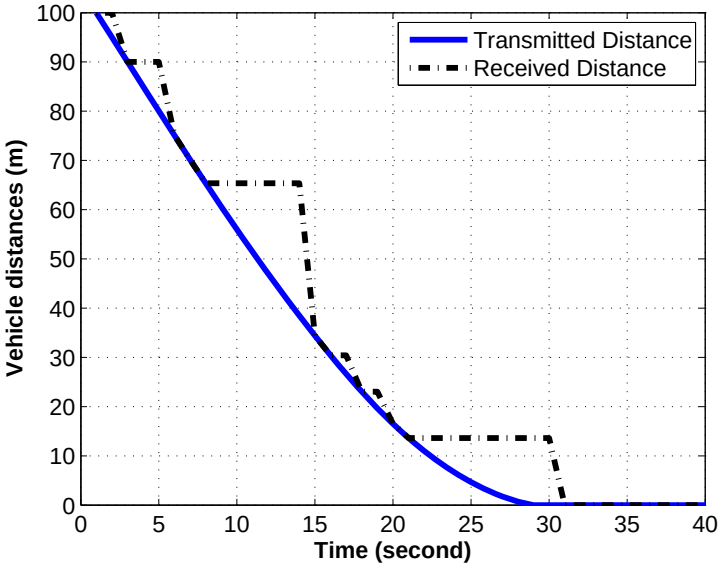

Figure 46: Transmitted d_k and received $\tilde{d}_k$

To give a sense on how the PDR will influence the vehicle safety, we consider a simplified two-vehicle model, with vehicles V_0 and V_1 shown in Fig. 47. In this model, the actual inter-vehicle distance is d but the vehicle controller on V_1 can only use the received $\tilde{d}$, rather than the actual distance d, to control its braking action.

The vehicle velocities are v_0 and v_1, respectively. Define $v = v_1 - v_0$. Then the two-car system dynamics is

$$\begin{cases} \dot{v} &= -\frac{f(\tilde{d})}{m_0} \\ \dot{d} &= -v. \end{cases} \tag{5.7}$$

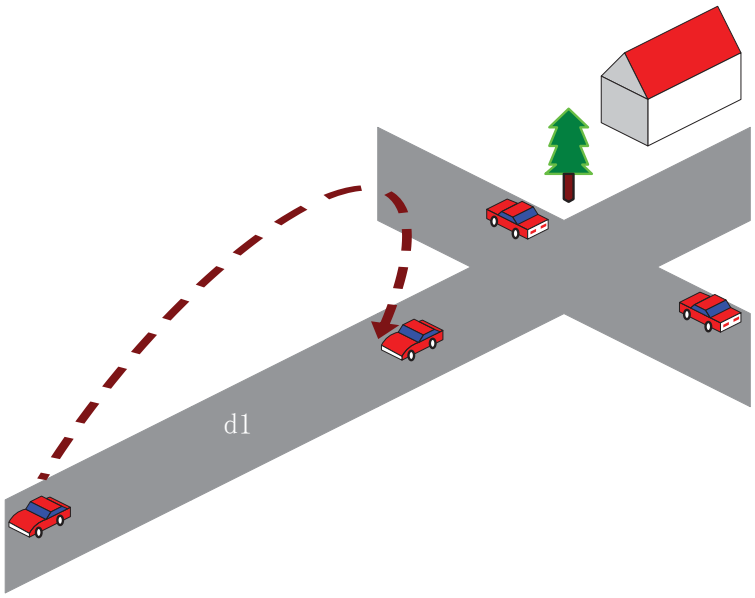

Figure 47: Two Vehicles Model with Distance Information Only

The received distance information under sampling interval τ_0 can be represented by

$$\tilde{d}_k = \begin{cases} d_k, & if \quad \gamma_k = 1 \\ \\ \tilde{d}_{k-1}, & if \quad \gamma_k = 0. \end{cases} \tag{5.8}$$

Example 23 Without loss of generality, assume $v_0 = 0$. Then $v = v_1$. Vehicle masses $m_0 = m_1 = 1500$. The initial speed $v(0) = 25$ m/s and the nominal inter-vehicle distance $d_{ref} = 80$ m. The simplified feedback control function is

$$g_1(\tilde{d}) = \max\{k_1(\tilde{d} - d_{ref}), -F_{max}\} \tag{5.9}$$

where $k_1 = 115$, $F_{max} = 10000$ (N). Suppose that the communication channel PDR is $\rho = 70\%$ and sampling time $\tau_0 = 0.2$ second. The plot of Fig. 48 is the probabilistic

distribution of the final inter-vehicle distances under 1000 repeated runs. The sample average of the final distance is $E(d_{final}) = 3.6603$ (m) and variance $\sigma^2 = 1.0757$.

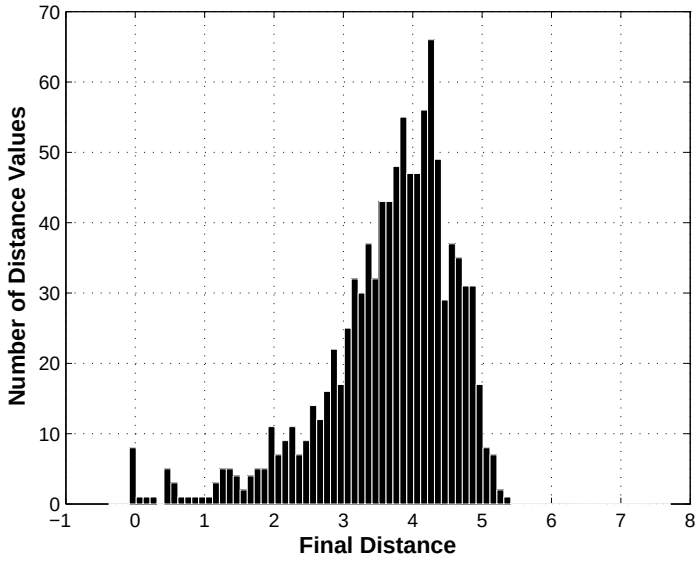

Figure 48: Final distance distribution with repeating 1000 times

Example 24 Under the same configuration of Example 23, we now consider time-varying PDR value ρ that is a function of the distance. The simulation results in Fig. 49 show the average final distance as a function of ρ.

Fig. 49 indicates a monotone relationship between ρ and final distance d_{final}: The higher the PDR ρ, the earlier vehicle 1 stops. On the other hand, if we choose a shorter sampling interval $\tau_0' < \tau_0$, namely using a faster sampling system, then more re-transmission is allowed with a given control updating interval, leading to a higher probability of data receipt. To show this, we fix PDR to $\rho = 30\%$. The simulation results in Fig. 50 demonstrate the average final distance as a function of sample time

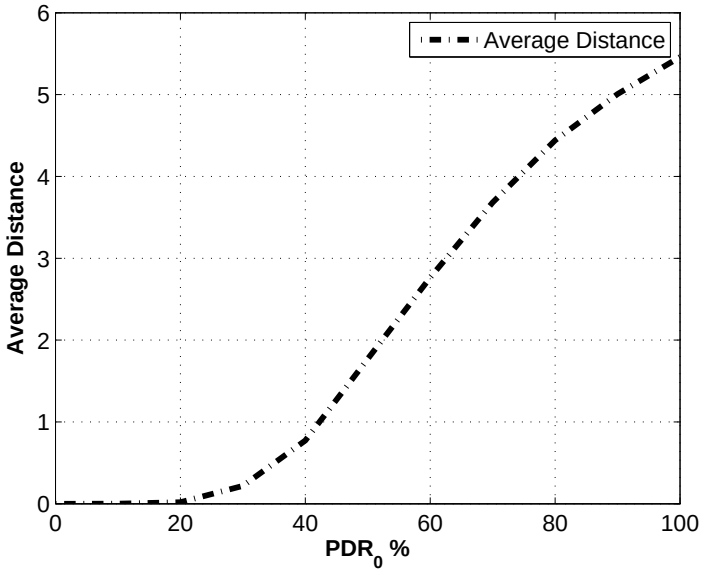

Figure 49: Average final distance vs. distance-dependent PDR ρ

τ_0. It shows a monotone relationship: the shorter the base sampling interval, the earlier the vehicle stops.

5.2.3 Impact of Transmission Power and Modulation Rate

We perform two case studies in this subsection with two commonly used transmission parameters: transmission power and data modulation rate. Vehicular ad hoc network (VANET) designers can control these parameters to meet platoon safety requirements. The coverage distance by a single radio link, which ranges from 10 m to 1 km in IEEE 802.11p, depends on the transmission power, channel environment, modulation and coding schemes.

Example 25 We first exam the impact of transmission power. Wireless devices are

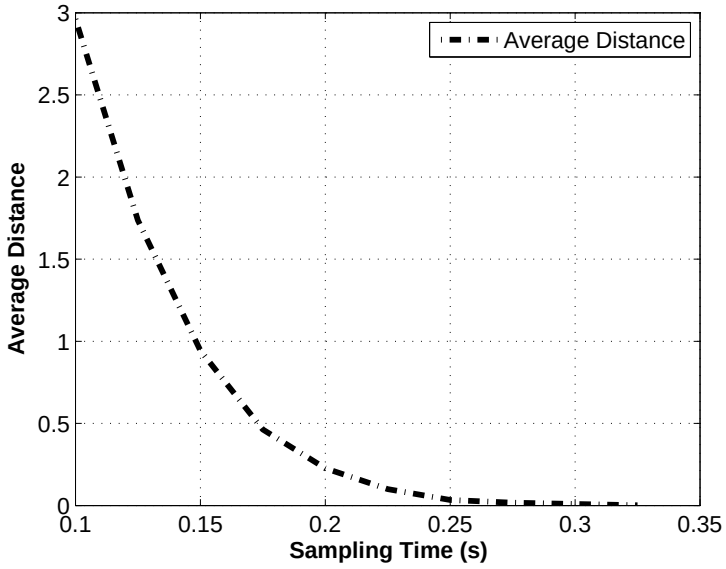

Figure 50: Average final distance vs. varying sampling time

assumed to have maximum transmission power from 0 dBm to 28.8 dBm. Fig. 51 from [34] is an experimental result relating the PDR to transmission distances. The figure describes how the PDR varies with the inter-vehicle distance under different transmission power levels while keeping other factors fixed. The transmission power varies from 10 dBm to 20 dBm in a rural road environment. It shows that higher transmission power generates higher PDRs. For example, under the same system and operating condition as Example 19, by applying the PDR curve with 20 dBm transmission power, the left plots of Fig. 52 implies that the minimum distance is 14.92 (m).

When the transmission power is reduced to 10 dBm, the right plots of Fig. 52 give a minimum distance 6.88 (m). It is no longer an acceptable distance.

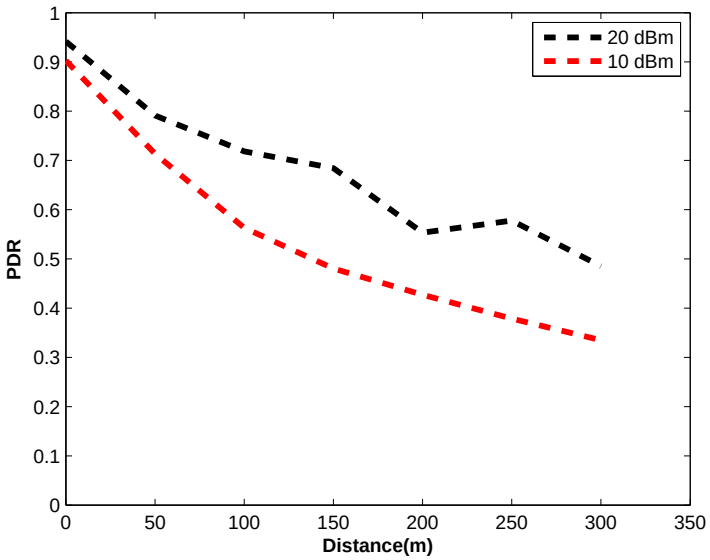

Figure 51: PDR vs. distance under different transmission power settings in the rural road (RR) environment (with 95% confidence interval). Here, the transmission power is 10 dBm and 20 dBm. The data rate is 6 Mbps.

Example 26 We now exam the impact of modulation rate. A typical curve from [34] is re-generated in Fig. 17. The figure describes how the PDR varies with the distance under different modulation rates. By applying the first PDR under modulation rate 6 Mbps, the simulation in Fig. 53 shows that the minimum distance is 12.44 (m).

On the other hand, if the modulation rate is increased to 18 Pbps, Fig. 53 shows that the minimum distance is reduced to 0 (m) and a collision occurs.

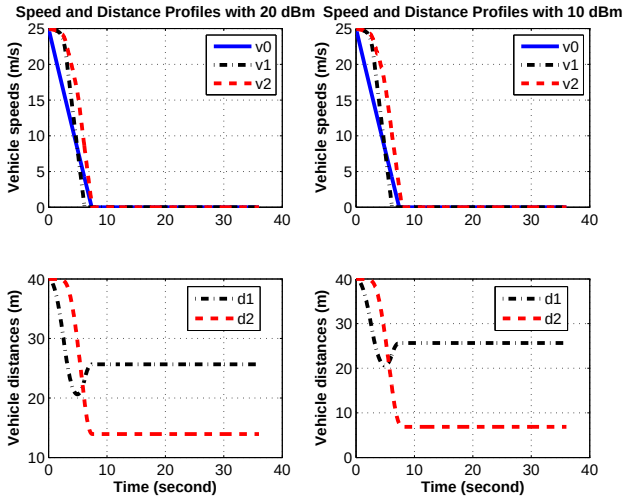

Figure 52: Distance and speed trajectories with the leading vehicle speed information under different transmission powers.

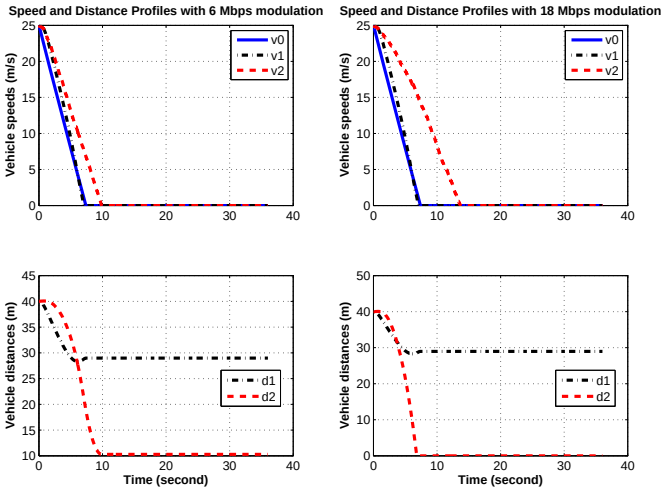

Figure 53: Distance and speed trajectories with braking information under modulation rate of 6 Mpbs and 18 Mpbs.

6 INFORMATION HARMONIZATION MODULE DESIGN

6.1 Multi-Information Structure

In two vehicle models, we assume braking information F_0 of $v0$ is transmitted to $v2$. $v2$ performs F_0 braking force instantly. A simulation shows $d^2_{final} = 54.35$. By additional information of F_0, the collision is avoided. However, d^2_{final} is not an acceptable distance in the sense of highway usage. This becomes more obvious by following Example 27.

Example 27 We assume 25 vehicles form a typical 1 (km) platoon. When Vehicle $V0$ applies a braking force, vehicle $j, \{j = 1, 2, \ldots, 23\}$ perform braking action based on inter-vehicle distance d^j, and ending vehicle $V24$ follows $V0$'s braking actions. We assume $d^{23}_{final} \to 0$ and

$$\Delta d^{final} = \frac{1}{24}\sum_{i=1}^{24}(d^i_{final} - d^{i-1}_{final}) = 1.6(m).$$

It can be found that $d^{final}_{24} = 480$ (m). Obviously, It is not an acceptable distance. The last second vehicle v^{23} is in a collision situation while the last vehicle is far behind the platoon. It occupies half of the platoon distance.

From Example 27 and previous safety discussion, neither distance information d^2 or leading vehicle braking information F^0 can guarantee a successful state updating. Moreover, Vehicle ad hoc network (VANET) enabled vehicles can access multi-information from neighor and networked vehicles.

In VANET, vehicles are equipped with on-board systems that allows them to exchange messages with each other in Vehicle-to-Vehicle communication (V2V) and also to exchange messages with a roadside network infrastructure (Vehicle-to-Roadside Communication V2R).

With the integration of VANET as shown at Fig. 54, a platoon can access information from access point, cellular tower, satellite and other VANET enabled vehicles.

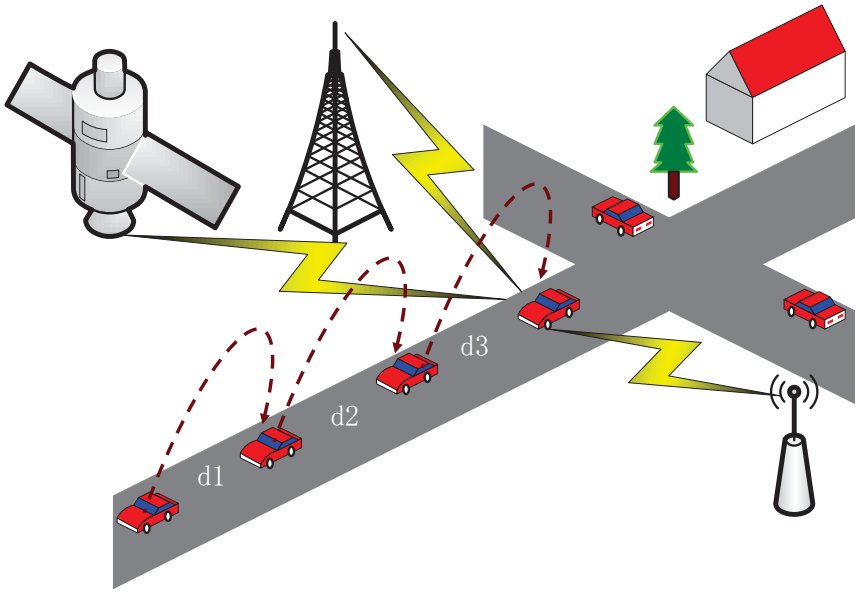

Figure 54: Platoon in VANET Framework

In general, a platoon consists r vehicles, namely vehicle 0 to vehicle $r-1$. For example, the ending vehicle can access multi-information of d_i, v_i, F_i, $i \in \{0, 1, \ldots, r-1\}$. Now, it comes out a direct question in order to achieve a consensus: which information content we should select and how to use the selected information? This will be answered in next Information Harmonization Module (IHM) analysis and

design sections.

6.2 Weighted Multi-information Structure Control Method in IHM

There are two control methods in IHM. We first use the broadcast/receiving schema to analyze the Weighted Multi-information Structure Control.

6.2.1 Analysis of Multi-inforation Structure Weighted Coefficients Selections

The main object of this method is to achieve a vehicle control goal by coordinating available information. For the clarity of our investigation, we assume vehicle j, $j \in \{0, 1, \ldots, r-1\}$ receives information of I_1 and I_2 only. Without lose the generality, we use the braking force of $f'(I_1, t) \geq f(I_2, t)$. For example, I_1 is the leading vehicle's braking information F_0, and I_2 is distance information of d^j. The main idea of this analysis is to investigate a weighted coefficient γ on each braking force so that the output of control effort can successfully meet the control goals. The output control effort $f(t, \eta)$ is a new braking function

$$f(t, \eta) = \gamma_1 f'(I_1, t) + \gamma_2 f(I_2, t). \tag{6.6}$$

where we assume $\gamma_1 + \gamma_2 = 1$ and η is a variable depends on the selections of γ.

Suppose that both information I_1 and I_2 are transmitted without any communication uncertainties, and following assumptions are also imposed.

Assumption 3 (1) The leading vehicle and following vehicle travel at the cruising condition with distance d_{ref} and speed $v(0)$. (2) The information of I_1 at $t = 0$ is immediately transmitted to vehicle j without a communication delay. (3) vehicle j use I_1 and I_2 information only. (4) Platoon starts with $f'(I_1, t) \geq f(I_2, t)$ and might stops at $f'(I_1, t) \geq f(I_2, t)$ at the same time intervals.

For notation simplification, we denote $f(I_1, t)$ as $f'(t)$ or f' and $f(I_2, t)$ as $f(t)$ or f. Let $\gamma_1 = p$, Then (6.6) becomes

$$f(t, \eta) = pf'(t) + (1 - p)f(t). \tag{6.7}$$

Theorem 28 *Under Assumption 3, total travel time T and weighted coefficient p satisfies*

$$p = \frac{v(0) - \int_0^T \frac{f(\tau)}{m} d\tau}{\int_0^T (\frac{(f'(\tau) - f(\tau))}{m}) d\tau}. \tag{6.8}$$

Proof: Since

$$\int_0^T \frac{f(\tau, \eta)}{m} d\tau = v(0).$$

We have

$$\begin{aligned}
\textstyle\int_0^T \frac{f(\tau,\eta)}{m} d\tau &= \int_0^T \frac{(pf'(\tau) + (1 - p)f(\tau))}{m} d\tau \\
&= \int_0^T \frac{p(f'(\tau) - f(\tau)) + f(\tau)}{m} d\tau \\
&= p \int_0^T \frac{f'(\tau) - f(\tau)}{m} d\tau + \int_0^T \frac{f(\tau)}{m} d\tau \\
&= v(0)
\end{aligned}$$

Let p represent by T, it is easy to get (6.8). □

Lemma 29 *From Theorem 28, if we choose two different weighted coefficient p^1,p^2, and $p^1 > p^2$, the total travel time $T^1 < T^2$*

Proof: From (6.8), we have

$$\frac{dp}{dT} = \frac{-\frac{f}{m}(\tau)\int_0^T \frac{f'(\tau)-f(\tau)}{m}d\tau - (v(0) - \int_0^T \frac{f(\tau)}{m}d\tau)\frac{(f'-f)}{m}}{(\int_0^T \frac{f'(\tau)-f(\tau)}{m}d\tau)^2} \tag{6.9}$$

Under Assumption 3, we have

$$\int_0^T \frac{f'(\tau)}{m}d\tau > \int_0^T \frac{f(\tau)}{m}d\tau \tag{6.10}$$

From (6.9) and (6.10), we get

$$\frac{dp}{dT} < 0, \tag{6.11}$$

this complete the proof. □

Define L_j as total travel distance of vehicle j, d^j_{final} as the final inter-vehicle distance when the speed of vehicle j first time reaches 0. Then we have

$$d^j_{final} = d_{ref} - (L_j - L_{j-1}), \tag{6.12}$$

Since varying p can affect the L_j if we consider the vehicles ahead of vehicle j, we only need focus on the L_j instead of d^j_{final}. IHM is to find such a p or p's that $d^j_{final} = d_{ref}$, it can be equivalently represented by total travel distance $L^j = L^j_{ref}$.

One of the extreme case is that

$$L^j_f = v(0)T - \int_0^T \int_0^t \frac{f(\tau)}{m}d\tau dt < L^j_{ref},$$

where L_n^f is the total travel length with speed information I_1 only. From 6.10, it is not difficult to verify that

$$L_{f'}^j = v(0)T - \int_0^T \int_0^t \frac{f'(\tau)}{m} d\tau dt < L_f^j < L_{ref}^j.$$

This implies that none of $p \in [0,1]$ satisfies the d_{ref} requirement.

Similarly, the other extreme case is that

$$L_{ref}^j < L_{f'}^j < L_f^j.$$

It is obvious that such a set up does not satisfy the $d_{final}^j = d_{ref}$ requirement.

Hence, we are only interesting the third case that

$$L_n^{f'} < L_{ref}^j < L_f^j.$$

Theorem 30 *If $L_n^{f'} < L_{ref}^j < L_f^j$, For a given required reference distance d_{ref}, there is a p^0 which satisfies*

$$L^j(p^0) = L_{ref}^j, \tag{6.13}$$

, where

$$L^j(p^0) = v(0)T - p^0 \int_0^T \int_0^t \frac{f'(\tau) - f(\tau)}{m} d\tau dt - \int_0^T \int_0^t \frac{f(\tau)}{m} d\tau dt \tag{6.14}$$

Proof: Let

$$\phi(T, \eta) = v(0)T - p \int_0^T \int_0^t \frac{f'(\tau) - f(\tau)}{m} d\tau dt - \int_0^T \int_0^t \frac{f(\tau)}{m} d\tau dt$$

We have

$$\frac{d\phi(T,\eta)}{dT} = v(0) - \int_0^T \frac{f(\tau)}{m} d\tau - \frac{dp}{dT} \int_0^T \int_0^t \frac{f'(\tau) - f(\tau)}{m} d\tau dt - p \int_0^T \frac{f'(\tau) - f(\tau)}{m} d\tau.$$

From 28,

$$v(0) - \int_0^T \frac{f(\tau)}{m} d\tau = p \int_0^T \frac{f'(\tau) - f(\tau)}{m} d\tau,$$

and together with (6.9), we have

$$\frac{d\phi(T,\eta)}{dT} > 0 \tag{6.15}$$

Since $L^j = \phi(T,\eta)$, together with (6.15) and (6.9), It is valid that $L^j(p^0) = L_{ref}$ and hence $d^j_{final} = d_{ref}$ when $p = p^0$. This complete the proof. □

Corollary 31 *In particular, for collision avoidance, $d_{ref} = 0$, a requirement of p_{min} must be met, and p_{min} satisfies*

$$v(0)T - p_{min} \int_0^T \int_0^t \frac{f'(\tau) - f(\tau)}{m} d\tau dt - \int_0^T \int_0^t \frac{f(\tau)}{m} d\tau dt = d_{ref} L^{j-1}$$

Proof: From (6.12),

$$d^j_{final} = 0 = d^j_{ref} - (L^j - L^{j-1}),$$

it is easy to get

$$L^j = d_{ref} + L^{j-1},$$

and this complete the proof. □

6.2.2 Simulation and Verification of Weighted Multi-information Structure Control

Example 32 when we apply weighted coefficient γ^2 on vehicle 2. Set $\gamma_1^2 = p$ on leading vehicle barking information and $\gamma_2^2 = 1 - p$ on d^2. The output control effort

from IHM of vehicle 2 becomes:

$$F^2(t) = p \times F^0(t) + (1-p) \times max(k_1 * (d^2(t) - d_{ref}) + k_2 \times (d^2(t) - d_{ref})^3, -F_{max}).$$

where $k_1 = 50$ and $k_2 = 4$.

By varying p from 0 to 1, d^2_{final} increase from 0 (m) to 54.35 (m) as shown at Fig. 55.

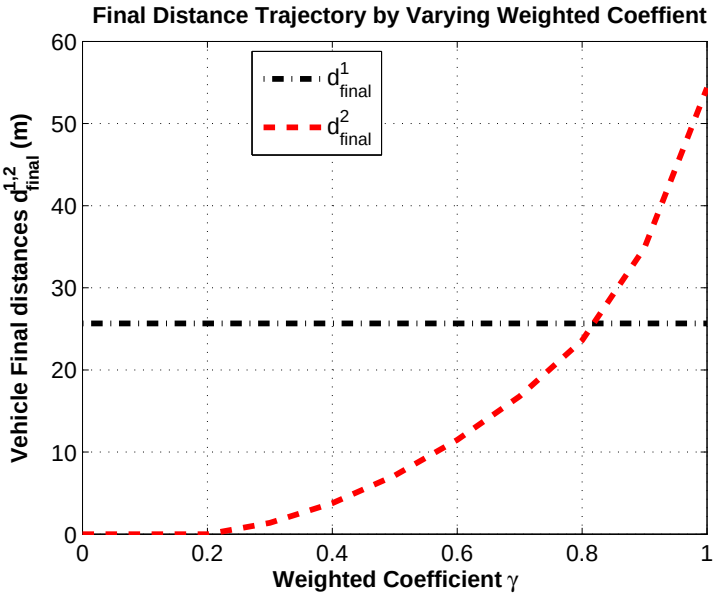

Figure 55: Inter-vehicle Distances Based on varying γ^2

When $p = p^0 = 0.91$, $d^2_{final} = d_{ref}$. Since vehicle 2 is located at the end of platoon, d^1_{final} stays at 25.65 (m). There is no effect on vehicle 0 and vehicle 1 by changing p since both are located in front of vehicle 2.

We now consider more general cases. Each vehicle j (IHM) receives multi-information and adjusts inter-vehicle distance by weighted coefficients γ^j. Any changes of γ^j affect vehicles i, where $i > j$.

Example 33 Following Example 32, we apply weighted coefficient γ^1 on vehicle 1. Set $\gamma_1^1 = p$ on leading vehicle barking information and $\gamma_2^1 = 1 - p$ on d^1. The output control effort from IHM of vehicle 1 becomes:

$$F^1(t) = p \times F^0(t) + (1-p) \times max(k_1 * (d^1(t) - d_{ref}) + k_2 \times (d^1(t) - d_{ref})^3, -F_{max}).$$

where $k_1 = 50$ and $k_2 = 4$.

As shown at Fig. 56, by varying p from 0 to 1, d^1_{final} decreases from 25.65 (m) to 20.80 (m) at the point of $p = 0.59$ then increases to $d_{ref} = 40$ (m) at the end. It is understandable that vehicle 1 can only keep the reference distance 40 (m) if vehicle 1 takes the same braking actions at the same time.

Comparing with the Example 32, vehicle 1 needs more contribution from leading vehicle's braking information than vehicle 2 in order to achieve $d_{final} = d_{ref}$. This also explains the scenario of Example 27 with 25 vehicles. Since the ending vehicle 24 takes braking actions based on the leading vehicle's braking information F^0, vehicle 24 stops too early.

Since γ^1 affects the performance of vehicle 2, d^2_{final} increases from 0 to 33.87 (m) at the point of $p = 0.8$, then drops to 25.68 (m). $d^2_{final} \neq d_{ref}$ at any point with this setup.

Example 34 Following Example 32 and Example 33, now we apply weighted coefficient γ^1 on vehicle 1 and γ^2 on vehicle 2. Set $\gamma_1^1 = \gamma_1^2 = p$ on leading vehicle barking information and $\gamma_2^1 = \gamma_2^2 = 1 - p$ on both d^1,d^2. The output control effort from IHM of vehicle 1, 2 are the same with Example 32 and Example 33 individually.

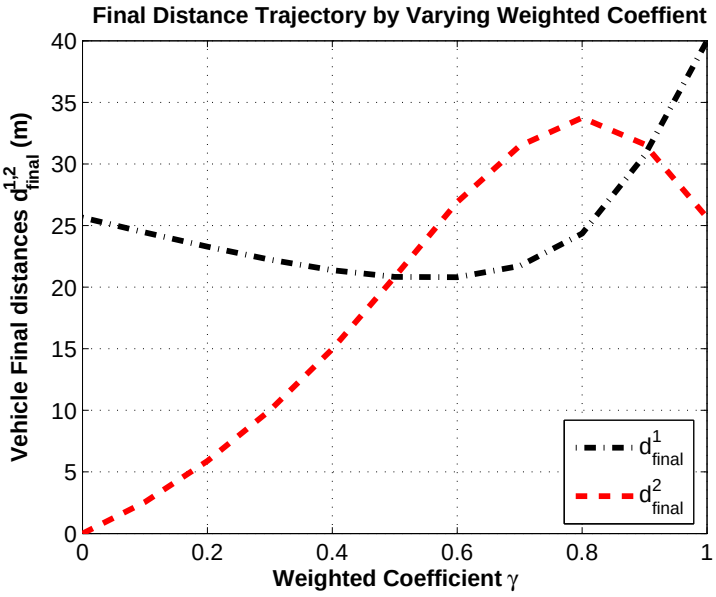

Figure 56: Inter-vehicle Distances Based on varying γ^1

As shown at Fig. 57, by varying p from 0 to 1, d^1_{final} keeps the same trajectory with Example 33 as we expected. While d^2_{final} increases 0 (m) to 40 (m). Vehicle 2 reaches d_{ref} at the point of $p = p^0 = 1$.

Again, γ^1 affects the performance of vehicle 2, by varying γ^2, we can get the point of $d^2_{final} = d_{ref}$.

6.3 Data Rate Control method in IHM

Now we exam the second control method in IHM. The main idea of data rate control is to choose information content I and request an idea data rate of I. As shown at Fig. 58, IHM can also screen available information based on control goals, and directly request data and data rate based on the system state feedback. This request/response

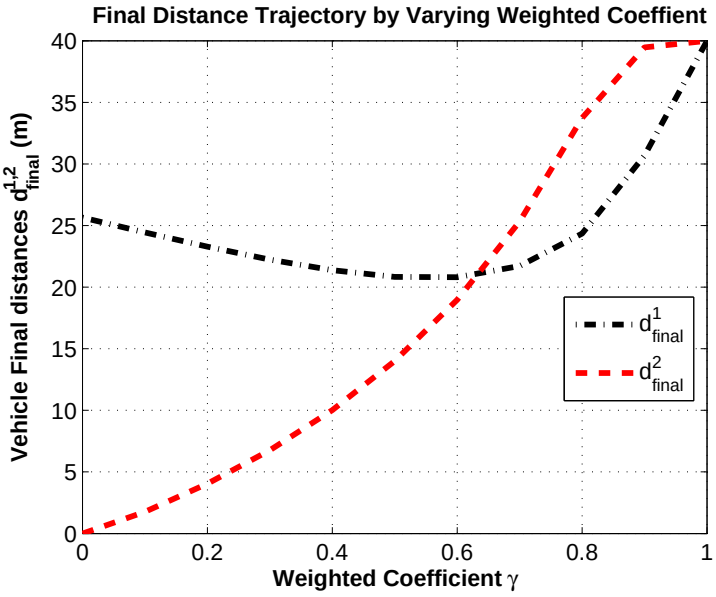

Figure 57: Inter-vehicle Distances Based on varying $\gamma^{1,2}$

schema can dramatically improve the network resources usage. Such a schema is called Information on Demand (IOD).

We now investigate why IOD can fit in this framework. From Example 32, when $\gamma_1 = 0.91$ and $\gamma_2 = 0.19$, control goal of $d_{final} = dref$ can be achieved. It means a full contribution from communication information of F^0 and d_2 are not necessary in this scenario. Then IHM informs VANET a slower data rate of both F^0 and d_2, and consequently improves the bandwidth usage of overall network. We illustrate the relationship of data rate and control goal d_{final} by a simplified two vehicles model. With vehicles V_0 and V_1 shown in Fig. 47. In this model, we only use inter-vehicle distance $d = d_1$ to control vehicle 1.

The vehicle velocities are v_0 and v_1, respectively. Define $v = v_1 - v_0$. Then the

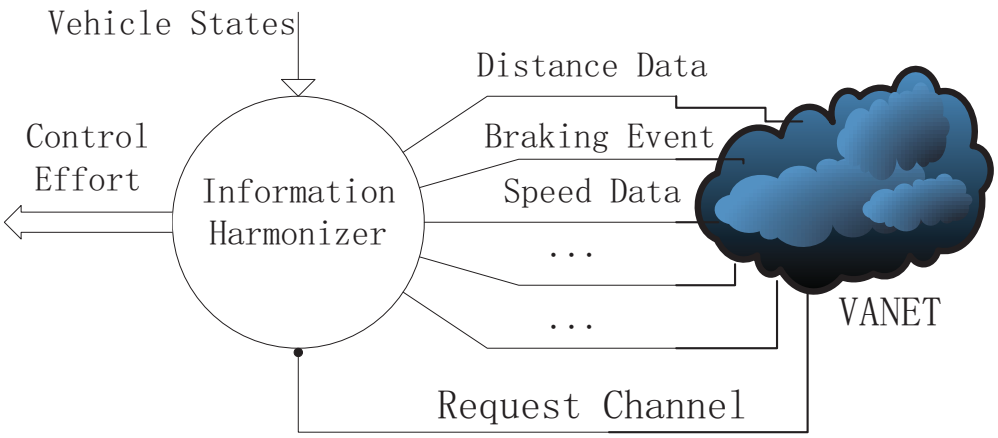

Figure 58: IHM and VANET Interactive Architecture

two-car system dynamics is 5.7

The received distance information is represented by $d_{k\tau}$, $k \in \{1, 2, \ldots\}$. Time interval τ depends on communication data rate R. Smaller τ implies faster transmission data rate. For example, a very slower communication link has a round trip time $\tau_r = 341$ (ms). Each round trip can successfully deliver a m bytes package. The package includes full information of d_k. In this case, data rate $R = m/\tau_r$, time interval between d_k and d_{k+1} is $\tau_r = \tau$. Vehicle 2 keeps using the same braking force $f(d_k)$ between time interval $k\tau$ and $(k+1)\tau$. Then, the two-vehicle system becomes

$$\begin{cases} v_{k+1} &= v_k - \tau \frac{f(d_k)}{m_0} \\ \\ d_{k+1} &= d_k - \tau v_k \end{cases} \tag{6.16}$$

Since τ is inversely proportional to data rate R, we use τ to illustrate following

examples.

Example 35 Without loss of generality, assume $v_0 = 0$. Then $v = v_1$. Vehicle masses $m_0 = m_1 = 1500$. The initial speed $v(0) = 25$ m/s and the nominal inter-vehicle distance $d_{ref} = 80$ m. The simplified feedback control function is

$$g_1(d_k) = \gamma \max\{k_1(d_k - d_{ref}), -F_{max}\} \tag{6.17}$$

where $k_1 = 115$, $F_{max} = 10000$ (N).

Suppose time interval $\tau = 0.025$ second. By varying γ, the plot at Fig. 59 shows the simulation result of the final distance d_{final}. d_{final} increases from 0 (m) to 52.19 (m) when γ changes from 0 to 1. We are interested in the point that $d_{final} = 40.75$ (m) when $\gamma = 0.8$.

Again, a partial contribution of information d is enough to achieve the control goal of $d_{final} \doteq 40$ (m).

We now exam less information contribution by decreasing increasing τ or decreasing R.

Example 36 We use the same setup as Example 35, $v_0 = 0$ and Vehicle masses $m_0 = m_1 = 1500$. The initial speed $v(0) = 25$ m/s and the nominal inter-vehicle distance $d_{ref} = 80$ m. The feedback control function is

$$g_1(d_k) = \max\{k_1(d_k - d_{ref}), -F_{max}\} \tag{6.18}$$

where $k_1 = 115$, $F_{max} = 10000$ (N).

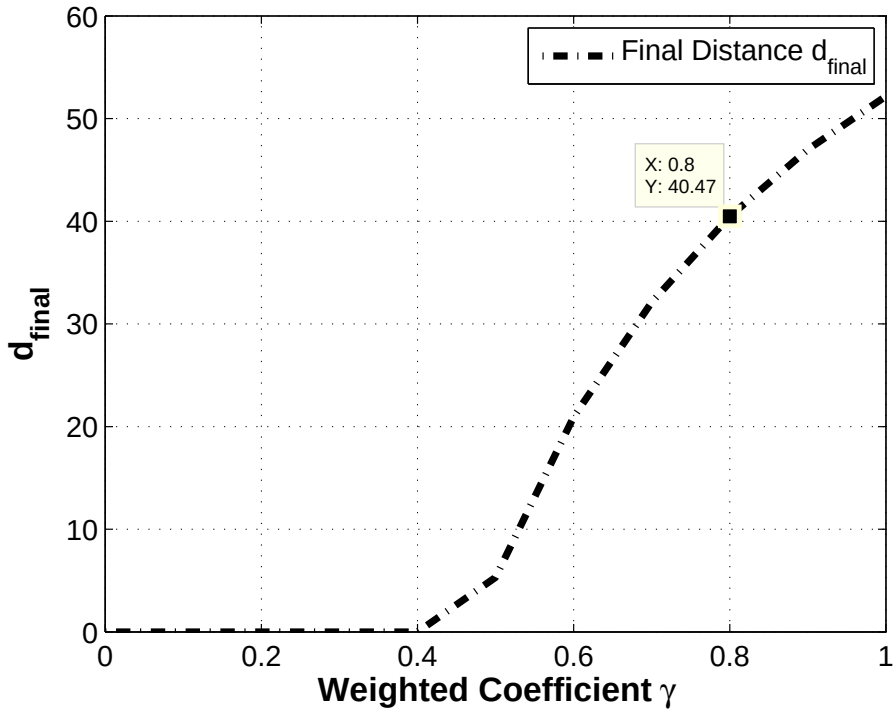

Figure 59: Final Distance vs Varying γ

We can combine (6.18) and (6.16),

$$d_{k+2} - 2d_{k+1} + (1 + \tau^2 c_0)d_k - \tau^2 c^0 d_r = 0, \tag{6.19}$$

where $c_0 = \frac{k_1}{m_0}$ is a constant. The final distance d_{final} can be represented by a function of τ, namely $d_{final} = \Theta(\tau)$ by solving the difference equation (6.19).

We assume all packages are successfully delivered. By varying time interval τ from 0.025 to 1.5, Fig 60 plots the relationship of d_{final} and time interval τ. It demonstrates function of Θ. It shows a monotone relationship: the shorter the communication round time interval, the earlier the vehicle stops.

Example 36 shows that a control goal $d_{final} \doteq 39.92$ (m) can be achieved when

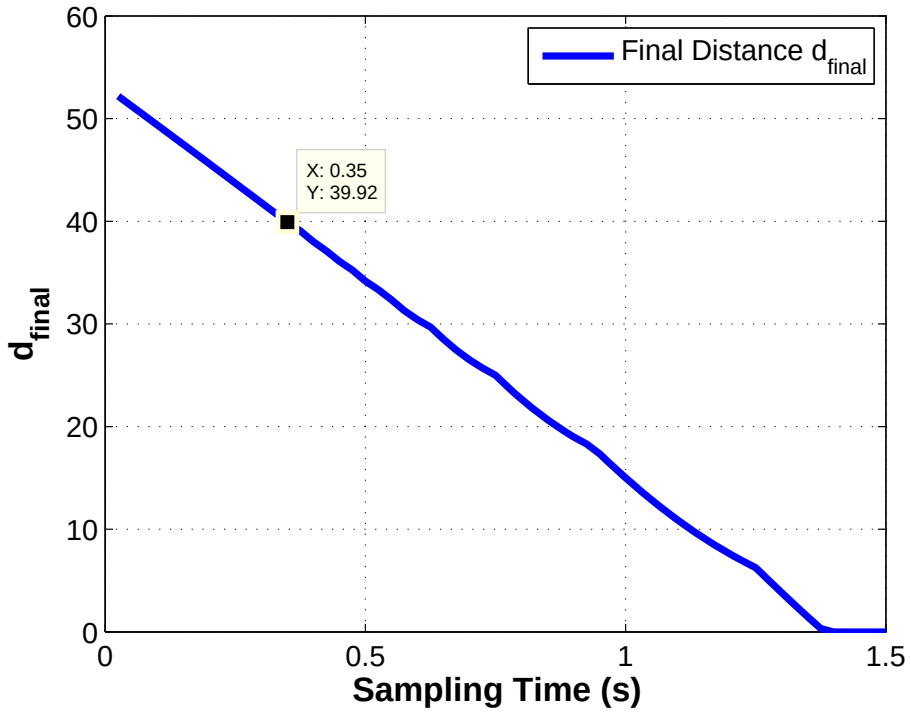

Figure 60: Final Distance vs Sampling Interval

$\tau = 0.35$. It means IHM requests a much less data rate. We use a typical Directed Short Range Communication data package size as an example. Assume a typical IPv6+UDP/TCP protocols is used in such systems, each package includes IPv6 overhead, data, error checking bits and acknowledgement. IHM requests only $0.025/0.35 = 7.1\%$ data to meet the control goal, it dramatically improves the bandwidth usage.

6.4 Case Study of Platoon Control via Data Rate Control Method

Dedicated short-range communications (DSRC) becomes a strong candidate for V2V communication technologies in VANET framework. The US Federal Communications Commission (FCC) has allocated 75MHz of spectrum in the 5.9GHz band for DSRC. We will use data rate selection/control or message rate selection/control of DSRC in this case study.

6.4.1 Data Rate Selection For DSRC

DSRC Standards include IEEE 802.11p (MAC and PHY standards) and IEEE Std 1609.1 to 1609.4. IEEE 802.11p follows IEEE 802.11e's Quality of Service support and both can provide multiple priorities to different applications by differentiating distributed coordination function (DCF)-based channel access parameters. Consequently, DCF-based schema enabled antennas can response different data rate/message rate requested by IHM as shown at Table 2 [38]. The options of data rate ranges from 3 Mbps to 27 Mbps based on modulation rate, code rate and Signal to Interference plus noise ratio (SINR) for frame reception. The higher data rate leads to shorter MAC Frame transmission duration and causes more errors with the same transmission power. On the other hand, more communication power is necessary in order to keep the same bit error rate (BER) with higher data rate.

6.4.2 IHM in DSRC

Fig. 61 shows data flow for a complete request/response round trip. For example, IHM on vehicle 1 first requests an ideal data rate for information I_j from vehicle 0.

Table 2: Data Rate Supported in DSRC

Modulation Technique	Coded Bit Rate (Mbps)	Coding Rate	Data Rate (Mbps)	Data Bits per OFDM symbols	SINR threshold (dB)
BPSK	6	1/2	3	24	5
BPSK	6	3/4	4.5	36	6
QPSK	12	1/2	6	48	8
QPSK	12	3/4	9	72	11
16-QAM	24	1/2	12	96	15
16-QAM	24	3/4	18	144	20
64-QAM	64	2/3	24	192	25
64-QAM	64	3/4	27	216	NA

IHM on vehicle 0 processes the requests and responses an approximate data rate.

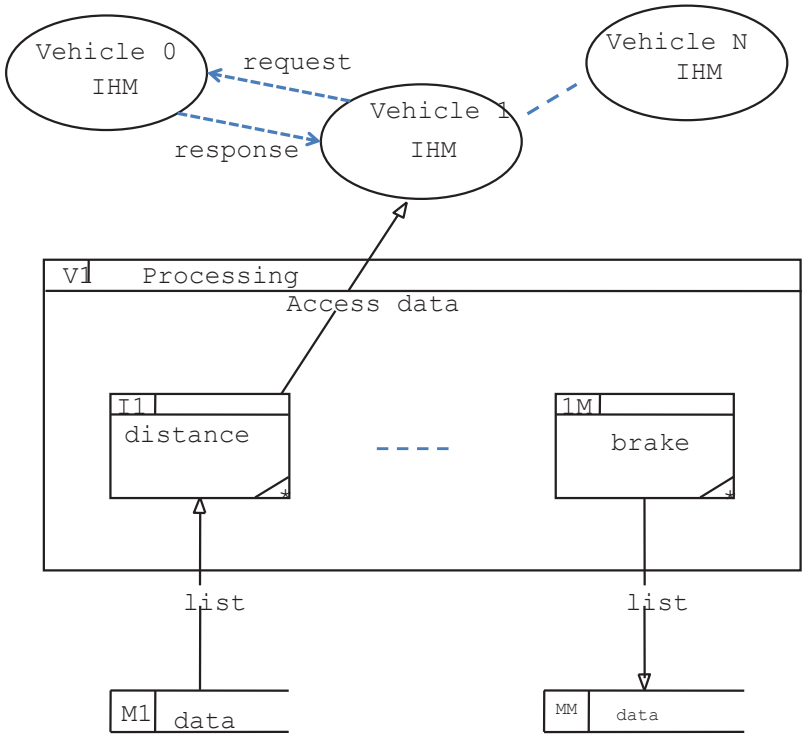

Figure 61: Request/Response Schema Data Flow

This request/response is different from client/server request/response model. Since IHM requests are based on vehicle control, any delayed process will be discarded. For example, if d_k are not processed while d_{k+1} is ready to be sent. With Redis schema, d_{k+1} is sent first then d_k. But in our schema, d_k will be discarded by IHM.

6.5 Platoon Control with Selections of DSRC Data Rate

Now we exam the platoon control with selections of DSRC data rate.

Example 37 We use the same setup as Example 36, $v_0 = 0$ and Vehicle masses

$m_0 = m_1 = 1500$. The initial speed $v(0) = 25$ m/s and the nominal inter-vehicle distance $d_{ref} = 80$ m. We assign 10% of communication usage to this link since this two vehicles are from a group of platoon. Each data package includes full information of d_k.

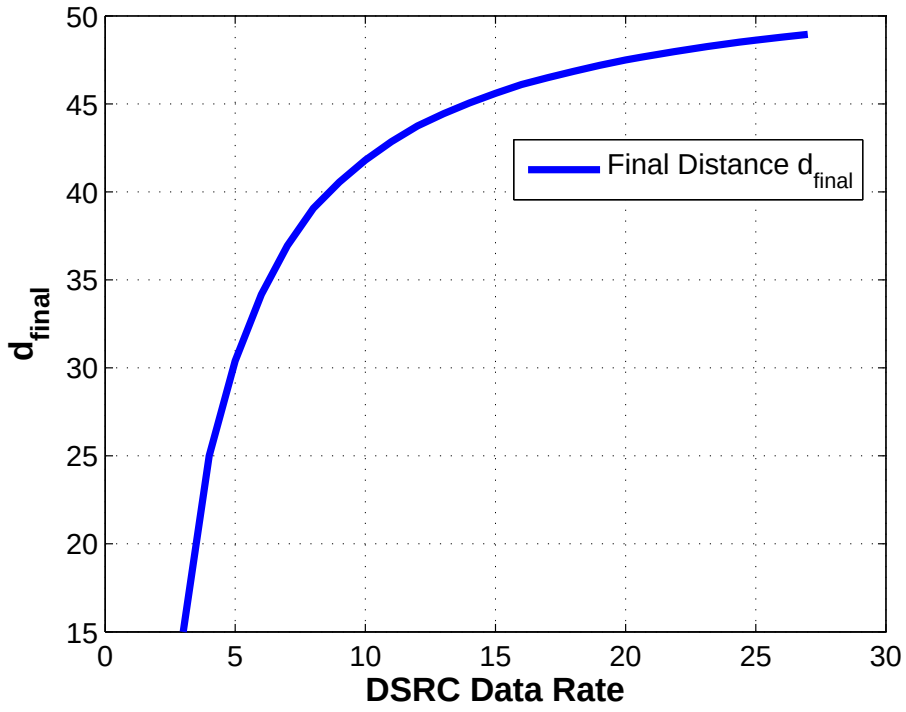

Figure 62: Final Distance vs DSRC Data Rate Selections

Fig. 62 plots the final distances with varying DSRC Data Rate from 3 (Mbps) to 27 (Mbps).

6.6 TDMA Design Considerations with Data Rate Control Method

It is likely that TDMA becomes a strong candidate for inter-vehicle communications. As shown at Fig. 63, vehicles take turns to transmit packages. The transmission slot (and packets) are constant t^0, which includes necessary guard times for modem preambles and Tx-Rx switch over latencies. A frame is of duration T_{fr}. Frame dimension or size $fr = T_{fr}/t^0$. fr is a variable. In this work, fr depends on data rate requested from platoon control side.

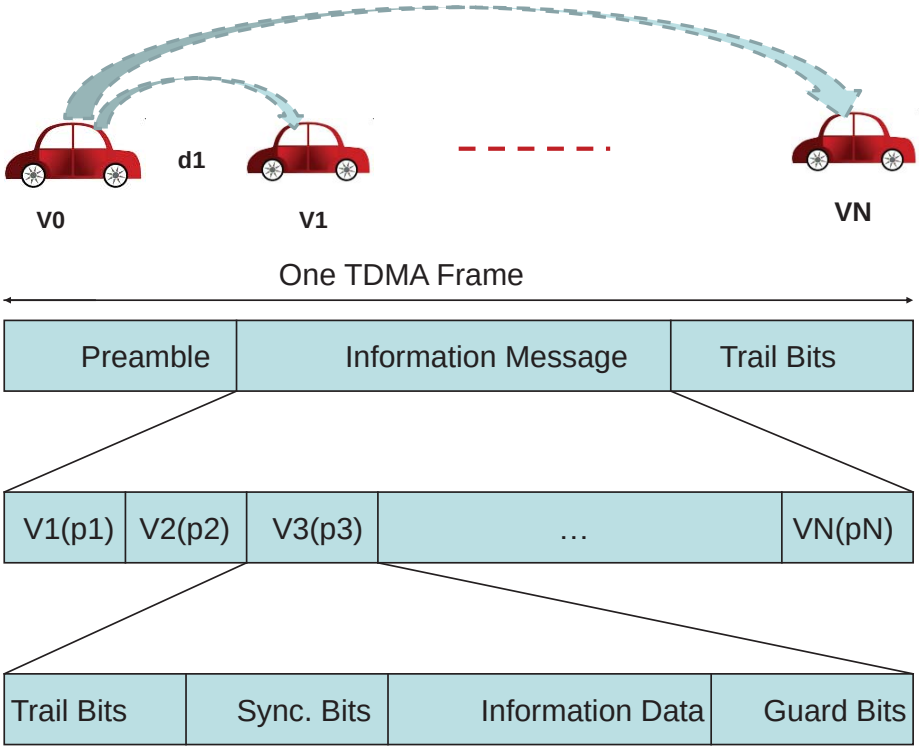

Figure 63: TDMA Slot Allocation Schema

Since an ideal data rate

$$R = [R_1, R_2, \ldots, R_N]'$$

is known, we propose a new optimal TDMA scheduling algorithm. Let

$$R_{max} = \max R_1, R_2, \ldots, R_N.$$

Theorem 38 *A time slot scheduling is optimal when*

$$\bar{fr} = \frac{1}{R_{max}} \sum_{i=1}^{N} R_i \tag{6.20}$$

Proof: Assume data size of each slot/packet is m^0 (Mb). Vehicle j needs to transmit m_j (Mb) data. Vehicle with R_{max} transmits m_{max}. Then

$$m_j = m_{max} \frac{R_j}{R_{max}}.$$

Each frame allows transmit each vehicle at most one packet. Then the total frames fr_{total} are decided by the minimum number of packets/slots for R_{max}.

$$fr_{total} = fr_{min} = S_{max} = \frac{m_{max}}{m^0}. \tag{6.21}$$

where S_{max} is the number of slots for vehicle with R_{max}. Since all R_j, $j \in \{1, 2, \ldots, N\}$ are known parameters, we can get slots for each vehicle

$$S_i = \frac{m_{max R_j}}{m^0 R_{max}}.$$

Then number of total slots can be represented by

$$S_{total} = \frac{m_{max}}{m^0} \frac{1}{R_{max}} \sum_{i=1}^{N} R_i,$$

together with the total frames of (6.21), we can (6.20). This completes the proof. □

Now we propose a new scheduling schema to meet the optimal slots allocation requirement.

Data Rate Based Priority: Due to the different data rate requests from different users/vehicles, we set higher priority for higher data rate vehicle. For example, a slot is assigned to vehicle j as long as there is no higher priority vehicles in the same frame.

Data Rate Based Allocation Probability: The probability p^j of allocating vehicle j a slot depends on data rate also. Assume it is vehicle j's turn to be assigned a slot, the probability

$$p^j = \frac{R_j}{R_{max}}.$$

If vehicle j get a slot successfully, then this slot i is not available anymore. Otherwise, slot i will be considered for next vehicles with lower priority than vehicle j.

Theorem 39 *Data rate based scheduling leads to an optimal TDMA slots allocation,*

$$\mathbb{E}(fr) = fr_{min}. \tag{6.22}$$

Proof: A slot time duration of vehicle j is t^j. Since

$$\mathbb{E}(t_j) = p^j t^0 = \frac{R_j}{R_{max}} t^0,$$

then a frame duration

$$\mathbb{E}(T_{fr}) = \frac{t^0}{R_{max}} \sum_{i=1}^{N} R_i.$$

Recall that t^0 is a constant, then number of frames

$$\mathbb{E}(fr) = \frac{1}{R_{max}} \sum_{i=1}^{N} R_i = fr_{min}.$$

This completes the proof. □

Synchronization with Platoon Control: Above setup can guarantee a relative data rate response for all requests. Now we only need to synchronize communication with control steps. If TDMA allocation is faster than control requirements, TDMA leaves certain slots for other random access usage. If control demands a faster response, TDMA begins to borrow slots from next frequencies. Overall, data rate can successfully achieved for platoon control objects.

6.7 Considerations of Communication Uncertainties

When we consider the communication uncertainties, IHM design involves stochastic analysis of information contents since communication introduces uncertainties such as delay, jitter and package loss. We use the setup of two vehicles platoon model for this analysis.

Following Example 36, we assume vehicle 1 can access the distance information d by wireless communication or radar frequency. The first step of platoon control is to select one from these two options.

(1) Package Delivery Digital Wireless Communication Model We model wireless communication as package delivery model. In this model, vehicle 1 either

receives d or none. The system 5.7 becomes

$$\begin{cases} \dot{v} &= -\frac{f(\tilde{d})}{m_0} \\ \\ \dot{d} &= -v \end{cases} \tag{6.23}$$

where

$$v = v_1 - v_0.$$

The received distance information under sampling interval τ can be represented by

A link-connection variable γ_k to indicate if the packet is delivered ($\gamma_k = 1$) or lost ($\gamma_k = 0$). As a result, assuming that γ_k is i.i.d., we denote the package delivery rate (PDR) by $\rho = P\{\gamma_k = 1\}$.

(2) Resolution Based Radar Frequency Model Taking into consideration radar resolution, the measured distance is $\widehat{td} = d + \gamma\delta$, where γ is a resolution level and δ is a standard Gaussian noise $\mathcal{N}(0, 1)$.

If we select radar frequency, the system becomes

$$\begin{cases} \dot{v} &= -\frac{f(\widehat{td})}{m_0} \\ \\ \dot{d} &= -v \end{cases} \tag{6.24}$$

Both information resources have random characteristics. We need to analyze the problem from the stochastic perspectives.

Example 40 Following Example 36, we first select wireless communication with package delivery rate $\rho = 70\%$. The plot at Fig. 64 shows final distance d_{final} distribution at sampling interval $\tau = 0.1$ (second).

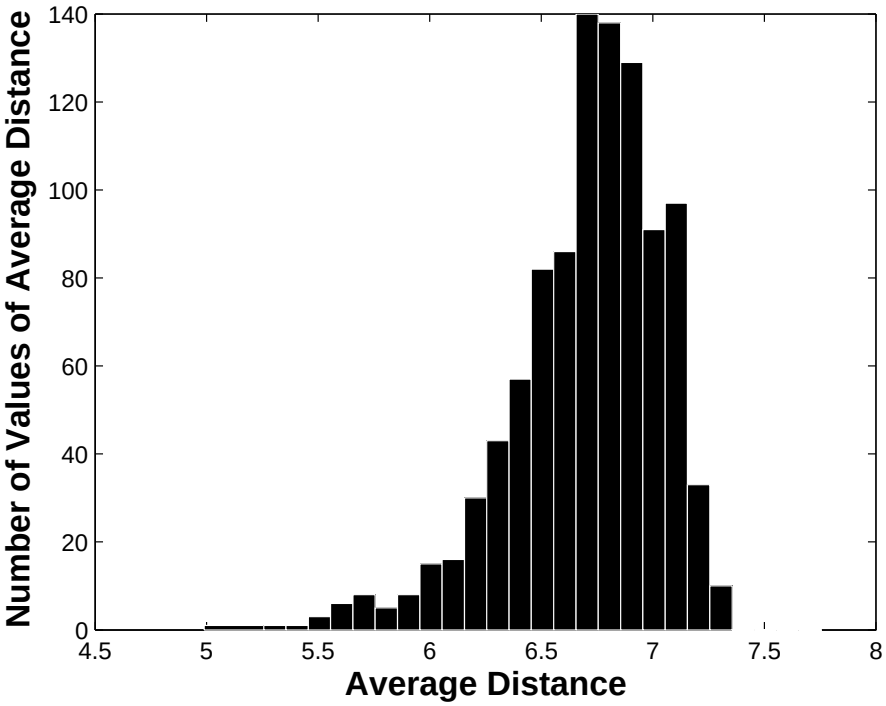

Figure 64: Final Distance Distribution with Wireless Communication at $\rho = 70\%$

We use the same setup, but select Radar wit resolution level 1 (m). Simulation result is shown at Fig. 65 with the same sampling interval $\tau = 0.1$ (second).

Comparing these two resources, the mean value of final distance $\mathbb{E} = 6.84$ (m) for wireless communication while it is 49.32 (m) for radar. But if we look at the details of final distance distribution, it is easy to find the probability of collision is very high with radar frequency.

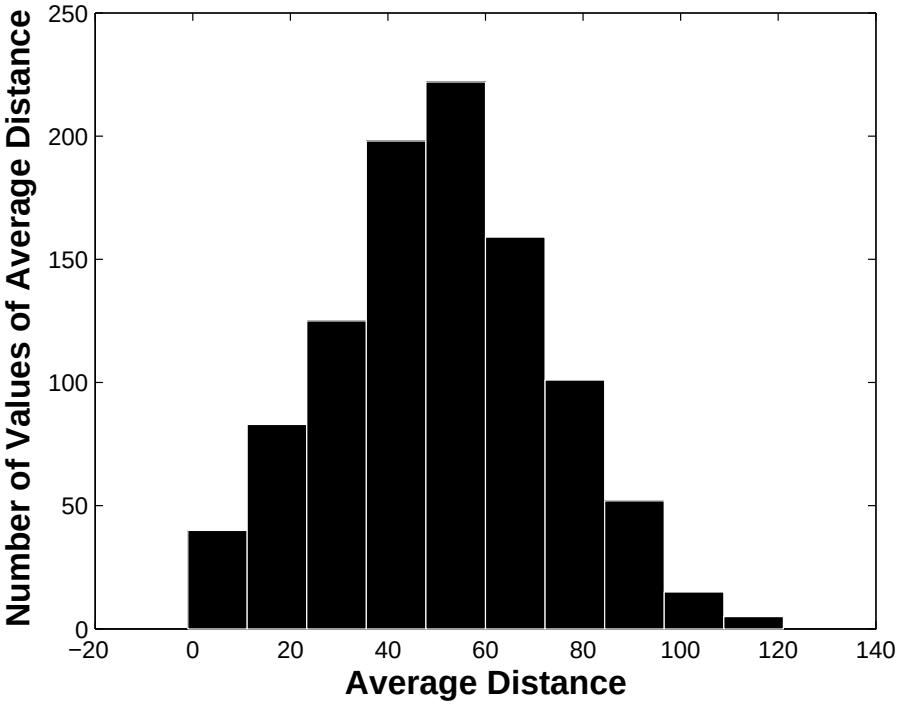

Figure 65: Final Distance with Radar Frequency at Resolution Level 1 (m)

Information content selection becomes very complicated due to the stochastic features of transmissions. IHM needs a very careful design when we consider such uncertainties including package loss, delay and jitter.

7 ENHANCED NETWORK ROBUSTNESS BY DITHERS

This section investigates impact of communication channels on feedback stability and performance and introduces new schemes to enhance feedback robustness against communication channel uncertainties. While communication systems may be integrated into a feedback system through different configurations, such as sensor networks, distributed actuators, topology -constrained team coordinations, to gain a fundamental understanding of the issues involved, this thesis will focus on the basic feedback system in which the output of a plant is processed and communicated through a communication system to form a feedback look, shown Figure 66. In principle, a control system may use either a shared network or a dedicated link for communications to connect. This section will use the dedicated link for remote control systems as a benchmark, see the right-side configuration in Figure 66.

The combined plant $P(s)$ and the controller $C(s)$ form the open-loop system denoted by G. Suppose G has a state space realization

$$\begin{cases} \dot{x}(t) = Ax(t) + Bu(t) \\ \\ y(t) = Cx(t) \end{cases}$$

Without uncertainties from communication channels, the control is the negative unity

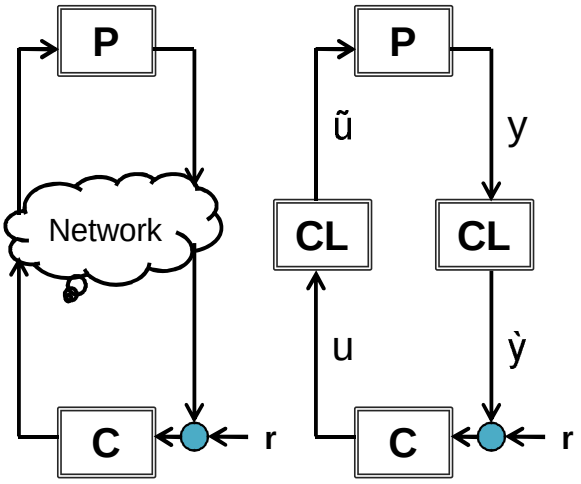

Figure 66: Feedback System over Communication Channel

feedback $u = -y$, and the close-loop system is

$$\begin{cases} \dot{x}(t) = Ax(t) + Bu(t) = (A - BC)x(t) = A_0 x(t) \\ \\ y(t) = Cx(t) \end{cases} \tag{7.1}$$

When a communication link is inserted in the feedback loop, the output signal must be sampled. Although periodic sampling is commonly used, communication scheduling and event-based sampling often lead to irregular sampling. This thesis will accommodate general sampling schemes. Suppose that τ_k is the sampling interval which may change with time. Then, the open-loop system may be approximated by

$$\begin{cases} x_{k+1} = x_k + \tau_k(Ax_k + Bu_k) \\ \\ y_k = Cx_k \end{cases} \tag{7.2}$$

Note that for $t_0 = 0$ and $t_k = \sum_{i=1}^{k} \tau_i$, $x_k = x(t_k)$ and $y_k = y(t_k)$. Under the standard zero-order hold (ZOH) framework $u(t) = u_k, t \in [t_k, t_{k+1})$.

7.1 Preliminaries of Stochastic Dithers

7.1.1 Systems

The basic feedback system consists of a plant whose output is processed and communicated through a dedicated communication link to form a feedback loop. The plant $P(s)$ and controller $C(s)$ are combined to form the open-loop system G that has a state-space realization

$$\begin{cases} \dot{x}(t) = Ax(t) + Bu(t) \\ \\ y(t) = Cx(t). \end{cases}$$

Without uncertainties from communication channels, the feedback loop is formed by the negative unity feedback $u = -y$, and the resulting closed-loop system is

$$\dot{x}(t) = Ax(t) + Bu(t) = (A - BC)x(t) = A_0 x(t). \tag{7.3}$$

When communication channels are involved, the output signal $y(t)$ will be sampled. Suppose that τ_k is the kth sampling interval which may change with time. For

small τ_k, the open-loop system is approximated by

$$\begin{cases} x_{k+1} = x_k + \tau_k(Ax_k + Bu_k) \\ \\ y_k = Cx_k \end{cases} \tag{7.4}$$

where starting at $t_0 = 0$ with $t_k = \sum_{i=1}^{k} \tau_i$, we denote $x_k = x(t_k)$ and $y_k = y(t_k)$. The feedback control is $u_k = -y_k$. Under the standard zero-order hold (ZOH) framework, $u(t) = u_k, t \in [t_k, t_{k+1})$.

Typical digital communications consist of several essential function blocks, such as sampling, data compression, quantization, source coding, channel coding, and modulation at the sending side; and demodulation, decoding, and signal reconstruction at the receiving side [40]. Communication channels introduce uncertainties of various types. In this thesis, we consider combined additive and multiplicative communication uncertainties

$$\widehat{y}_k = g_k y_k + e_k \tag{7.5}$$

where e_k is an additive noise and g_k is the gain uncertainty, both being random. Since the additive noise e_k is independent of the signal y_k, it will affect system performance, such as control accuracy and error bounds, but not robust stability. With the feedback control $u_k = -\widehat{y}_k = -g_k y_k - e_k$, the closed-loop system becomes

$$x_{k+1} = x_k + \tau_k((A - g_k BC)x_k - Be_k). \tag{7.6}$$

Note that for constant uncertain gains $g_k = g$, stability of the closed-loop system is determined by $A - gBC$.

The random gain g_k will affect stability directly. The robustness of a feedback system against gain uncertainties is often quite limited. For example, consider the open-loop system

$$\dot{x}(t) = ax(t) + bu(t)$$

with $a > 0$ and $b > 0$, This system can be stabilized by a constant feedback $u = -gx$, if $a - bg < 0$. The robustness range for the uncertain gain g is $(a/b, \infty)$. Obviously, the feedback mechanism cannot tolerate sign changes in transmission gains.

7.1.2 Scaled Dithers

Instead of sending only y_k, a scaled dither is now added to form a new signal z_k to be sent through the communication channel

$$z_k = y_k + \alpha(\tau_k, y_k)d_k \tag{7.7}$$

where d_k is the stochastic dither. The scaling factor $\alpha(\tau_k, y_k)$ is both signal dependent and sampling interval dependent, and selected as

$$\alpha(\tau_k, y_k) = \frac{\gamma}{\sqrt{\tau_k}} y_k, \tag{7.8}$$

for some design variable $\gamma > 0$. The reason for this choice will become clear soon. The communication channel introduces uncertainties as in (7.5) and generates a received signal $\widehat{z}_k$

$$\widehat{z}_k = g_k z_k + e_k. \tag{7.9}$$

Then the feedback becomes $u_k = -\widehat{z}_k$.

Assumption 1 (1) $\{d_k\}$ is an independent and identically distributed (i.i.d) Gaussian distributed random dither such that $Ed_k = 0$ and $Ed_k^2 = 1$.

(2) The unknown gain $\{g_k\}$ is a bounded sequence of stationary, uniform mixing process ([39, pp. 350-351]), independent of $\{d_k\}$ such that its mixing measure ψ_k satisfies $\sum_{k=0}^{\infty} \psi_k^{1/2} < \infty$ and that $Eg_k = \overline{g}$.

(3) $\{e_k\}$ is another sequence of stationary mixing process such that $Ee_k = 0$ and $E|e_k|^{2+q} < \infty$ for some $q > 0$, and that its mixing measure $\widetilde{\psi}_k$ satisfies $\sum_k \widetilde{\psi}_k^{q/(1+q)} < \infty$.

From (7.4) and (7.9), the control signal is

$$u_k = -g_k(y_k + \frac{\gamma}{\sqrt{\tau_k}} y_k d_k) - e_k = -g_k(Cx_k + \frac{\gamma}{\sqrt{\tau_k}} Cx_k d_k) - e_k. \tag{7.10}$$

Consequently, the closed-loop system becomes

$$x_{k+1} = x_k + \tau_k(A - g_k BC)x_k - \sqrt{\tau_k} g_k \gamma BCx_k d_k - \tau_k Be_k, \tag{7.11}$$

where the sampling interval sequence $\{\tau_k\}$ is interpreted interchangeably as *the stepsize*, and assumed to satisfy $\tau_k > 0$, $\tau_k \to 0$ as $k \to \infty$, and $\sum_{j=0}^{\infty} \tau_j = \infty$. In applications of periodic sampling, τ_k is a small constant τ. So we will also consider a constant stepsize algorithm of the form

$$x_{k+1} = x_k + \tau(A - g_k BC)x_k - \sqrt{\tau} g_k \gamma BCx_k d_k - \tau Be_k. \tag{7.12}$$

For simplicity, assume that x_0 is not random and not dependent on τ. Both (7.11) and (7.12) are Euler-Maruyama types of recursion. In fact, they can be studied by means of stochastic approximation methods [51].

To relate them to continuous-time dynamic systems, for the decreasing stepsize algorithm (7.11), we define t_k as before, introduce piecewise constant interpolations $x^0(\cdot)$ as $x^0(t) = x_k$ for $t \in [t_k, t_{k+1})$, and denote the shifted sequence of functions $x^k(t) = x^0(t + t_k)$, and $m(t) = \max\{k : t_k \leq t\}$. For the constant stepsize algorithm (7.12), we define $x^\tau(t) = x_k$ for $t \in [\tau k, \tau k + \tau)$. Consider, for instance, the case of constant stepsize algorithm and the scaled noise

$$\widetilde{w}^\tau(t) = \sqrt{\tau} \sum_{k=0}^{t/\tau - 1} g_k d_k,$$

where $t/\tau = \lfloor t/\tau \rfloor$ is the integer part of t/τ (for notational simplicity, we suppress the floor function notation henceforth). Under Assumption 1, as $\tau \to 0$, $\widetilde{w}^\tau(\cdot)$ converges weakly to $\widetilde{w}(\cdot)$, a Brownian motion with covariance $\widehat{g}^2 t$ and

$$\widehat{g}^2 = E g_0^2 d_0^2 + 2 \sum_{k=1}^{\infty} E g_k d_k g_0 d_0 = E g_0^2.$$

Likewise, we can define for the algorithm (7.11)

$$\widehat{w}^k(t) = \sum_{j=k}^{m(t+t_k)-1} \sqrt{\tau_j} g_j d_j.$$

We can also show that $\widehat{w}^k(\cdot)$ converges weakly to a Brownian motion $\widehat{w}(\cdot)$ with covariance $\widehat{g}^2 t$.

The Brownian motion limits obtained above can be represented by using the above observations and the techniques of stochastic approximation. Under constant step sizes, $x^\tau(\cdot)$ converges weakly to $x(\cdot)$ that is a solution of a stochastic differential equation (SDE). In this process, the noise e_k and the signal g_k vary much faster than that of the "state" x. As a result, e_k is averaged to 0, and the drift involving g_k

is averaged to $\overline{g} = Eg_k$. Furthermore, the Brownian motion $\widetilde{w}(\cdot)$ (or $\widehat{w}^k(\cdot)$) can be replaced by a standard Brownian motion $w(\cdot)$. The proof of the following theorem is omitted and the reader is referred to [51, Chapters 7 & 10] for further details. Consequently, the stability of (7.11) or (7.12) can be analyzed by using its limit SDE.

Theorem 41 *Under Assumption 1, both $x^\tau(\cdot)$ and $x^k(\cdot)$ converge weakly to $x(\cdot)$ such that $x(\cdot)$ is a solution of the stochastic differential equation*

$$dx = (A - \overline{g}BC)xdt + \widehat{g}\gamma BCxdw \tag{7.13}$$

where $w(\cdot)$ is a standard Brownian motion.

7.2 Feedback Robustness against Gain Uncertainties

7.2.1 Stochastic Differential Equations and Itô's Formula

The enhancement of stability robustness by the scaled dither is based on Itô's Formula in stochastic differential equations [52, 41, 42]. In its applications to linear time-invariant systems, suppose that $x(t) \in \mathbb{R}^n$ is a real-valued stochastic process satisfying

$$x(t) = x(t_0) + \int_{t_0}^{t} Mx(r)dr + \int_{t_0}^{t} Hx(r)dw(r), \tag{7.14}$$

where $M, H \in \mathbb{R}^{n\times n}$ and $w(\cdot)$ is the one-dimensional standard Brownian motion. The solution $x(\cdot)$ can also be written as

$$dx = Mxdt + Hxdw. \tag{7.15}$$

In our approach, the diffusion is created by the added scaled dither.

Definition 42 *The SDE (7.15) is said to be exponentially stable w.p.1 if its Liapunov exponent satisfies*

$$\limsup_{t\to\infty} \frac{1}{t} \log |x(t)| < 0 \quad w.p.1,$$

where $|\cdot|$ *is the Euclidean norm.*

From (7.13), we have $M = A - \overline{g}BC$ and $H = \widehat{g}\gamma BC$, with $\overline{g} = Eg_k$ and $\widehat{g} = E\widehat{g}_0^2$. For the case of scalar systems, x is a scalar and

$$dx = mxdt + hxdw. \tag{7.16}$$

By Itô's Formula [52, 42], the solution to (7.16) is

$$x(t) = e^{(m-\frac{1}{2}h^2)t+hw}x(0), \tag{7.17}$$

with the given initial condition $x(0)$. By the local martingale convergence theorem [43], $w(t)/t \to 0$ w.p.1. As a result,

$$\limsup_{t\to\infty} \frac{\log |x(t)|}{t} = m - \frac{1}{2}h^2. \tag{7.18}$$

Consequently, the SDE (7.16) is exponentially stable if $m - \frac{1}{2}h^2 < 0$. The dither term $-\frac{1}{2}h^2$ provides a stabilizing effect.

7.2.2 Impact of the Scaled Dither on Gain Robustness

To proceed, we now explore first-order systems in detail. In this case, $A = a$, $B = b$, $C = c$, all scaler constants. For the system to be controllable and observable, it requires that $b \neq 0$ and $c \neq 0$. By (7.18) with $m = a - \overline{g}bc$ and $h = \widehat{g}\gamma bc$, the stability

condition becomes

$$f_c(\overline{g}, \widehat{g}^2) = m - \frac{1}{2}h^2 = a - \overline{g}bc - \frac{1}{2}\widehat{g}^2\gamma^2 b^2 c^2 < 0. \tag{7.19}$$

Suppose that the uncertainty on g_k is characterized by an uncertainty set Ω on $(\overline{g}, \widehat{g}^2)$. Then the robust stability requires that

$$\sup_{(\overline{g},\widehat{g}^2)\in\Omega} f_c(\overline{g}, \widehat{g}^2) < 0, \tag{7.20}$$

or equivalently

$$\sup_{(\overline{g},\widehat{g}^2)\in\Omega} (\widehat{g}^2\gamma^2 b^2 c^2 + 2\overline{g}bc - 2a) > 0. \tag{7.21}$$

By expressing $g_0 = \overline{g} + \varepsilon_0$ where $E\varepsilon_0 = 0$ and $E\varepsilon_0^2 = \sigma_g^2$, we have

$$\widehat{g}^2 = Eg_0^2 = \overline{g}^2 + \sigma_g^2.$$

Hence, the condition (7.19) is equivalent to

$$\overline{g}^2\gamma^2 b^2 c^2 + 2\overline{g}bc - 2a + \sigma_g^2\gamma^2 b^2 c^2 > 0. \tag{7.22}$$

Theorem 43 *Suppose that σ_g^2 is bounded below by some constant μ, $\sigma_g^2 \geq \mu > 0$. If γ is designed to satisfy*

$$\gamma^2 > \frac{a + \sqrt{a^2 + \mu b^2 c^2}}{\mu b^2 c^2} \tag{7.23}$$

then the SDE (7.16) is exponentially stable for all $\overline{g}$ and $\sigma_g^2 \geq \mu$.

Proof: The roots of the polynomial (as a function of $\overline{g}$)

$$\overline{g}^2\gamma^2 b^2 c^2 + 2\overline{g}bc - 2a + \sigma_g^2\gamma^2 b^2 c^2 = 0$$

are

$$\lambda_{1,2} = \frac{-bc \pm |bc|\sqrt{1 + 2a\gamma^2 - \sigma_g^2\gamma^4 b^2 c^2}}{\gamma^2 b^2 c^2}. \tag{7.24}$$

Observe that the condition for $\lambda_{1,2}$ to be complex is

$$1 + 2a\gamma^2 - \sigma_g^2\gamma^4 b^2 c^2 < 0. \tag{7.25}$$

By solving γ^2 from

$$1 + 2a\gamma^2 - \sigma_g^2\gamma^4 b^2 c^2 = 0$$

we obtain the positive solution as

$$\gamma^2 = \frac{a + \sqrt{a^2 + \sigma_g^2 b^2 c^2}}{\sigma_g^2 b^2 c^2}. \tag{7.26}$$

Since the right hand side of (7.26) is monotone with respect to σ_g^2, if (7.23) is satisfied,

$$1 + 2a\gamma^2 - \sigma_g^2\gamma^4 b^2 c^2 < 0.$$

This implies that $\lambda_{1,2}$ are complex. Consequently, (7.22) is satisfied. This implies that the SDE (7.16) is exponentially stable. Since this is valid for for all $\overline{g}$ and any $\sigma_g^2 \geq \mu$, the proof is complete. □

In the special case of deterministic but unknown g_k, namely $\sigma_g^2 = 0$, the above analysis can be directly applied to the degenerative stability condition

$$\overline{g}^2\gamma^2 b^2 c^2 + 2\overline{g}bc - 2a > 0.$$

In this case the following results hold.

Theorem 44 *(1) If $a < 0$, representing stable open loop systems, then by selecting $\gamma^2 > 1/(2|a|)$, the closed-loop system is stable for all $\overline{g}$.*

(2) If $a \geq 0$, representing unstable open-loop systems, then for any given γ, the closed-loop system is stable for all $\overline{g} \in \Omega = (-\infty, \lambda_1) \cap (\lambda_2, \infty)$, where

$$\lambda_1 = \frac{-bc - |bc|\sqrt{1+2a\gamma^2}}{\gamma^2 b^2 c^2}, \lambda_2 = \frac{-bc + |bc|\sqrt{1+2a\gamma^2}}{\gamma^2 b^2 c^2}.$$

Proof: Note that the roots of the polynomial $\gamma^2 \overline{g}^2 b^2 c^2 + 2\overline{g}bc - 2a$ are

$$\lambda_{1,2} = \frac{-bc \pm |bc|\sqrt{1+2a\gamma^2}}{\gamma^2 b^2 c^2}.$$

(1) If $a < 0$ and $\gamma^2 > 1/(2|a|)$, λ_1 and λ_2 are complex. As a result, $\gamma^2 \overline{g}^2 b^2 c^2 + 2\overline{g}bc - 2a > 0$ for all $\overline{g}$. This implies that the SDE (7.16) is exponentially stable for all $\overline{g}$.

(2) If $a \geq 0$, then $1 + 2a\gamma^2 \geq 0$. It follows that $\gamma^2 \overline{g}^2 b^2 c^2 + 2\overline{g}bc - 2a > 0$ if and only if $\overline{g} < \lambda_1$ or $\overline{g} > \lambda_2$.

□

Remark 45 Note that $\lim_{\gamma\to\infty} \lambda_1 = 0$, $\lim_{\gamma\to\infty} \lambda_2 = 0$. As a result, for any compact set $\Omega_0 \subset (-\infty, 0) \cap (0, \infty)$, there exists γ such that the closed-loop system is robustly stable for all $g_0 \in \Omega_0$. The added dither creates a desirable stabilizing factor that can tolerate random uncertain gains with sign changes. Such robustness cannot be achieved by a deterministic feedback.

7.2.3 Robustness Bounds on Relative Gain Uncertainties

It is common in practice that gain uncertainties are expressed in relative terms: $g_k = (1 + \delta_k)\overline{g}$, where $\overline{g}$ is the nominal gain and δ_k is the relative gain uncertainty.

Assumption 2 *δ_k is i.i.d. with $E\delta_k = 0$ and $E\delta_k^2 = \sigma_\delta^2 > 0$.*

Under Assumption 2, $Eg_0 = \overline{g}$ and $Eg_k^2 = \overline{g}^2(1+\sigma_\delta^2)$. In this case, the stability condition (7.21) takes the form

$$\overline{g}^2(1+\sigma_\delta^2)\gamma^2 b^2 c^2 + 2\overline{g}bc - 2a > 0. \tag{7.27}$$

The following results hold. While the results cannot be directly derived from Theorem 44, the proof is similar, and hence omitted.

Theorem 46 *(1) If $a < 0$, representing stable open loop systems, then by selecting $\gamma^2 > 1/(2|a|(1+\sigma_\delta^2)$, the closed-loop system is stable for all $\overline{g}$.*

(2) If $a \geq 0$, representing unstable open-loop systems, then for any given γ, the closed-loop system is stable for all $\overline{g} \in \Omega = (-\infty, \lambda_1) \cap (\lambda_2, \infty)$, where

$$\lambda_1 = \frac{-bc - |bc|\sqrt{1+2a\gamma^2(1+\sigma_\delta^2)}}{\gamma^2(1+\sigma_\delta^2)b^2c^2}, \lambda_2 = \frac{-bc + |bc|\sqrt{1+2a\gamma^2(1+\sigma_\delta^2)}}{\gamma^2(1+\sigma_\delta^2)b^2c^2}.$$

Example 47 Consider the system $\dot{x} = 2x + u$. We compare the closed-loop systems with or without the added dithers. We consider the deterministic unknown gains g_0. Suppose that the gain uncertainty satisfies $|g_0| \geq 1$. Figure 67 shows three cases: (a) Nominal feedback with $g_0 = 3$; (b) The gain is perturbed to a much reduced value $g_0 = 1$; (c) When channel uncertainties result in a sign change on the gain to $g_0 = -1$. Without the dither, the closed-loop system is unstable under (b) and (c). The simulation results demonstrate that with the added dither, the feedback system retains stability under all perturbed gains, hence is more robust.

7.2.4 Pure Dither Feedback

It is possible to use a pure dither feedback to gain robust stability. Suppose that instead of (7.7), we only use $z_k = \frac{\gamma y_k}{\sqrt{\tau_k}} d_k$. Then, the SDE (7.16) becomes

$$dx = axdt + \widehat{g}\gamma bcdw.$$

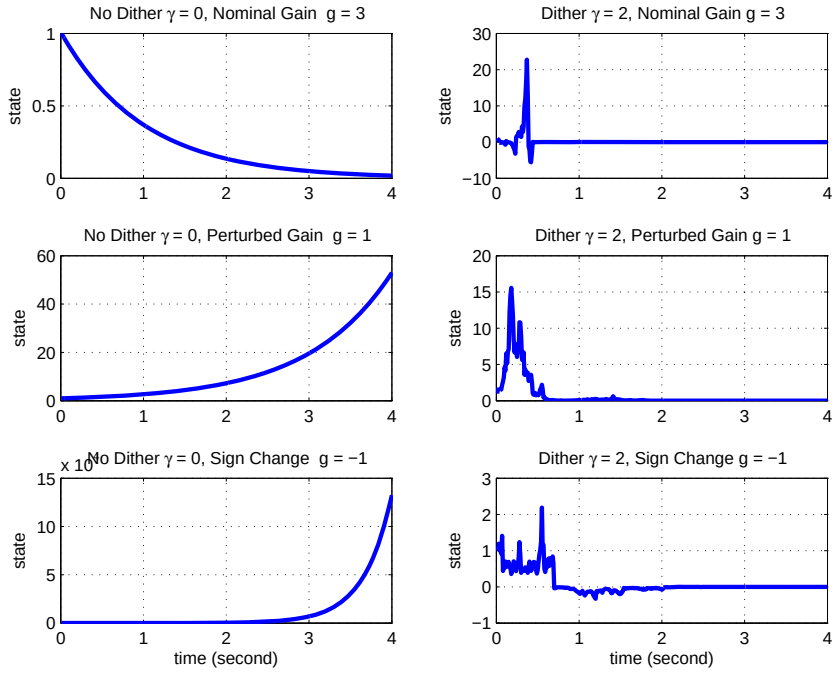

Figure 67: Comparison between a deterministic feedback and a feedback with a stochastic dither: The left-side plots show feedback without added dithers. (a) Top: Nominal feedback. The closed-loop system is stable. (b) Middle: The gain is perturbed from 3 to 1. The closed-loop system is unstable. (c) Bottom: The sign of the gain is changed to negative. The closed-loop system is unstable. The right-side plots show feedback with an added dither of $\gamma^2 = 4$. (a) Top: Nominal feedback. The closed-loop system is stable. (b) Middle: The gain is perturbed from 3 to 1. The closed-loop system remains stable. (c) Bottom: The sign of the gain is changed to negative. The closed-loop system remains stable.

The stability condition is simplified to

$$a - \frac{1}{2}\widehat{g}^2\gamma^2 b^2 c^2 < 0.$$

Theorem 48 *Suppose that for some constant $\mu > 0$,*

$$\gamma^2 > \frac{2|a|}{\mu b^2 c^2}. \tag{7.28}$$

Then the closed-loop system is robustly stable for all $\widehat{g}^2 \geq \mu > 0$.

Proof: Under (7.28), if $\widehat{g}^2 \geq \mu > 0$

$$a - \frac{1}{2}\widehat{g}^2\gamma^2 b^2 c^2 \leq a - \frac{1}{2}\mu\gamma^2 b^2 c^2 < 0 \tag{7.29}$$

This implies stability. □

Remark 49 In some sense, the condition $\widehat{g}^2 \geq \mu > 0$ is necessary. If $\widehat{g}^2 = 0$, then the communication channel is disconnected with probability one. In this case the feedback is running in open loop. So, if the open-loop system is unstable, feedback stability is lost, regardless what feedback control is used.

7.3 Robust State Observers

In this section, we briefly describe potential usage of stochastic dithers to achieve robustness in state observers. Standard full-order observers, Luenberger observers, Kalman filters assume the complete knowledge of the system parameters in their designs. In general, they are not robust with respect to model uncertainties.

Consider a first-order state space system

$$\begin{cases} \dot{x} &= ax + bu \\ \\ y &= cx \end{cases} \tag{7.30}$$

For simplicity, we assume $b = 1$ (just group bu as the new u) and $c = 1$ (just group y/c as y). Hence,

$$\begin{cases} \dot{x} &= ax + u \\ \\ y &= x \end{cases} \tag{7.31}$$

For a meaningful discussion on stabilization, we assume $a > 0$ (so the open-loop system is unstable). The standard state estimators assume the full knowledge of system parameters.

Luenberger Observers:

For this basic system, the Luenberger observer will simply use

$$\widehat{x} = y$$

as a reduced order observer. Now, suppose that there is a multiplicative uncertainty of transmitting y with

$$\widetilde{y} = gy$$

and g is an uncertainty. Consequently, the Luenberger observer becomes

$$\widehat{x} = \widetilde{y} = gy.$$

If $g \neq 1$, then the Luenberger observer will fail to get the correct state estimate. Since this is an open-loop observer, it is not robust to such multiplicative uncertainties. If this state estimator is used for feedback design, we have $u = -K\widehat{x}$. This leads to a closed-loop system

$$\dot{x} = (a - Kg)x. \tag{7.32}$$

Apparently, if g can assume both positive and negative values, there exists no feedback gain K that can robustly stabilize the system. In other words, the Luenberger observer is fundamentally non-robust in this specific sense.

Now, let us add a dither to the transmission line. Following the same development as in Section 7.1 that leads to (7.13), the resulting system is modified from (7.32) to a stochastic differential equation

$$dx = (a - Kg)xdt + g\gamma Kxdw \tag{7.33}$$

where $w(\cdot)$ is a standard Brownian motion. Consequently, the results of Theorems 44 and 46 are applicable. In other words, by appropriate selections of γ, stability of (7.33) will be guaranteed for a much larger range of gain uncertainty on g.

Full-Order Observers:

Next, we will try the full-order observer which involves a feedback mechanism.

The observer structure is

$$\begin{cases} \dot{\widehat{x}} &= a\widehat{x} + u - L(\widehat{y} - \widetilde{y}) \\ \widehat{y} &= \widehat{x} \end{cases} \tag{7.34}$$

where $\widetilde{y} = gy$ and g is the gain uncertainty. Let the state estimation error be $e = \widehat{x} - x$. The error dynamics can be easily derived as

$$\dot{e} = (a - L)e - L(1 - g)x \tag{7.35}$$

which has an additional term due to gain uncertainty.

Next, we design a state feedback $u = -K\widehat{x}$. It can be derive that

$$\dot{x} = ax - L(e + x) = (a - K)x - Ke.$$

The overall system dynamics become

$$\begin{cases} \dot{x} &= (a - K)x - Ke \\ \dot{e} &= (a - L)e - L(1 - g)x \end{cases} \tag{7.36}$$

For stability, L and K are designed to be $a - L = -\lambda_1$, $a - K = -\lambda_2$ with $\lambda_1 > 0$ and $\lambda_2 > 0$. So, we have

$$\begin{cases} \dot{x} &= -\lambda_2 x - Ke \\ \dot{e} &= -\lambda_1 e - L(1 - g)x \end{cases} \tag{7.37}$$

The system matrix is

$$M = \begin{bmatrix} -\lambda_2 & -K \\ -L(1-g) & -\lambda_1 \end{bmatrix}$$

Its characteristic polynomial is

$$(s+\lambda_1)(s+\lambda_2) - KL(1-g) = s^2 + (\lambda_1+\lambda_2)s + \lambda_1\lambda_2 - KL(1-g).$$

For robust stability, we must have $\lambda_1\lambda_2 - KL(1-g) > 0$, or equivalently,

$$g > 1 - \frac{\lambda_1\lambda_2}{KL}. \tag{7.38}$$

Since $\lambda_1 = L - a$, $\lambda_2 = K - a$, and $a > 0$, we have $0 < 1 - \frac{\lambda_1\lambda_2}{KL} < 1$. Consequently, the condition (7.38) will always be violated if g can take negative values. In other word, regardless how K and L are designed, the robustness with respect to the gain uncertainty cannot tolerate sign changes on g.

It is easy to see that Kalman filters will have the same robustness issues as the full-order observers.

Using Stochastic Dithers to Enhance Observer Robustness:

Without going into too much technical details, we note that adding stochastic dithers amounts to introduce a diffusion term. By suitable choices of dithers and their locations, the observer/feedback system will be modified to a stochastic differential

equation in the form of

$$d\begin{bmatrix} x \\ \\ e \end{bmatrix} = \begin{bmatrix} -\lambda_2 & -K \\ \\ -L(1-g) & -\lambda_1 \end{bmatrix} \begin{bmatrix} x \\ \\ e \end{bmatrix} dt + B \begin{bmatrix} x \\ \\ e \end{bmatrix} dw \tag{7.39}$$

where w is the standard Brownian motion and B is a suitable 2×2 matrix. We note that

$$\mathrm{tr}M = \mathrm{tr} \begin{bmatrix} -\lambda_2 & -K \\ \\ -L(1-g) & -\lambda_1 \end{bmatrix} = -\lambda_1 - \lambda_2 < 0.$$

By [44], see also [45], the asymptotic stability in probability of (7.39) can be achieved if and only if $\mathrm{tr}M < 0$. Since this condition is satisfied here, robust observers can be achieved. Detailed analysis will belong to general higher dimensional cases and will be treated in a separate paper.

7.4 Discussions on Scaled Dithers for Higher-Dimensional Systems

The scaled dithers are effective in providing enhanced robustness in first-order systems. Extension of this idea to higher-dimensional systems can also be beneficial, but requires caution. This is due to more complicated stability conditions and impact of the diffusion term on stability. In general, adding a dither without careful assessment of system structures may destabilize a stable system. However, in the important area

of networked consensus control, when properly designed, adding scaled dithers will enhance robust stability. This will be reported in a separate paper [46].

A complete investigation of such scenarios is beyond the scope of this thesis. In this section, we use an example to demonstrate effects of adding dithers in improving robustness in consensus control.

7.4.1 A Case Study

The constrained consensus was introduced in [47] and applied to several application problems such as power systems in [48]. A networked system consists of r node states denoted by $x_n = [x_n^1, \ldots, x_n^r]'$. At the control step n, the state will be updated from x_n to x_{n+1} by the amount u_n

$$x_{n+1} = x_n + u_n \tag{7.40}$$

with $u_n = [u_n^1, \ldots, u_n^r]'$. The node subsystems are linked by a network, represented by a directed graph $\mathcal{G}$ whose element (i, j) indicates a connection between node i and node j, namely estimation of the state x_n^j by node i via a communication link. Skipping derivation details, the state updating algorithm leads to the dynamic equation

$$x_{n+1} = x_n + \mu_n(Mx_n + Wd_n)$$

where the matrices M and W are determined by the network topology and d_n represents observation noises.

Consider a power management problem in microgrids. A five-bus grid has transmission lines between Buses 1 and 2, 2 and 3, 3 and 4, and 4 and 5, shown in Figure

68(a). The initial per-unit load distributions on the buses are not balanced with $x_0 = [0.1, 0.2, 0.3, 0.4, 0]'$.

Under suitable selection of link gains, we have

$$M = \begin{bmatrix} -0.6 & 0.6 & 0 & 0 & 0 \\ 0.6 & -1.8 & 1.2 & 0 & 0 \\ 0 & 1.2 & -3 & 1.8 & 0 \\ 0 & 0 & 1.8 & -3.8 & 2 \\ 0 & 0 & 0 & 2 & -2 \end{bmatrix}$$

;

$$W = \begin{bmatrix} 0.3 & -0.3 & 0 & 0 & 0 & 0 & 0 & 0 \\ -0.3 & 0.3 & 0.5 & -0.7 & 0 & 0 & 0 & 0 \\ 0 & 0 & -0.5 & 0.7 & 0.9 & -0.9 & 0 & 0 \\ 0 & 0 & 0 & 0 & -0.9 & 0.9 & 1 & -1 \\ 0 & 0 & 0 & 0 & 0 & 0 & -1 & 1 \end{bmatrix}$$

In this case, the eigenvalues of M are -6.0125, -3.2432, -1.5016, -0.4426, 0. Since all eigenvalues (except the single eigenvalue at 0) are stable, the control achieves the

weighted consensus, as shown in Figure 68(b).

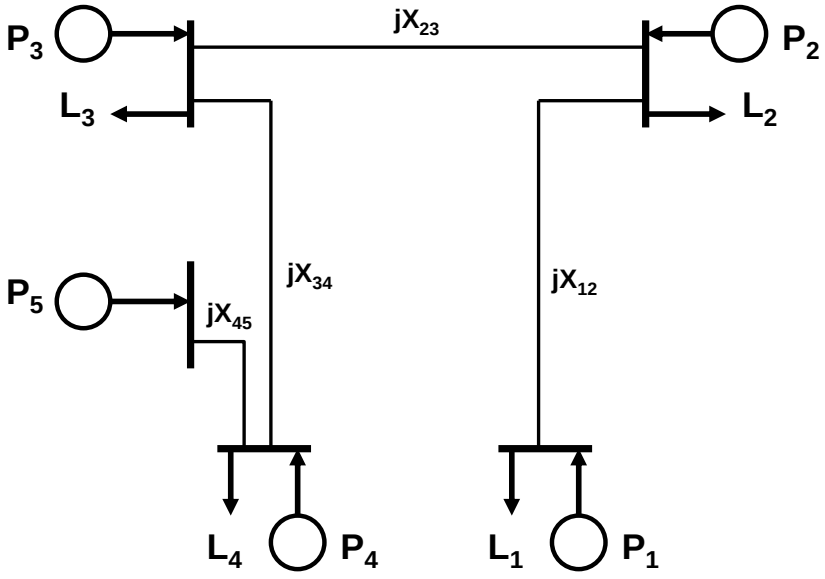

(a) A grid of five buses

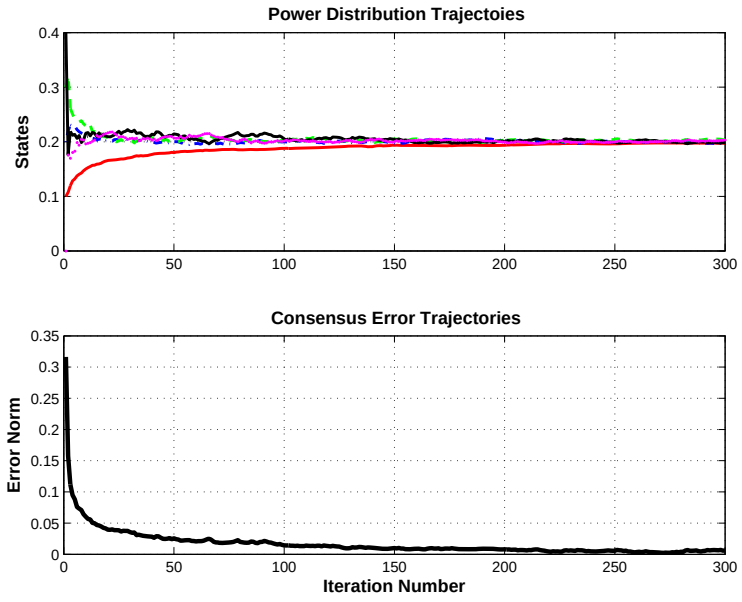

(b) Power flow control under positive link gains

Figure 68: Power management in microgrids

Now, suppose that communication channel gain uncertainties cause the link gain

matrix to change its values to $G = \text{diag}[0.3, 0.3, 0.5, -0.7, -0.9, 0.9, 1, 1]$. Correspondingly, the M matrix is changed to

$$M = \begin{bmatrix} -0.6 & 0.6 & 0 & 0 & 0 \\ 0.6 & -0.4 & -0.2 & 0 & 0 \\ 0 & -0.2 & 0.2 & 0 & 0 \\ 0 & 0 & 0 & -2 & 2 \\ 0 & 0 & 0 & 2 & -2 \end{bmatrix}$$

whose eigenvalues are -4, -1.1211, 0.3211, 0, 0. The inclusion of an unstable eigenvalue indicates that the consensus control becomes unstable. This is shown in Figure 69(a). By adding a dither with $\sigma^2 = 9$, we witness a restoration of stable eigenvalues, recovering convergence of the consensus control under communication uncertainty, shown in Figure 69(b).

7.4.2 Stability Analysis

For multidimensional systems (7.14), we can employ the idea from Khasminskii [49] to examine stability of the SDE (7.15). Define the normalized state

$$\zeta(t) = \frac{x(t)}{|x(t)|}.$$

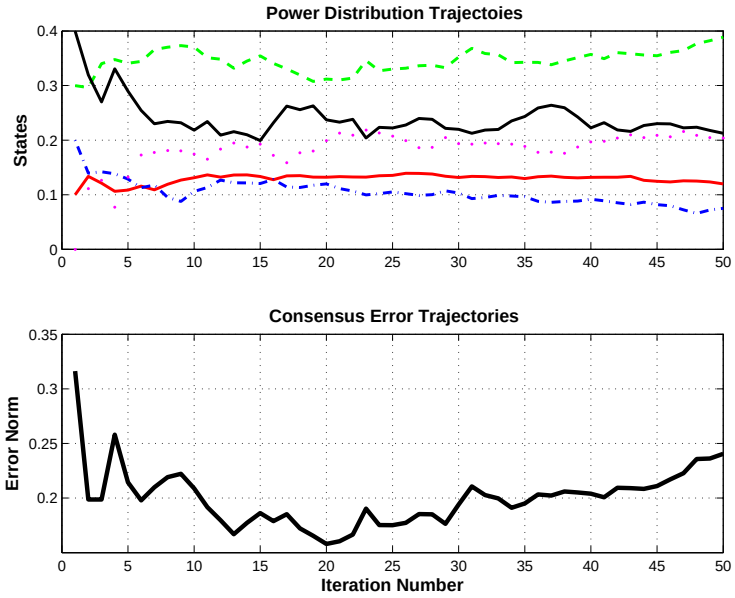

(a) Power flow control under perturbed link gains

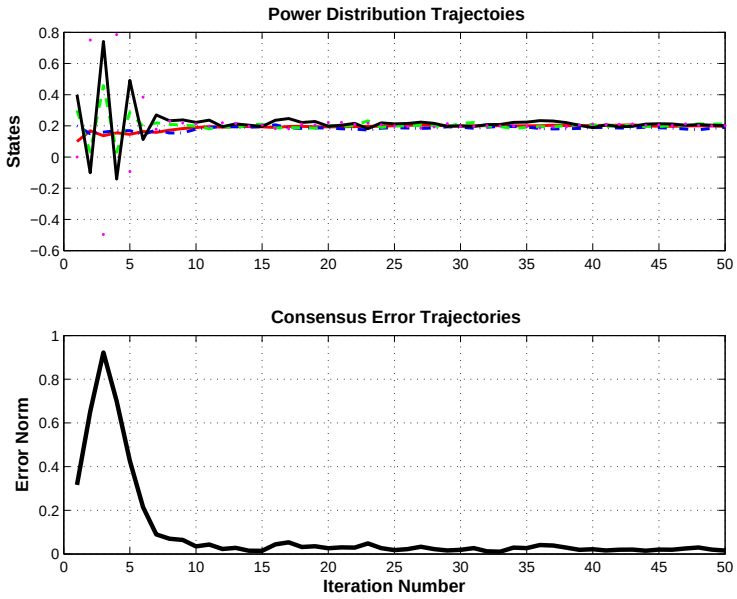

(b) Power flow control under perturbed link gains but with a scaled dither added to each observation link

Figure 69: Consensus robustness with and without scaled dithers

By virtue of Itô's Formula,

$$\begin{aligned} d\zeta(t) = &\Big[M\zeta(t) - \zeta'(t)H\zeta(t)]H\zeta(t) \\ &+\Big(-\zeta'(t)M\zeta(t) + \frac{1}{2}\big[-|H\zeta(t)|^2 + 3|\zeta'(t)H\zeta(t)|^2\big]\Big)\zeta(t)\Big]dt \\ &+\Big(H\zeta(t) - [\zeta'(t)H\zeta(t)]\zeta(t)\Big)dw(t). \end{aligned} \tag{7.41}$$

Let $H = [h_{ij}]$. Denote

$$q_{ij}(x) = \sum_{l_1,l_2} h_{l_1 i}h_{l_2 j}x_{l_1}x_{l_2}, i, j = 1, \ldots, n$$

and $Q(x) = [q_{ij}(x)]$. Define

$$\rho(t) = \ln|x(t)|.$$

As stated in [49, pp. 220–221], since $\zeta(t)$ is a diffusion on $\mathbb{S} = \{\zeta : |\zeta| = 1\}$ (the unit sphere), $\zeta(t)$ is ergodic with a unique invariant measure $P(\cdot)$ if

$$\xi'Q(x)\xi = (\xi'Hx)^2 \geq K_0|x|^2|\xi|^2. \tag{7.42}$$

By Itô's Formula,

$$d\rho(t) = [\zeta'(t)M\zeta(t) + \frac{1}{2}\mathrm{tr}Q(\zeta(t)) - \zeta'(t)Q(\zeta(t))\zeta(t)]dt + \zeta'(t)H\zeta(t)dw(t).$$

We obtain the following result.

Theorem 50 *Assume that (7.42) is satisfied. Let*

$$\lambda_0 = \int_{\mathbb{S}} \Big[\zeta'M\zeta + \frac{1}{2}\big(|H\zeta|^2 - 2|\zeta'H\zeta|^2\big)\Big]P(d\zeta), \tag{7.43}$$

where $P(\cdot)$ is the invariant measure. Then the linear SDE (7.15) is almost surely exponentially stable (resp., unstable) if and only if $\lambda_0 < 0$ (resp., $\lambda_0 > 0$).

The proof of the theorem is omitted. Some details of the proof can be found in [49] for diffusion processes and in [50] for switching diffusion processes. The stability condition (7.43) is reduced to (7.19) for first-order systems, which can be analyzed directly. In general, however, the condition (7.43) needs to be verified numerically.

8 CONCLUSION AND FUTURE WORK

This thesis investigates the interaction between control and communications, in the framework of highway platoon safety. Information structure, information content, and information reliability have been taken into consideration in this study. It is well perceived that communication systems introduce uncertainties that are of many types and values. To be concrete, we have selected communication latency as a key uncertainty in this study.

One of the main results of this thesis demonstrate that communications provide critical information that can enhance vehicle safety effectively beyond distance sensors. In fact, from our simulation studies, platoon control may mandate communications for additional information. Although traditionally, distance and vehicle speed are immediate candidates for transmission, our results show that drivers' braking events contain very effective information for platoon management. Our simulations suggest that platoon communications place event data under more prominent considerations. This thesis shows that communication latency is a critical factor in information exchange. Large latency can diminish values of data communication in platoon control. It is a common framework in multi-vehicle communication scenarios that vehicles within an interference radius do not transmit simultaneously. A direct consequence is that latency becomes larger. For instance, under the IEEE 802.11p standard, transmission radius can reach 1 km. If 50 vehicles are in this region and each transmission (or broadcasting) takes 30 ms, a delay of 1.5 second will occur

between consecutive transmissions of a given vehicle. Our study shows that such a delay has an alarmingly high impact on vehicle safety. This issue deserves further studies.

To be concrete, we selected communication PDRs as another key uncertainty in this study.The main results of this thesis demonstrate that communications provide critical information that can enhance vehicle safety effectively beyond distance sensors. In fact, from our simulation and analysis studies, platoon control may mandate communications for additional information. Although traditionally, distance and vehicle speed are immediate candidates for transmission, our results show that drivers' braking events contain very effective information for platoon management while it is very sensitive to packet loss. Our study shows that communication is a critical factor in information exchange. Large packet loss can diminish values of data communication in platoon control.

This thesis also investigates the IHM design considerations in the DSRC framework. Weighted multi-information control and DSRC data rate control designs are proposed based on the reality that vehicles can access information from neighbors or VANET enabled vehicles. The results of this this demonstrate that by choosing information content and data rate, a vehicle control goal can be achieved. Although traditionally, control gain design are immediate candidates for platoon control, our results show that a proper selection of information content and data rate can also be applied to the platoon control and potentially improve the communication resources usage. We believe that our analysis may contribute to implementing control/communication

interface design to improve highway and communication resource usages. We hope that our findings may influence standard planning for WAVE. We have only considered basic driving conditions: Straight lanes, dry surface conditions, good weather conditions, and no lane changes or platoon re-formation after vehicle departure or addition. System integration with VANET framework is a worthy topic to pursue.

This thesis also introduces the approach of adding scaled dithers to expand robustness capabilities of feedback systems. The approach is introduced in feedback systems with communication channels which involve random gain uncertainties including possible sign changes. It is shown that adding a state and sampling-rate dependent dither can enhance feedback robustness beyond the optimal gain margin in deterministic systems. A more comprehensive study of feasibility and limitations of this method is of interest. Utility of this method in systems involving random delays and phase shifts are currently under investigation.

REFERENCES

[1] J.K. Hedrick, D. McMahon, D. Swaroop, Vehicle modeling and control for automated highway systems, PATH Research Report, UCB-ITS-PRR-93-24, 1993.

[2] P. Ioannou and C. Chien, Autonomous intelligent cruise control, *IEEE Transactions on Vehicular Technology*, Vol. 42, No. 4, pp. 657672, 1993.

[3] R. Rajamani, H.S. Tan, B. Law and W.B. Zhang, Demonstration of integrated lateral and longitudinal control for the operation of automated vehicles in platoons, *IEEE Transactions on Control Systems Technology*, Vol. 8, No. 4, pp. 695-708, 2000.

[4] F. Knorr, D. Baselt, M. Schreckenberg, and M. Mauve, Reducing traffic jams via VANETs, *IEEE Transactions on Vehicular Technology*, Vol. 61 , Iss. 8, pp. 3490-3498, 2012.

[5] K.S. Chang, W. Li, P. Devlin, A. Shaikhbahai, P. Varaiya, J.K. Hedrick, D. McMahon, V. Narendran, D. Swaroop, J. Olds, Experimentation with a vehicle platoon control system, Vehicle Navigation and Information Systems Conference, pp. 1117-1124, 1991.

[6] D.H. Narendran, V.K. Swaroop, D. Hedrick, J.K. Chang, K.S. Devlin, P.E., Longitudinal Vehicle Controllers for IVHS: Theory and Experiment McMahon,American Control Conference, 1992 Publication Year: 1992 , Page(s): 1753 - 1757 Seattle, 1995.

[7] Y.F. Zhao, H. Ogai, Development of a platooning control algorithm based on RoboCar, ICE Annual Conference (SICE), pp. 352-355, 2011.

[8] J. Bom, B. Thuilot, F. Marmoiton, P. Martinet, A global control strategy for urban vehicles platooning relying on nonlinear decoupling laws, Intelligent Robots and Systems, pp. 2875-2880, 2005.

[9] G. Guo and W. Yue, Autonomous platoon control allowing range-limited sensors, *IEEE Transactions on Vehicular Technology*, Vol. 61, Iss. 7, pp. 2901-2912, 2012.

[10] C.Y. Liang and H. Peng, String stability analysis of adaptive cruise controlled vehicles, JSME International Journal Series C, Volume: 43, Issue: 3, pp. 671-677, 2000.

[11] L.Y. Wang, A. Syed, G. Yin, A. Pandya, H.W. Zhang, Coordinated vehicle platoon control: weighted and constrained consensus and communication network topologies, *Proceedings of CDC 2012*, Hawaii, pp. 4057-4062, Dec. 2012.

[12] Le Yi Wang, Ali Syed, George Yin, Abhilash Pandya, Hongwei Zhang, Control of vehicle platoons for highway safety and efficient utility: Consensus with communications and vehicle dynamics, *Journal of Systems Science and Complexity*, accepted and to appear in 2013.

[13] G. N. Nair and R. J. Evans, Exponential stabilisability of finite-dimensional linear systems with limited data rates *Automatica*, 39 (2003) 585-593.

[14] R. Obstovasky, Y. Radbani, L. J. Schulman, "Error-Correcting Codes for Automatic Control, " *Information Theory*, IEEE Transactions 2009

[15] J. S. Freudenberg and R. H. Middleton, Feedback control performance over a noisy communication channel. *Proceedings of the 2008 Information Theory Workshop*, Porto, Portugal, pp. 232-236, May 2008.

[16] J. Nilsson, B. Bernhardsson, B. Wittenmark, "Stochastic analysis and control of real-time system with random time delays." *Auomatica*, vol.34,pp.57-64. 1998.

[17] Le Yi Wang, George Yin, Ji-feng Zhang, Yanlong Zhao, System Identification with Quantized Observations, Boston, MA: Birkhäuser, 2010 (ISBN: 978-0-8176-4955-5).

[18] R. Luck and A. Ray, Experimental verification of a delay compensation algorithm for integrated communication and control system. *International Journal of Control*, vol. 59, pp. 1357-1372, 1994.

[19] A. J. Rojas, J. H. Braslavsky, and R. H, Middleton, Fundamental limitations in control over a communication channel *Automatica*, Vol. 44, pp. 3147-3151, 2008.

[20] R.T. O'Brien, Vehicle lateral control for automated highway systems, *IEEE Transactions on Control Systems Technology*, Vol. 4, Iss. 3, pp. 266 - 273, 1996.

[21] S. Sheikholeslam, C.A. Desoer, Longitudinal control of a platoon of vehicles with no communication of lead vehicle information: a system level study, *IEEE Transactions on Vehicular Technology*, Vol. 42, Iss. 4, pp. 546 - 554, 1993.

[22] D.H. McMahon, J.K. Hedrick, S.E. Shladover, Vehicle modelling and control for automated highway systems, *Proceedings of American Control Conference*, San Diego, CA, USA, pp. 297 - 303, May 23-25, 1990.

[23] M.J. Neely and Eytan Modiano, Capacity and delay tradeoffs for Ad-Hoc mobile networks, *IEEE Tran. on Information Theory*, Vol. 51, No. 6, pp. 1917-1936, 2005.

[24] K.A. Hafeez, L. Zhao, B. Ma, J.W. Mark, Performance analysis and enhancement of the DSRC for VANET's safety applications, *IEEE Transactions on Vehicular Technology*, Vol. 62 , Iss. 7, pp. 3069-3083, 2013.

[25] A. Kumar, D. Manjunath, J. Kuri, Wireless Networking, Elsevier, 2008.

[26] L.L. Peterson, B.S. Davie, Computer Networks (2nd Ed.), Morgan Kaufmann, San Francisco, CA, USA, 2000.

[27] W. Stevens, TCP/IP Illustrated (Vol. 1, The Protocols), Addison-Wesley, Reading, MA, USA, 1994.

[28] A. Lapidoth, The performance of convolutional codes on the block erasure channel using various finite interleaving techniques, *IEEE Trans. on Inform. Theory*, vol. 40, no. 5, pp. 1459-1473, Sept. 1994.

[29] R. Knopp and P. Humblet, On coding for block fading channels, *IEEE Trans. on Inform. Theory*, vol. 46, no. 1, pp. 1643-1646, July 1999.

[30] A. Guillen, I. Fabregas, and G. Caire, Coded modulation in the blockfading channel: Code construction and coding theorems, *IEEE Trans. on Inform. Theory*, vol. 52, no. 1, Jan. 2006.

[31] T. Richardson and R. Urbanke, Modern Coding Theory, Cambridge University Press, 2008.

[32] A. Papoulis and S.U. Pillai, Probability, Random Variables and Stochastic Processes, 4th Edition, McGraw-Hill Europe, 2002.

[33] J.G. Proakis and M. Salehi, Digital Communications, 5th Edition, McGraw-Hill High Education, 2008.

[34] F. Bai, D.D. Stancil, H. Krishnan, Toward understanding characteristics of dedicated short range communications (DSRC) from a perspective of vehicular network engineers, *Proceedings of MobiCom10*, Chicargo, IL, USA, pp. 329 - 340, September 20-24, 2010.

[35] L. Cheng, B.E. Henry, D.D. Stancil, F. Bai, and P. Mudalige, Mobile vehicle-to-vehicle narrow-band channel measurement and characterization of 5.9 GHz dedicated short range communication (DSRC) frequency band, *IEEE Journal on Selected Areas in Communication*, Vol. 25, Issue 8, pp. 1501-1516, October 2007.

[36] John Turner, Automotive Sensors, Momentum Press, 2009.

[37] R.G.Gallager, Principles of Digital Communication, 1st Edition, Cambridge University Press, 2008.

[38] IEEE Std 802, Wireless LAN Medium Access Control (MAC) enhancements for Quality of Service (QoS), 2005.

[39] S.N. Ethier and T.G. Kurtz, *Markov Processes: Characterization and Convergence*, J. Wiley, New York, NY, 1986.

[40] S. Haykin, Communication Systems, 4th Ed., John Wley & Sons, 2001.

[41] P. Kloeden, E. Platen, Numerical Solutions to Stochastic Differential Equations, 3rd Ed., Springer-Verlag, 1999

[42] B. Oksendal, Stochastic Differential Equations: An Introduction with Applications, 6th Ed., Springer, 2007.

[43] R. Liptser, A strong law of large numbers for local martingales, Stochastics 3 (1980) 217–228.

[44] L. Arnold, H. Crauel, and V. Wihstutz, Stabilization of linear systems by noises, SIAM J. Control and Optimization, Vol. 21, No. 3, pp. 451-561, 1983.

[45] G. Yin and C. Zhu, Hybrid Switching Diffusion: Properties and Applications, Springer, New York, 2010.

[46] L.J. Xu, L.Y. Wang, G. Yin, W.X. Zheng, Robust consensus control by state-dependent dithers, in preparation.

[47] G. Yin, Y. Sun, and L.Y. Wang, Asymptotic properties of consensus-type algorithms for networked systems with regime-switching topologies, *Automatica*, 47 (2011) 1366–1378.

[48] Wang, L.Y.; Wang, C.; Yin, G.; Wang, Y.; Weighted and Constrained Consensus for Distributed Power Flow Control, 12th International Conference on Probabilistic Methods Applied to Power Systems PMAPS 2012, Istanbul, Turkey, 2012.

[49] R.Z. Khasminskii, Stochastic Stability of Differential Equations, Sijthoff and Noordhoff, 1981.

[50] X. Mao, G. Yin, C. Yuan, Stabilization and destabilization of hybrid systems of stochastic differential equations, Automatica 43 (2007) 264–273.

[51] H.J. Kushner, G. Yin, Stochastic Approximation Algorithms and Applications, 2nd Ed., Springer-Verlag, New York, 2003.

[52] L.C. Evans, An Introduction to Stochastic Differential Equations, Version 1.2. Online Resource: http://math.berkeley.edu/ evans/SDE.course.pdf

ABSTRACT

COMMUNICATION PROTOCOL DESIGN CONSIDERATIONS FOR HIGHWAY VEHICLE PLATOONS AND ENHANCED NETWORKED ROBUSTNESS BY STOCHASTIC DITHERS

by

LIJIAN XU

May 2014

Advisor: Dr. Le Yi Wang

Major: Electrical and Computer Engineering

Degree: Doctor of Philosopy

Highway platooning of vehicles has been identified as a promising framework in developing intelligent transportation systems. By autonomous or semi-autonomous vehicle control and inter-vehicle coordination, an appropriately managed platoon can potentially offer enhanced safety, improved highway utility, increased fuel economy, and reduced emission. This thesis is focused on quantitative characterization of impact of communication information structures and contents on platoon safety. By comparing different information structures which combine front sensors, rear sensors, and wireless communication channels, and different information contents such as distances, speeds, and drivers' actions, we reveal a number of intrinsic relationships between vehicle coordination and communications in platoons. Typical communication standards and related communication latency and package loss are used as benchmark cases in our study. These findings provide useful guidelines for information harmonization module (IHM) design in sensor selections, communication resource allocations, and vehicle coordination. Two new weighted multi-information structure control and information data rate control are proposed. Both control methods have been validated by experimental simulation and finite element analysis, and

also show a surprising improvement of communication resources usage with data rate control. The results for the proposed module are new in the literature for vehicle platoon control. A new method is introduced to enhance feedback robustness against communication gain uncertainties. The method employs a fundamental property in stochastic differential equations to add a scaled stochastic dither under which tolerable gain uncertainties can be much enlarged, beyond the traditional deterministic optimal gain margin. Algorithms, stability, convergence, and robustness are presented for first-order systems. Extension to higher-dimensional systems is further discussed. Simulation results are used to illustrate the merits of this methodology.

AUTOBIOGRAPHICAL STATEMENT

LIJIAN XU

Education

- Ph.D in Electrical and Computer Engineering, May 2014
  Wayne State University, Detroit, Michigan
- M.S. in Computer Engineering, August 2001
  University of Central Florida, Orlando, Florida

Experience

- Graduate Research/Teaching Assistant, September, 2011—April, 2014
  Department of Electrical & Computer Engineering, Wayne State University, Detroit, Michigan
- Engineer and Engineering Manager, September, 2001—January,2008
  AT&T, Telus Communication

Awards

- Olbrot Travel Awards for Excellence in Graduate Student Research,
  Department of ECE, Wayne State University, 2013
- Best Paper Award,
  2012 IEEE International Conference on Electrical/Information technology, 2012
- Thomas C. Rumble University Graduate Fellowship Award,
  Wayne State University, 2012
- 2011 ECE Travel Grant,
  Wayne State University, 2011

Accepted/Published Journal Papers:

1. **Lijian Xu**, Le Yi Wang, George Yin, Hongwei Zhang, "Coordinated Control and Communication for Enhanced Safety of Highway Vehicle Platoons", *IEEE Transactions on Vehicular Technology*, accepted and to appear in 2014.

2. **Lijian Xu**, Le Yi Wang, George Yin, Weixing Zheng, "Enhanced Feedback Robustness against Communication Channel Uncertainties via Scaled Dithers in Network Systems", *Systems & control Letters*, accepted and to appear in 2014.

Under-review Journal Papers:

1. **Lijian Xu**, Le Yi Wang, George Yin, Hongwei Zhang, "Impact of Communication Erasure Channels on Safety of Highway Vehicle Platoons", *IEEE Transactions on Intelligent Transportation System.*

2. Le Yi Wang, Ge Chen., George Yin, **Lijian Xu**, "Integration of Subsystem Dynamics and Weighted and Constrained Consensus: Convergence, Stability, and Robustness", *IEEE Transactions on Automatic Control.*